Cross-Layer Design of All-Optical Networks Incorporating Crosstalk Effects

A Dissertation

Presented to

the faculty of the School of Engineering and Applied Science

University of Virginia

In Partial Fulfillment

of the requirements for the Degree

Doctor of Philosophy

Electrical and Computer Engineering

by

Yvan Pointurier

August 2006

Approvals

This dissertation is submitted in partial fulfillment of the requirements for the degree of

Doctor of Philosophy

Electrical and Computer Engineering

Yvan Pointurier

Approved:

Maïté Brandt-Pearce (Advisor)

Stephen G. Wilson (Chair)

Malathi Veeraraghavan

Ira Jacobs (Virginia Tech)

Toby Berger

Accepted by the School of Engineering and Applied Science:

James H. Aylor (Dean)

August 2006

Abstract

The performance of current optical networks is inherently limited by the speed of electronic components, and especially the electronic switches; a new generation of optical networks, referred to as all-optical networks, overcome this limitation by switching data entirely optically using all-optical crossconnects (OXCs). However, all-optical networks are prone to phenomena that are unknown to current optical networks. For instance, OXCs are subject to optical leaks, resulting in unwanted components called node crosstalk being added to transmitted signals. Node crosstalk is propagated over long paths without any signal regeneration.

We study the interplay between nonlinear fiber and node crosstalk signals over long distance as a source of Quality of Service (QoS) degradation, measured in terms of bit-error rate (BER). We present a crosstalk model for all-optical networks and give exact expressions for the performance degradation resulting from the joint propagation of a signal and node crosstalk in large networks. Realizing that crosstalk can be a serious impairment for proper network operation, we propose to mitigate physical layer impact (including node crosstalk) at call admission time using specifically designed QoS-aware Routing and Wavelength Assignment (RWA) algorithms (a network-layer technique). Our new RWA algorithms choose a route and a wavelength for incoming calls in all-optical networks (viewed as circuit-switched networks) depending on the physical-layer state, making RWA algorithms and all-optical networks design a cross-layer issue.

We show that our new RWA algorithms outperform traditional RWA algorithms while exhibiting additional interesting properties, such as enhancing the fairness among the users in the network. Our RWA algorithms are evaluated with simulations on realistic large-scale metropolitan and regional network topologies. To decrease the time to evaluate QoS-aware RWA algorithms, we also present an analytical technique to evaluate the performance of a class of RWA algorithms incorporating multiple physical layer impairments including node crosstalk. Our analytical technique is shown by simulation on various network topologies to model accurately all-optical network behavior.

Acknowledgments

This work was carried under the supervision of Prof. Maïté Brandt-Pearce. Maïté always supported me throughout the past four years, from advising me towards a good choice for my Ph.D dissertation topic to giving me job advice. I greatly benefited from her insight when I thought I was stuck with a difficult problem, finding ways to bypass the difficulty when it seemed a straightforward solution was not available. I would like to thank Maïté for her always friendly attitude towards me, and for sharing many of her experiences including a semester-long trip to the French Riviera and a trip to Istanbul for the International Conference on Communications (ICC) highlighted by a best paper award; the work presented in this dissertation would not have been made possible without her. Maïté actually took over a process started up by my former advisor Jörg Liebeherr; Prof. Liebeherr initiated me not only to research, but also to good practice in research. May he be thanked for this.

I would also like to acknowledge the support from the National Science Foundation and hence the American taxpayer, which funded me for the duration of my graduate studies.

Many people in addition to Maïté have supported me in one way or another during my Ph.D studies; among them, Nicolas Christin has given me numerous advice which helped me professionally, and Bo Xu and Satya Ponnaluri have greatly helped me with my transition from the Computer Science department to the Electrical and

Computer Engineering department, sharing with me their deep background in my (then) new field. Satya also assisted me many times at more difficult times during the past four years and I am deeply thankful for this.

Last but not least, I want to thank my parents for supporting my choices even when that meant being away from home for extended periods of time. They set up a great educational background during my upbringing without which I never would have received a doctoral degree.

Contents

List of Figures

List of Tables

List of Acronyms

ASE	Amplified spontaneous noise
BER	Bit-error rate
CW	Continuous wave
DC	Dispersion compensation
DWDM	Dense wavelength division multiplexing
NZ-DSF	Non-zero dispersion-shifted fiber
FEC	Forward error correction
FFT	Fast Fourier transform
FWM	Four wave mixing
Gbps	Gigabit per second
HQ	Highest Q factor
ISI	Intersymbol interference
MEMS	Micro-electro-mechanical systems
MMQ	Max-min Q factor
MMQ2	Max-min Q factor with protecting threshold
NRZ	Non-return to zero
NSF	National Science Foundation
OBS	Optical burst switching

OXC	Optical crossconnect
PMD	Polarization mode dispersion
QoS	Quality of service
RWA	Routing and wavelength assignment
RZ	Return to zero
SMF	Single-mode fiber
SNR	Signal to noise ratio
SP	Shortest path
SP2	Shortest path with protecting threshold
SPM	Self-phase modulation
SSF	Split-step Fourier
TCP	Transmission control protocol
XPM	Cross-phase modulation
WDM	Wavelength division multiplexing

Chapter 1

Introduction

All-optical networks have emerged as a solution to keep up with the always increasing throughput demand. In today's transport networks, data are transmitted over optical fibers and optical-electro-optical conversion is needed at the nodes to perform routing. These networks can achieve a throughput of up to several hundreds of Gbits/s using Wavelength Division Multiplexed (WDM) channels. Yet optical fibers have a potential capacity of several tens of terabits/s per channel. Electronic switches are not able to sustain such transmission rates and have become complex and costly, making it highly desirable to replace them with all-optical switches where no electric conversion is needed at all. Deploying such all-optical networks is promising but also challenging and novel issues have to be anticipated. In this dissertation, we study one of these issues, impairment by optical leaks, called node crosstalk, which takes place in switches; we show how to mitigate node crosstalk as well as other physical impairments using crosslayer techniques consisting of routing and wavelength assignment algorithms that account for physical impairments.

All-optical switches, or Optical Crossconnects (OXCs), remove the electrical conversion step in switching hardware. In addition to the gain in network data rate, all-

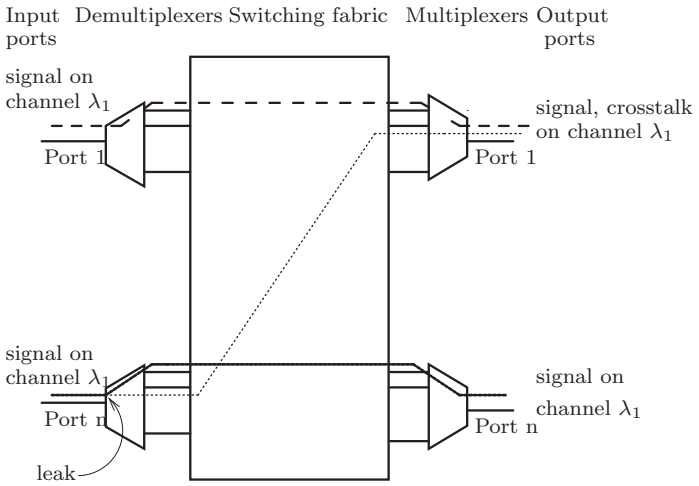

Figure 1.1: Example of source of in-band node crosstalk: due to filter imperfection in the OXC, a small amount of the input signal on channel λ_1 on the n^{th} input port is allowed in the switching fabric via the input reserved for channel λ_2.

optical switches are expected to become simpler to implement and therefore cheaper than their electrical counterparts. Moreover, all-optical switches allow for improved data rate flexibility in networks. All-optical switches have been the subject of much research in the recent years and some are already commercially available [1, 2]. The function of an all-optical switch is to transmit an incoming signal arriving along a certain optical fiber on a certain wavelength to a different optical fiber. Although several architectures have been proposed, all-optical switches contain the same functional elements: demultiplexers, a switching fabric, optional wavelength converters, and multiplexers, as depicted in Fig. 1.1; a comprehensive review of enabling technologies for all-optical networks, including several OXC architectures and numerical data for all-optical components parameters, is available in [3]. In our work, we do not consider wavelength conversion nor optical regenerators, as those devices are still at the experimental stage and are likely to be costly.

A key feature of optical networks is their capability to deliver data with low bit-error rates (BER) over long distances. However, as transmission distances increase,

signals are subject to more severe physical impairments: intersymbol interference (ISI) appears because of the fiber chromatic dispersion, nonlinear effects (Self Phase Modulation, SPM), and polarization mode dispersion (PMD); noise that is generated in optical amplifiers accumulates; and nonlinear interchannel interference, or *nonlinear crosstalk*, appears in WDM and more particularly in dense WDM (DWDM) systems due to fiber nonlinear effects (cross-phase modulation, XPM, and four wave mixing, FWM) [4]. These effects impair traditional optical networks and are enhanced by the propagation distances involved in all-optical networks.

In addition, signals can leak within an OXC due to the physical imperfections of the components. The *node crosstalk* phenomenon refers to the presence of unwanted components (*node crosstalk signals*) at the output of the switch because of leaks of the input signal. Node crosstalk can be in-band (the node crosstalk component and the input signal are on the same channel) or out-of-band (the channels are different). It has been shown that the node crosstalk effects on signal transmission are largely dominated by in-band node crosstalk in [5], and therefore we consider here in-band node crosstalk only. More details about node crosstalk, including classification into broad classes, are available in [6] and [7]. For example, consider the OXC with n ports in Fig. 1.1, where we assume that channel λ_1 from the first input port is routed to the first output port, channel λ_1 from the n^{th} input port is routed to the n^{th} output port, and channel λ_2 from the n^{th} input port is routed to the first output port. In Fig. 1.1, a leak occurs in the n^{th} input demultiplexer that allows part of signal on channel λ_1 to leak, to travel with λ_2 within the switching fabric, and to be present at the output of the first output demultiplexer. In this particular example, node crosstalk is the result of leaks at the demultiplexers. In this work, we actually use more elaborate models for the origin of node crosstalk that are presented in [8] and reviewed in Chapter 3.

Because of the large transmission distances involved in all-optical networks, fiber dispersion and nonlinearity are important sources of performance degradation. These effects are complex and interdependent, making simulation an appropriate tool for design and analysis [9]. Although impairments due to node crosstalk in all-optical networks have been observed in the past [10], observed experimentally [11] and included in OXC design [12, 13, 14, 15], an analytical model for nonlinear propagation of node crosstalk in all-optical networks has never been proposed. Such a model is essential in the study of this important phenomenon, and eventually in our goal to alleviate its effect in all-optical network. We envision two different techniques to reach such a goal. A first solution is to design all-optical networks carefully, i.e., with node crosstalk in mind since the earliest design stages. Unfortunately, much fiber (called *dark fiber*) is already in place and waiting to be used, making it too costly to change the network design [16]. Moreover, much research has been carried on in the past decades to reduce physical impairments at the physical layer, leading for instance to the development of low-noise amplifiers and the design of complex dispersion maps, dispersion compensation devices, and multi-user detectors; however, residual degradation still remains, and crosstalks for instance cannot be filtered out at the physical layer since leaked signal and legitimate signal share the same band. Therefore, accounting for node crosstalk in the physical layer design of all-optical networks is a limited option. Another technique to reduce node crosstalk impairment in all-optical networks is to route and assign wavelengths to calls with appropriate Routing and Wavelength Assignment (RWA) algorithms that account for node crosstalk. This is the solution we retained in this dissertation.

Routing and Wavelength Assignment has emerged as a method to mitigate physical impairments in all-optical networks at the network layer. Since wavelength conversion is not yet mature for commercial deployment, a call in an all-optical network

must use the same wavelength from source to destination, a constraint known as the *wavelength continuity constraint*. The role of RWA algorithms is to assign a route and a wavelength — the combination of which is called a *lightpath* [17] — to incoming calls in a network, in order to satisfy an optimization goal, such as the minimization of the average call blocking probability in the network [18].

In current all-optical networks, packet switching is not available as the switching matrices are not fast enough to switch each packet individually. Therefore, current all-optical networks are circuit-switched networks where a lightpath represents a circuit. Currently, most wavelengths are leased over long periods of time (up to months), and therefore much of the lightpaths are currently established in a preplanned manner in current optical networks. However, lease times are already decreasing such that wavelengths will be considered as circuits in the near future, thereby making blocking probability studies in all-optical networks relevant [19]. An example of the applications that benefit from short, on-demand circuit durations, is e-science collaboration [20], and technology to facilitate shortening of wavelength lease durations is already available (for instance, GMPLS, a new standard that is increasingly implemented in network equipment, enables on-demand lightpath establishment [21]). Moreover, although all-optical switching at the packet granularity is currently not available, Optical Burst Switching (OBS), which fills the gap between packet and circuit-switching, makes it possible to utilize wavelength-routed all-optical networks in a packet-switched environment such as the Internet: OBS aggregates packets with same source and destination in long bursts, which are then transmitted over short-lived circuits [22]. In this dissertation, we therefore view an all-optical network as a circuit-switched network where calls arrive randomly and circuits must be established and torn down on-demand, making blocking probability a meaningful performance metric.

All-optical networks are subject to physical impairments that are static and depend on the network topology only, such as ISI and noise, but also other physical impairments that are dynamic and can vary with the network state, such as nonlinear crosstalk and node crosstalk. As a result, Quality of Service (QoS) of signals in a network, as measured by their BER, is also dependent on the network state. Since QoS in all-optical networks depends on the network state, not only must RWA algorithms find a lightpath that meets the wavelength continuity constraint, but also the selected lightpath must meet a *QoS constraint*; in this dissertation, a QoS constraint is a fixed BER threshold that each lightpath cannot exceed at any time. In addition to minimizing blocking probability, it is desirable for RWA algorithms to exhibit high QoS (i.e., low average call BER) instead of only ensuring that each call satisfies a minimum level of QoS. Indeed, operating a network far from the BER threshold permits more flexibility in the network. It improves the network scalability, as adding links or nodes, and therefore increasing the amount of crosstalk injected in the network, moves the BER of lightpaths closer to, rather than across, the BER threshold. Similarly, operating with a BER margin mitigates the effects of hardware aging, and finally lower BERs can help increase the actual data throughput in the network by limiting the number of retransmissions at higher layers, such as TCP for instance.

The RWA problem has been given attention recently for problems involving QoS-awareness; for instance, one or more of the following impairments: noise, PMD, Four Wave Mixing, residual dispersion and average nonlinear phase variation, and electrical regeneration cost, have already been included in various RWA algorithms [23, 24, 25, 26, 27, 28, 29]. These works overlook node crosstalk. The algorithms presented in [30, 31] incorporate many impairments, including node crosstalk, at the admission control step only. The same impairments are accounted for in [32] in the case of translucent networks where some nodes can regenerate signals electronically;

in this dissertation, we consider transparent networks where the only regeneration mechanism available at the nodes is optical linear amplification. In the past, RWA algorithms that incorporate node crosstalk both at the admission control and at the route selection step [33] or wavelength assignment step [8] were proposed. These algorithms were based on fixed alternate routing algorithms. In this dissertation, we propose new RWA algorithms based on *adaptive RWA algorithms* [34], which are known to reduce the blocking probability due to the wavelength continuity constraint.

In addition to QoS-awareness, another desirable property for RWA algorithms is *fairness*. Fairness was defined and quantified by a *fairness index*, a number between 0 and 1, in the general context of circuit-switched networks in [35] and refers to how resources are shared between users: a fairness index of 1 means that resources are equally shared between users while a low fairness index indicates that some users enjoy access to the resources when others do not. Fairness in the context of RWA has received little attention. In [36], the authors presented techniques to improve blocking probability fairness. These techniques were assessed graphically rather than with a metric in the context of alternate routing in [37]. In [38], the authors evaluate fairness in terms of used capacity in traffic grooming situations where flows with different bitrates are aggregated over high capacity lightpaths. In [39], blocking probability fairness is evaluated in translucent networks where electronic regeneration is available. In this dissertation, we present new RWA algorithms that perform well in terms of QoS (BER) and fairness (both blocking probability and BER fairness) without sacrificing low blocking probabilities. We consider the case of large metropolitan-sized networks where distances are short enough for the network to accommodate uncoded lightpaths. We also consider the case of larger regional-sized networks where some paths are too long and require Forward-Error Correction (FEC) coding to achieve the desired QoS level. In both cases, our network-layer algorithms are shown to

remove most of the physical layer impairments. Our algorithms are evaluated by computationally-intensive simulations on realistic networks.

Evaluation by simulation of RWA is a time-consuming process, and alternate analytical methods are needed. Although the problem of analytically computing blocking probability in all-optical networks has been studied in the past, using various models and assumptions, the physical layer has barely been accounted for to this point in any analytical work. In [40], the problem of partial wavelength conversion is touched upon, and in [41] the authors determine the blocking due to outdated information in the network. In all previous works that provide an analysis of blocking in all-optical networks, links are always assumed to transmit data error-free. In this dissertation, we present an analytical method to compute blocking probabilities in all-optical networks, accounting for the blocking due to QoS — including both topology-only dependent effects (ISI, noise) and also load-dependent effects (node crosstalk). Our method is based on [19], which scales well with the network size and is applicable to large arbitrary topologies, but does not include blocking due to QoS.

The contributions of this dissertation are highlighted by its structure, which is as follows. In Chapter 2, we present fast novel analytical and semi-analytical methods to assess the impact on network performance of node crosstalk transmission in non-linear fiber. In Chapter 3, we present new RWA algorithms that mitigate the effects of the physical layer, including node crosstalk, at the network layer, through appropriate Routing and Wavelength Assignment. Our RWA algorithms exhibit additional important properties, specifically, they improve the QoS in all-optical networks and increase fairness among users. In Chapter 4, we present a fast analytical method to assess the performance of a class of RWA algorithms. This method is the first of its kind to include physical-layer impairments. We conclude our dissertation in Chapter 5 and give directions for future work.

Chapter 2

Crosstalk Propagation in All-Optical Networks

In this chapter, we study the performance degradation in all-optical transport networks caused by node crosstalk originating from leaks in OXCs. Because of fiber nonlinearity and because signals are transmitted over long optical lightpaths with no further regeneration or reshaping than amplification, crosstalk is a major impairment in all-optical networks, and thus crosstalk should be accounted for at the design stage when planning for all-optical network deployment. Availability of a fast method to assess crosstalk impairment in future all-optical networks is important in certain applications such as crosstalk-aware Routing and Wavelength Assignment algorithms design, which we study in Chapters 3 and 4. In this chapter, we use the word "crosstalk" to designate "node crosstalk", that is, crosstalk that originates from OXCs. Parts of this chapter were published in [42, 43].

2.1 Introduction

Crosstalk accumulation, due solely to the concatenation of optical switches (i.e., ignoring transmission issues), is a well-known problem [5, 44]. The transmission of crosstalk has been studied in the past [6, 10, 11, 45], but not analytically. The primary focus of this chapter is on the analysis of the interplay between fiber physical parameters, especially fiber nonlinearity, and crosstalk. The study of the transmission effects on crosstalk in nonlinear fibers for modulated signals has not been carried out analytically before. We present a new method based on perturbation theory to analytically compute the impact of crosstalk on the performance of all-optical networks. We assess the performance of a network via its *Q factor*, from which a bit-error rate (BER) can be estimated. Our analysis first assumes the transmission of a continuous wave signal (CW pump) perturbed by crosstalk, viewed as small signals. The CW assumption models accurately transmission of NRZ signals. Under the continuous wave assumption, we are able to derive a fast and accurate means of studying signal transmission subject to crosstalk in optical fibers. We then remove the CW assumption at the expense of a moderate increase in computational complexity to model RZ signal transmission. Here, other impairments such as receiver noise, inter-channel interference, insertion loss due to the optical components, polarization mode dispersion (PMD), which have been studied in the past and could be incorporated in the model, are ignored for simplicity.

This chapter is organized as follows. The system of interest is described in Section 2.2. In Section 2.3, we model systems with NRZ signaling using a CW assumption and we present a perturbation theory based analysis of the impact of in-band crosstalk in all-optical networks with NRZ signaling. We relax the CW assumption in Section 2.4 to account for all-optical networks with RZ signaling.

2.2 System description

2.2.1 Network model

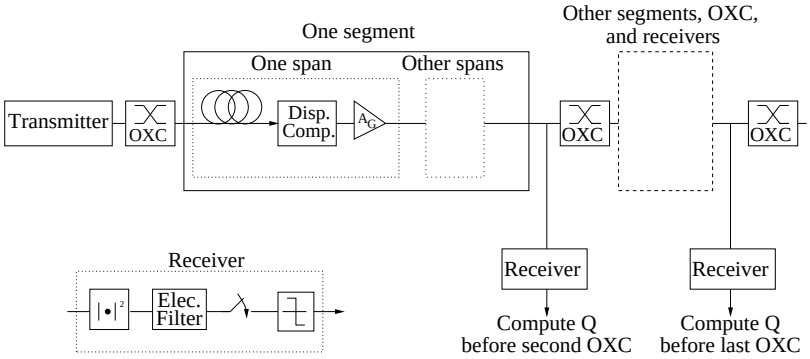

Figure 2.1: Simulated network: each OXC adds a crosstalk component to the input signals.

To carry out our analysis and simulations, we model a lightpath in an all-optical network as depicted in Fig. 2.1. In Section 2.3.1, we consider that the transmitter generates a CW signal with power P_0 and we conduct crosstalk transmission impairment analysis using a CW assumption. From Section 2.3.2 onwards, we consider that the transmitter generates a modulated signal with peak power P_0. The lightpath consists of N_s *segments* separated by OXCs that inject crosstalk in the system; we describe crosstalk modeling in Section 2.2.2. Each segment consists in turn of a fixed number N_f of fiber *spans* of length L. We assume that the number of spans is the same for each segment to simplify the notations, but generalization to different numbers of spans per segment can easily be included in our analysis. In each fiber span, an optical amplifier with gain A_G compensates exactly for the fiber loss and dispersion compensation may be used as depicted in Fig. 2.1.

The main signal and the crosstalk signals propagate from one end of the lightpath to the other; the propagation equation of an optical signal with slowly varying

complex envelope $A = A(t, z)$ at time t and position z along a fiber is given by the nonlinear Schrödinger equation [46]:

$$\frac{\partial A}{\partial z} = -\frac{\alpha}{2}A + \frac{j}{2}\beta_2 \frac{\partial^2 A}{\partial t^2} - j\gamma \left|A\right|^2 A \tag{2.1}$$

where α is the linear attenuation, β_2 the second-order dispersion, and γ the nonlinear parameter. Again, in our analysis, we assume that all fiber spans of the lightpath are physically identical but generalization to lightpaths which contain different types of fiber is straightforward.

We assess the performance of the lightpath via its *Q factor*. The Q factor is an electrical SNR expression related to the bit error rate (BER) of the system ($BER = \frac{1}{2}\text{erfc}\frac{Q}{\sqrt{2}}$) under a Gaussian assumption, which is more accurate as the number of crosstalk signals grows [47]. We calculate the Q factor at the output of (virtual) receivers placed at the end of each span. Since each OXC injects new crosstalk, by placing the receivers before an OXC, we are able to assess the impact of fiber crosstalk on the lightpath performance without having to account for crosstalk components injected by subsequent OXCs on the lightpath. Each receiver is modeled by an ideal photodetector (a square-law detector), an electrical filter with narrow bandwidth, and a sampler. The Q factor can be calculated as

$$Q = \frac{\mu_1 - \mu_0}{\sigma_0 + \sigma_1}, \tag{2.2}$$

where μ_0, μ_1 are the means of the received samples corresponding to (sent) "0" and "1" bits respectively, and σ_0 and σ_1 are the standard deviations.

In this dissertation, we model crosstalk impact, measured after photodetection, as an electrical noise variance term to account for the beating between the crosstalk sig-

nal and the "one" samples of the sent signal [47]. Assuming a good extinction ratio, we can ignore the crosstalk contributions to $(\mu_1 - \mu_0)$ and σ_0; using this model, we further assume that the effects of signal-signal and signal-crosstalk nonlinear transmission are independent and therefore the variance σ_1^2 can be split into two terms:

$$\sigma_1^2 = \sigma_i^2 + \sigma_{nx}^2, \tag{2.3}$$

one corresponding to the ISI and linear and nonlinear propagation effects on the main signal due to its transmission through the fiber (σ_i^2) and the other term due to the crosstalk (σ_{nx}^2). We estimate μ_0, μ_1, σ_0 and σ_i using a simulation of the transmission of a short pseudo-random sequence of bits through the modeled network. It is also possible to estimate the crosstalk variance σ_{nx}^2 by Monte-Carlo simulation, but doing so is a time-consuming technique due to the large number of random variables (bits, phase, delay) to consider. We present here faster, analytical (for NRZ signaling, in Section 2.3) or semi-analytical (for RZ signaling, in Section 2.4) techniques to compute σ_{nx}^2.

Because our main interest lies in the study of the interactions between fiber properties and crosstalk, we assume in the analytical part of our work that amplifiers do not add any noise to the signal. For the same reason, we ignore inter-channel interactions (which can be included using, for instance, the Volterra Series Transfer Function approach as in [48]). Although crosstalk can originate from demultiplexers that are inside OXCs in a WDM system, we view crosstalk as a perturbation to a main signal, and therefore we consider a single-channel system where the main signal propagates over the system single channel and is subject to perturbation by crosstalk, regardless of the crosstalk origin.

2.2.2 Crosstalk model

After describing the physical and topological properties of the system of interest, we now describe our crosstalk modeling. At each OXC, the main signal is corrupted by a certain number of crosstalk signals. We first consider a single crosstalk signal, and then extend our analysis to several crosstalk terms. Since the crosstalk component and the input signal come from two different sources, the crosstalk can be slightly detuned from the main signal by an angular frequency ω_s.

The polarization between the main signal and the crosstalk signal is random; however, it was shown in [49] that impairments due to crosstalk are dominated by the case where the main and the crosstalk signals are in the same polarization state, and hence systems should be designed for this worst case. In this work, we therefore assume that the main signal and the crosstalk signal are copolarized.

Crosstalk can originate from the switching fabric or from the input demultiplexers of an OXC. In this chapter, we assume that the crosstalk signal is an attenuated version of the input signal. This assumption accurately models crosstalk originating from the switching fabric, and also from the demultiplexers if we consider that the frequency response of the demultiplexers is flat over the cut-off band. However, this assumption is not essential in our work and can be relaxed easily. We call η the peak power ratio of the crosstalk to the main signal peak power. In practice, η is as high as -25 dB in Fiber Bragg Grating based switches which integrate the demultiplexing and the spatial switching functionalities in the same fabric. Although crosstalk can be lower than -60 dB for MEMS spatial switches that are used in commercial all-optical switches, in such switches crosstalk originates from the multiplexing/demultiplexing stages and can amount to -20 dB [3,50]. We describe more elaborate crosstalk models in Section 3.2.

Given a baseband pulse shape $h(t)$ for the transmitted (crosstalk) bits, normalized to unit amplitude, we write the complex envelope of the fiber input signal $s_0(t)$ as the sum of the main signal and a crosstalk bit:

$$s_0(t) = \sqrt{P(t)} + mg_0(t - \tau), \tag{2.4}$$

where m is 0 or 1 with equal probability, and $g_0(t)$ is the effective transmit pulse shape

$$g_0(t) = \sqrt{\eta P_0} h(t) e^{j\omega_s t + j\varphi}. \tag{2.5}$$

The phase φ and the delay τ of the crosstalk with respect to the input signal are assumed to be randomly distributed, respectively between 0 and 2π, and 0 and the bit duration T_b. In the case of crosstalk originating from demultiplexers, if the demultiplexer response cannot be considered to be flat, it is possible to let $h(t)$ be the actual crosstalk pulse shape (after the demultiplexer) in (2.5).

The goal of the following section is to obtain an analytical expression for the crosstalk variance of the output signal at different points along the network for a continuous wave main signal ($\sqrt{P(t)} = \sqrt{P_0}$) taken as an approximation to NRZ modulation.

2.3 Continuous wave approximation

We approximate NRZ modulation for the main signal with a continuous wave probe to analytically estimate the impairment by modulated crosstalk via the variance σ_{nx}^2 in Section 2.3.1. Then, we validate this approach using simulations in Section 2.3.2.

2.3.1 Analysis for NRZ signals

In this section, we apply perturbation theory results to the transmission of a CW signal perturbed by a small crosstalk signal, for single and multi-segment systems, and give a complexity analysis for our method.

2.3.1.1 Crosstalk impact in single-segment systems

We first focus on a single-segment lightpath of N_f fiber spans between 2 OXCs. A CW pump and a single crosstalk component are injected by the first OXC, and the signal is observed just before the second OXC so that we can ignore the impact of the second OXC on the system for now; how to deal with several OXCs is discussed in the next section.

Perturbation theory has successfully been applied to the study of transmission impairments due to noise [51, 52, 53] and fiber nonlinearity [4]. We consider only first-order interactions, that is, interactions between the CW pump and crosstalk, and neglect all higher order interactions such as crosstalk-crosstalk interaction. Since crosstalk can be considered as a small perturbation to the CW pump, previously published results hold. In this section, we first determine the pulse shape of a crosstalk bit after transmission through a nonlinear fiber, and then use this pulse shape to compute the variance σ_1 needed to determine the Q factor of a lightpath in an all-optical network.

First, we rewrite the signal $s_0(t) = \sqrt{P_0} + mg_0^I(t) + jmg_0^Q(t)$, where we split a crosstalk bit (detuned by ω_s, delayed randomly by τ and with the constant but random phase φ relatively to the CW pump) $g_0(t)$ into an in-phase term $g_0^I(t)$ and a quadrature term $g_0^Q(t)$ with respect to the CW pump phase. Suppose the input signal is transmitted through k spans. We denote by $g_k(t)$ and $G_k(\omega)$ the pulse shape

of the crosstalk bit at the output of the k^{th} span in the time and frequency domain respectively, and by g_k^I and g_k^Q the in-phase and quadrature pulse shapes relative to the output CW signal. The signal at the output of the k^{th} span $s_k(t)$ can be written as:

$$\begin{aligned} s_k(t) &= \sqrt{P_0}e^{jk\theta_{SPM}} + mg_k(t-\tau) && (2.6)\\ &= e^{jk\theta_{SPM}}\left(\sqrt{P_0} + m\left(g_k^I(t-\tau) + jg_k^Q(t-\tau)\right)\right), && (2.7)\end{aligned}$$

where $\theta_{SPM} \approx -\frac{\gamma P_0}{\alpha}$ is the rotation of the CW pump phase under Self-Phase Modulation (SPM), assuming $e^{-\alpha L} \ll 1$.

Now, $g_k^I(t)$ and $g_k^Q(t)$ can be split into 2 terms corresponding to conjugate terms, both independent of φ, such that:

$$\begin{aligned} g_k^I(t) &= g_k^{I+}(t)e^{j\varphi} + g_k^{I-}(t)e^{-j\varphi} = \mathcal{F}^{-1}\big(G_k^{I+}(\omega)\big)e^{-j\varphi} + \mathcal{F}^{-1}\big(G_k^{I-}(\omega)\big)e^{j\varphi}, && (2.8)\\ g_k^Q(t) &= g_k^{Q+}(t)e^{j\varphi} + g_k^{Q-}(t)e^{-j\varphi} = \mathcal{F}^{-1}\big(G_k^{Q+}(\omega)\big)e^{-j\varphi} + \mathcal{F}^{-1}\big(G_k^{Q-}(\omega)\big)e^{j\varphi} && (2.9)\end{aligned}$$

where $\mathcal{F}^{-1}$ denotes the inverse Fourier transform operator.

Small perturbation theory is now utilized to give a linear relation between the terms making up the output of the fiber span $G_k^{I+}(\omega)$, $G_k^{Q+}(\omega)$, $G_k^{I-}(\omega)$, $G_k^{Q-}(\omega)$ and those of the input of the fiber span $G_{k-1}^{I+}(\omega)$, $G_{k-1}^{Q+}(\omega)$, $G_{k-1}^{I-}(\omega)$, $G_{k-1}^{Q-}(\omega)$ in the frequency domain via a *transfer matrix* $T_k(\omega)$:

$$\begin{bmatrix} G_k^{I+}(\omega) \\ G_k^{Q+}(\omega) \end{bmatrix} = T_k(\omega)\begin{bmatrix} G_{k-1}^{I+}(\omega) \\ G_{k-1}^{Q+}(\omega) \end{bmatrix}, \begin{bmatrix} G_k^{I-}(\omega) \\ G_k^{Q-}(\omega) \end{bmatrix} = T_k(\omega)\begin{bmatrix} G_{k-1}^{I-}(\omega) \\ G_{k-1}^{Q-}(\omega) \end{bmatrix}. \quad (2.10)$$

Moreover, it can be shown that [53]:

$$T_k(\omega) = \begin{bmatrix} \frac{1}{2}e^{-j\theta_{SPM}} & \frac{1}{2}e^{j\theta_{SPM}} \\ \frac{1}{2j}e^{-j\theta_{SPM}} & -\frac{1}{2j}e^{j\theta_{SPM}} \end{bmatrix} \mathcal{D}(\omega)\mathcal{M}(\omega) \begin{bmatrix} 1 & j \\ 1 & -j \end{bmatrix}, \tag{2.11}$$

where:

$$\mathcal{M}(\omega) = \begin{bmatrix} \mathcal{M}_{1,1}(\omega) & \mathcal{M}_{1,2}(\omega) \\ \mathcal{M}^*_{1,2}(\omega) & \mathcal{M}^*_{1,1}(\omega) \end{bmatrix}, \tag{2.12}$$

$$\mathcal{M}_{1,1}(\omega) = e^{-\frac{\alpha}{2}L} A_G e^{-\frac{j}{2}\beta_2 L\omega^2} \left(1 - j\frac{2\gamma P_0}{\alpha} + \frac{\gamma^2 P_0^2}{2\alpha(\alpha - j\beta_2\omega^2)} - \frac{2\gamma^2 P_0^2}{\alpha^2}\right), \tag{2.13}$$

$$\mathcal{M}_{1,2}(\omega) = e^{-\frac{\alpha}{2}L} A_G e^{-\frac{j}{2}\beta_2 L\omega^2} \left(-j\frac{\gamma P_0}{\alpha - j\beta 2\omega^2} - \frac{2\gamma^2 P_0^2}{\alpha(2\alpha - j\beta_2\omega^2)}\right). \tag{2.14}$$

The transmission matrix $\mathcal{M}$ accounts for linear and nonlinear effects during the transmission, and $\mathcal{D}$ accounts for post-dispersion compensation, if any. If no post-dispersion compensation is provided then $\mathcal{D}(\omega)$ is equal to the 2×2 identity matrix $I_{2\times 2}$; otherwise

$$\mathcal{D}(\omega) = \begin{bmatrix} e^{\frac{j}{2}\beta_2 L_d\omega^2} & 0 \\ 0 & e^{-\frac{j}{2}\beta_2 L_d\omega^2} \end{bmatrix}, \tag{2.15}$$

where L_d is the amount of compensation provided by the dispersion compensators, that is, the fiber length for which compensation is provided. If pre-dispersion compensation is used instead of post-dispersion compensation, then the order of the $\mathcal{D}$ and $\mathcal{M}$ matrices has to be reversed.

We can extend this result to the transmission through k spans:

$$\begin{bmatrix} G_k^{I+}(\omega) \\ G_k^{Q+}(\omega) \end{bmatrix} = T_k(\omega)\dots T_1(\omega) \begin{bmatrix} G_0^{I+}(\omega) \\ G_0^{Q+}(\omega) \end{bmatrix}, \tag{2.16}$$

$$\begin{bmatrix} G_k^{I-}(\omega) \\ G_k^{Q-}(\omega) \end{bmatrix} = T_k(\omega)\dots T_1(\omega) \begin{bmatrix} G_0^{I-}(\omega) \\ G_0^{Q-}(\omega) \end{bmatrix}. \tag{2.17}$$

Here, the inputs $G_0^{I+}(\omega)$, $G_0^{Q+}(\omega)$, $G_0^{I-}(\omega)$ and $G_0^{Q-}(\omega)$ are given as a function of the input pulse shape ($h(t)$) in the frequency domain $H(\omega)$ by:

$$G_0^{I+}(\omega) = \sqrt{\eta P_0}\frac{e^{-j\omega\tau}}{2}H(\omega-\omega_s), \tag{2.18}$$

$$G_0^{I-}(\omega) = \sqrt{\eta P_0}\frac{e^{-j\omega\tau}}{2}H(\omega+\omega_s), \tag{2.19}$$

$$G_0^{Q+}(\omega) = \sqrt{\eta P_0}\frac{e^{-j\omega\tau}}{2j}H(\omega-\omega_s), \tag{2.20}$$

$$G_0^{Q-}(\omega) = -\sqrt{\eta P_0}\frac{e^{-j\omega\tau}}{2j}H(\omega+\omega_s). \tag{2.21}$$

We now determine the crosstalk variance σ_{nx}^2. We denote by $f(t)$ the electrical filter impulse response and by $*$ the convolution operation. We call ρ the responsivity of the square-law detector. Since the crosstalk pulse shape after k spans can be written as:

$$g_k(t) = (g_k^{I+}(t)e^{j\varphi} + g_k^{I-}(t)e^{-j\varphi}) + j(g_k^{Q+}(t)e^{j\varphi} + g_k^{Q-}(t)e^{-j\varphi}), \tag{2.22}$$

then the current $i(t,k)$ that corresponds to the power distortion due to the presence

of crosstalk in the system is, at the output of the k^{th} span and after photodetection:

$$
\begin{aligned}
i(t,k) &= \rho f(t) * \left(\left| \sqrt{P_0} e^{jk\theta_{SPM}} + m g_k(t-\tau) \right|^2 - P_0 \right) && (2.23)\\
&= \rho f(t) * \Big(\Big| \sqrt{P_0} e^{jk\theta_{SPM}} + m \Big((g_k^{I+}(t-\tau)e^{j\varphi} + g_k^{I-}(t-\tau)e^{-j\varphi}) \\
&\qquad + j(g_k^{Q+}(t-\tau)e^{j\varphi} + g_k^{Q-}(t-\tau)e^{-j\varphi}) \Big) e^{jk\theta_{SPM}} \Big|^2 - P_0 \Big) && (2.24)\\
&= \rho f(t) * \Bigg(2\sqrt{P_0} m \left(g_k^{I+}(t-\tau)e^{j\varphi} + g_k^{I-}(t-\tau)e^{-j\varphi} \right) \\
&\qquad + \left(m \Big((g_k^{I+}(t-\tau)e^{j\varphi} + g_k^{I-}(t-\tau)e^{-j\varphi}) \Big)^2 \right. \\
&\qquad \left. + \left(m \Big((g_k^{Q+}(t-\tau)e^{j\varphi} + g_k^{Q-}(t-\tau)e^{-j\varphi}) \Big)^2 \right) \Bigg) && (2.25)\\
&\approx 2\rho\sqrt{P_0} m f(t) * \left(g_k^{I+}(t-\tau)e^{j\varphi} + g_k^{I-}(t-\tau)e^{-j\varphi} \right) && (2.26)
\end{aligned}
$$

in a first-order approximation, neglecting the squared crosstalk term and ISI between the crosstalk bits. We now take the variance of this quantity with respect to the random delay τ, phase ϕ, and bits m:

$$
\begin{aligned}
\sigma_{nx}^2(t,k) &= \mathrm{Var}_{m,\tau,\varphi}[i(t,k)] && (2.27)\\
&= E_\tau E_m E_\varphi \left[(i_k(t))^2 \right] - E_\tau E_m E_\varphi \left[i_k(t) \right]^2 && (2.28)\\
&= E_\tau E_\varphi E_m \Bigg[\Big(2\rho\sqrt{P_0} m f(t) \\
&\qquad * (g_k^{I+}(t-\tau)e^{j\varphi} + g_k^{I-}(t-\tau)e^{-j\varphi}) \Big)^2 \Bigg] && (2.29)\\
&= 2\rho^2 P_0 E_\tau E_\varphi \Big[\left(f(t) * g_k^{I+}(t-\tau) \right)^2 e^{2j\varphi} + \left(f(t) * g_k^{I-}(t-\tau) \right)^2 e^{-2j\varphi} \\
&\qquad + 2 \left(f(t) * g_k^{I+}(t-\tau) \right) \left(f(t) * g_k^{I-}(t-\tau) \right) \Big] && (2.30)\\
&= 4\rho^2 P_0 E_\tau \left[\left| f(t) * g_k^{I+}(t-\tau) \right|^2 \right], && (2.31)
\end{aligned}
$$

since $E_\varphi \left[i_k(t) \right] = 0$, using the distributions of m and φ and noticing that $g_k^{I+}(t)$ and

$g_k^{I-}(t)$ are complex conjugates. Finally, the expectation with regards to time delay τ can be computed as:

$$\sigma_{nx}^2(t,k) = 4\rho^2 P_0 \int_{-\infty}^{\infty} \frac{1}{T_b} \left| f(t) * g_k^{I+}(t-\tau) \right|^2 \mathrm{d}\tau, \tag{2.32}$$

extending the integral from $[0, T_b]$ to $[-\infty, \infty]$ to account for crosstalk ISI. Finally, at the end of the lightpath, after N_f spans:

$$\sigma_{nx}^2 = \sigma_{nx}^2(T_b/2, N_f) = 4\rho^2 P_0 \int_{-\infty}^{\infty} \frac{1}{T_b} \left| f(t) * g_{N_f}^{I+}(t) \right|^2 \mathrm{d}t. \tag{2.33}$$

This analysis can be extended to the case where the OXC adds several crosstalk signals, possibly with different attenuations and detunings. Indeed, since the crosstalk signals come from different sources, their phases, delays and bit patterns are independent and thus the variance of the overall crosstalk signal is simply obtained by adding the variances corresponding to the transmission of each crosstalk signal taken individually.

2.3.1.2 Multi-segment system

We now derive the expression for the system performance in the multi-segment case, as an extension of the single-segment case. Because the crosstalk signals added by each OXC are independent of each other and of every other crosstalk signal introduced by any other OXC, we can simply add their variances. As in the previous section, we consider the case where each OXC introduces a single crosstalk signal. We are interested in the variance of the current distortion just before the $(N_s+1)^{\text{th}}$ OXC.

We examine in turn the contribution to the current distortion variance of the crosstalk signal injected by each OXC. The crosstalk signal injected by the i^{th}

OXC travels through all of the $(N_s - i + 1)N_f$ spans between the i^{th} and the last OXC in the lightpath, so the contribution of this crosstalk signal to σ_1^2 is $4P_0\rho^2 \int_{-\infty}^{\infty} \frac{1}{T_b} \left| f(t) * g^{I+}_{(N_s-i+1)N_f}(t) \right|^2 \mathrm{d}t$. By independence of the crosstalk terms, the variance σ_{nx}^2 due to crosstalk at the end of the lightpath is given by the sum of these contributions and:

$$\sigma_{nx}^2 = \sum_{i=1}^{N_s} 4P_0\rho^2 \int_{-\infty}^{\infty} \frac{1}{T_b} \left| f(t) * g^{I+}_{(N_s-i+1)N_f}(t) \right|^2 \mathrm{d}t. \tag{2.34}$$

We can easily extend this result to the case where each OXC adds more than one crosstalk signal, possibly with different parameters such as crosstalk attenuation or detuning, considering that all crosstalk components are independent from each other (since they come from different sources).

We have presented an analytical method to compute the Q factor of a lightpath in a network subject to crosstalk; we now show that this method is less computationally expensive than simulation.

2.3.1.3 Complexity analysis

In this section, we compare the computational time complexity of our algorithm with that of the conventional method which simulate signal propagation in fiber optics.

The conventional method used to compute the Q factor of the systems of interest involves performing Monte Carlo simulations and solving the nonlinear Schrödinger equation numerically with the Split-Step Fourier method (SSF) [46]. We assume for simplicity that we want to compute the Q factor for a lightpath of N_s segments, where each segment is N_f spans long. Additionally, the SSF algorithm splits each span into N_z smaller trunks; the number of trunks is dependent on both the span length and the signal parameters. More specifically, a larger number of trunks are

Table 2.1: Complexity analysis parameters

Symbol	**Meaning**
N_s	Number of segments
N_f	Number of spans per segment
N_z	Number of trunks per span
N_r	Number of bit frames simulated
N_b	Number of bits in the bit frames
N_{spb}	Number of samples per bit

required for higher signal powers. Each bit is sampled N_{spb} times, and we simulate the transmission of N_r frames of N_b bits each; each frame has its own random crosstalk bits, phase and delay. These parameters are summarized in Table 2.1.

Consider Monte Carlo simulations first. The SSF mainly consists of FFTs, hence a complexity of $N_{spb}N_b \log(N_{spb}N_b)$ per frame. We need to perform N_r SSF per span trunk and there are $N_zN_sN_f$ span trunks in the lightpath, so the overall time complexity is in the order of $N_zN_rN_sN_fN_{spb}N_b \log(N_{spb}N_b)$.

Now consider our analytical method. Our analytical method requires to simulate the transmission of one frame through the system to estimate μ_0, μ_1, σ_0, σ_i. This is done in time $N_zN_sN_fN_{spb}N_b \log(N_{spb}N_b)$. Then, we convert the signal from time to frequency domain (complexity: $N_{spb}N_b \log(N_{spb}N_b)$). Computing each T_k matrix is done in time $N_{spb}N_b$ (we need one matrix multiplication per sample in the frequency domain), and we need N_sN_f multiplications to compute the pulse shape of the crosstalk component introduced by the first OXC, $(N_s - 1)N_f$ for the crosstalk component introduced by the second OXC, etc. Overall we need $N_s^2N_f$ matrix multiplications, which takes time $N_s^2N_fN_{spb}N_b$, to get the pulse shapes of the crosstalk signals introduced by all OXCs. Addition and integration of each of the N_s pulse shapes (Eq. 2.34) is done in time $N_sN_{spb}N_b$, which is negligible with respect to the time taken to compute the pulse shapes. Overall the crosstalk analysis time com-

Table 2.2: Baseline system parameters for the analytical method

Param--eter	**Description**	**Baseline value**	**Range tested**
N_s	Number of segments	1	1 – 4
N_f	Number of fiber spans per segment	10	3 – 12
L	Span length	100 km	
P_0	Pump power	2 mW	1 – 10 mW
T_b	Crosstalk bit duration	100 ps (10 Gbps)	2.5, 10 Gbps
m	Pulse shape parameter	3 (Super-Gaussian)	
r	Pulse shape parameter	0.46 (NRZ)	
η	Crosstalk attenuation	-30 dB	-30 – -15 dB
ω_s	Crosstalk detuning	0 GHz	0 – 8 GHz
α	Fiber loss	0.2 dB/km	
γ	Nonlinear coefficient	2.2 (W km)$^{-1}$	
D	Chromatic dispersion	17 ps/nm/km (SMF)	
L_D	Dispersion compensation length	100 km	0, 100 km
NF	Spontaneous-emission factor	0 (no noise)	0, 2
ρ	Photodetector responsitivity	1 A/W	
	Photodetector bandwidth	$0.7/T_b$	

plexity is $N_s N_f N_{spb} N_b (N_z \log(N_{spb} N_b) + N_s)$.

In practice, computing Q through analysis is several thousands times faster than through simulation, because N_r has to be large: we need values of N_r of several thousands (in the next section, we use $N_r = 2048$) to get reliable values of Q because we must average the performance over three independent random variables.

2.3.2 Validation by simulation

In this section, we seek to validate with Monte Carlo simulations our analytical approach and to determine its limits over a wide range of physical parameters.

2.3.2.1 Baseline system

We use the following numerical values for a baseline lightpath from which all of our modeled lightpaths are simulated. For all plots, one or two parameters are varied, leaving the others as described here. These parameters are chosen to model large-scale metropolitan to continental networks. The lightpath consists of a single segment of 10 spans of SMF (single mode fiber, $D = -\beta_2\nu^2/(2\pi c) = 17$ ps/nm/km) with nonlinear coefficient $\gamma = 2.2$ W^{-1}km^{-1}. Each span is 100 km long. Amplifiers compensate exactly for the fiber loss (0.2 dB/km) and do not introduce any noise. Post-dispersion compensation is provided after each span and is assumed to compensate exactly for the SMF dispersion. The length of the dispersion compensating fibers is neglected. The peak power of the transmitted signal with no crosstalk is $P_0 = 2$ mW and the power attenuation of the unique crosstalk signal introduced by the first OXC is -30 dB. Main signal and crosstalk are a frame of NRZ super-Gaussian pulses not detuned from the main signal (f_s=$\omega_s/(2\pi) = 0$ GHz). These parameters are summarized in Table 2.2. In each Monte Carlo simulation, we transmit 2048 frames of 16 pulses, varying the phase and delay between the frames, to ensure tight confidence intervals on the Q factor (confidence interval tighter than 0.2 for $Q \approx 6$). For the analytical approach, we simulate the transmission of a single frame of 16 bits to estimate μ_1, μ_0, σ_0, σ_i. In each of the following plots, plain lines are obtained using the analytical model and dotted lines come from simulations.

In the systems we simulate, the main signal is modulated and its peak power varies slightly with the transmission distance. To account for this variation in the estimation of σ_{nx}, we replace P_0 in (2.33) by the value of μ_1 obtained from this short

simulation, such that:

$$\sigma_{nx}^2 = 4\mu_1\rho^2 \int_{-\infty}^{\infty} \frac{1}{T_b} \left| f(t) * g_{N_f}^{I+}(t) \right|^2 \mathrm{d}t. \tag{2.35}$$

Our analysis does not rely on a specific pulse shape for the input signal; however our numerical results assume Super-Gaussian pulse shaping [46], i.e.,

$$h(t) = \exp\left(-\frac{1}{2} \left(r \frac{t}{T_b} \right)^{2m} \right), \tag{2.36}$$

where T_b is the crosstalk bit duration, or, equivalently, the inverse of the system bitrate, and m and r are pulse shaping parameters.

2.3.2.2 Effects of fiber and crosstalk parameters

In the first simulation, we seek to verify that the CW assumption and the transmission effects on the main signal (accounted for by σ_i^2), the noise (accounted for by σ_n^2) and the impairment due to crosstalk (accounted for by σ_{nx}^2) are independent, such that:

$$\sigma_1^2 = \sigma_i^2 + \sigma_n^2 + \sigma_{nx}^2. \tag{2.37}$$

We also verify that simulating the propagation of a single frame is enough to estimate μ_1, μ_0, σ_0 and σ_i.

First consider Fig. 2.2(a), where the variances for transmission effects on the main signal, noise, and crosstalk, are plotted at the output of each span of our baseline network. For this case we consider that the optical amplifier after each span injects noise in the network. The analytical curves for crosstalk was obtained using the results of Section 2.3.1. The analytical curve for σ_n^2 was obtained using [53]. The "analytical" curve for σ_i^2 is actually the estimate obtained by a single-frame transmission simula-

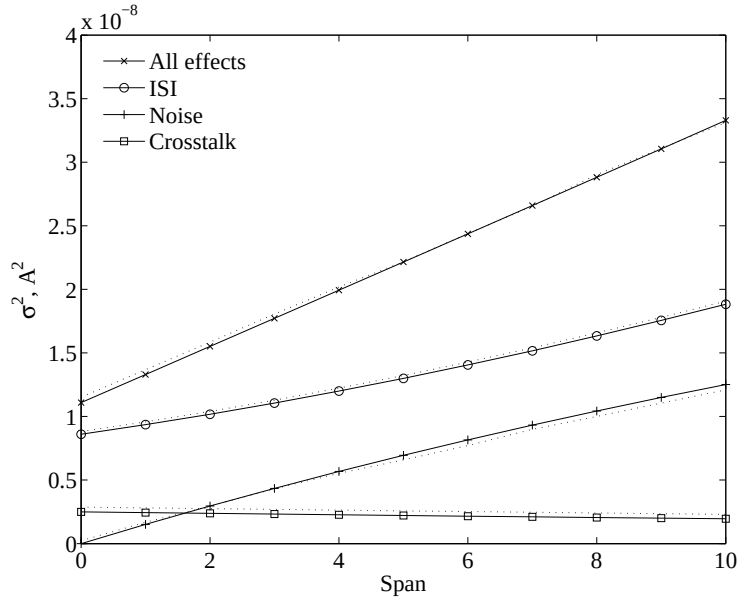

(a) Variance

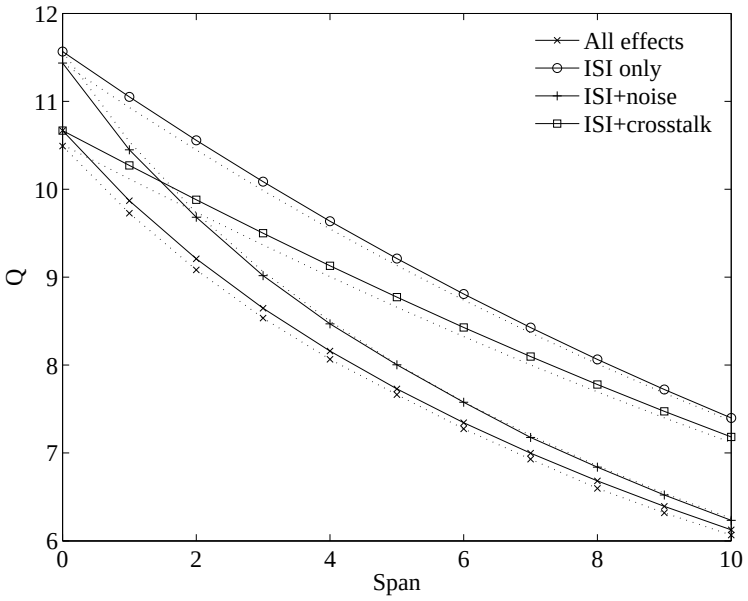

(b) Q factor

Figure 2.2: Details of the impact of each impairment on a 10 GHz dispersion-compensated system (noise, ISI, crosstalk).

tion. The analytical curve for all effects combined (σ_1^2) was obtained by summing up the variances σ_i^2, σ_n^2, σ_{nx}^2. The simulation curve for σ_1^2 was obtained by full-length Monte-Carlo simulation including random crosstalk and noise. We then ran three additional Monte-Carlo simulation: one with no crosstalk and no noise (from which we obtained the plot for σ_i^2), one with crosstalk but no noise, and one with noise but no crosstalk to deduce the plots for σ_{nx}^2 and σ_n^2.

The simulation (dotted) and analytical (plain) plots agree very well, after each span, for all the cases we consider — noise only, crosstalk only, transmission effects only, and all effects combined. For these parameters, σ_{nx}^2 from (2.35) slightly underestimates the crosstalk variance. In this dispersion compensated network, all effects have the same order of magnitude, although we consider only a single crosstalk component. It is easy to see that crosstalk can dominate after transmission through only a few OXCs. Also, in this case, crosstalk variance tends to decrease with the transmission distance, thereby alleviating the impact of crosstalk as compared with other transmission impairments. This is caused by the tight electrical filter that removes part of the crosstalk spectrally spread by the fiber nonlinearity.

In Fig. 2.2(b), we provide the Q factors for the ISI only, ISI+noise, ISI+crosstalk, and ISI+noise+crosstalk cases. Since the values for μ_1, μ_0 and σ_0 are dependent on the transmission length, Q accounts for transmission effects better than σ_1 only. Again, very good agreement is found between simulation and our analytical results. For the single crosstalk component case which is considered in this work, it is known that the Gaussian approximation is not accurate and overestimates the crosstalk variance and hence underestimates Q [47]. Nevertheless, since our technique is valid for any number of crosstalk components, obtaining accurate values for the Q factor for only one crosstalk signal ensures the attainment of accurate values of Q and thus of the BER with our technique in more realistic multi-crosstalk signals cases.

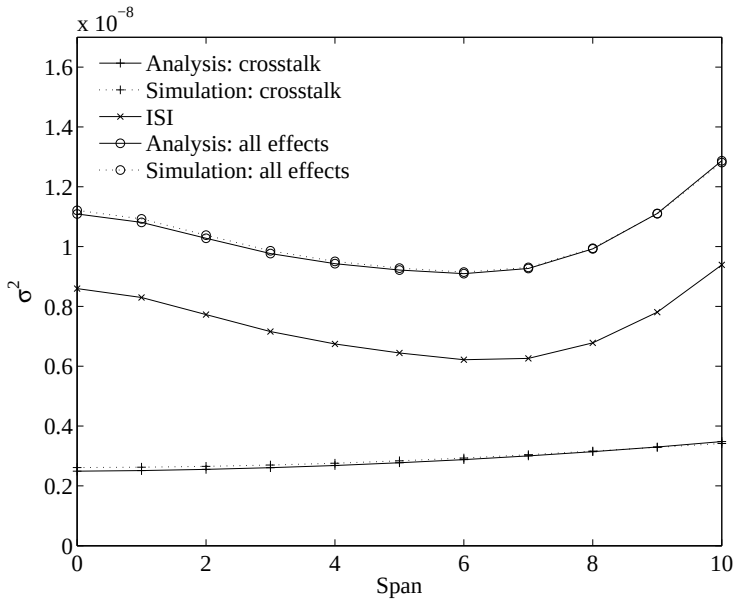

(a) Variance

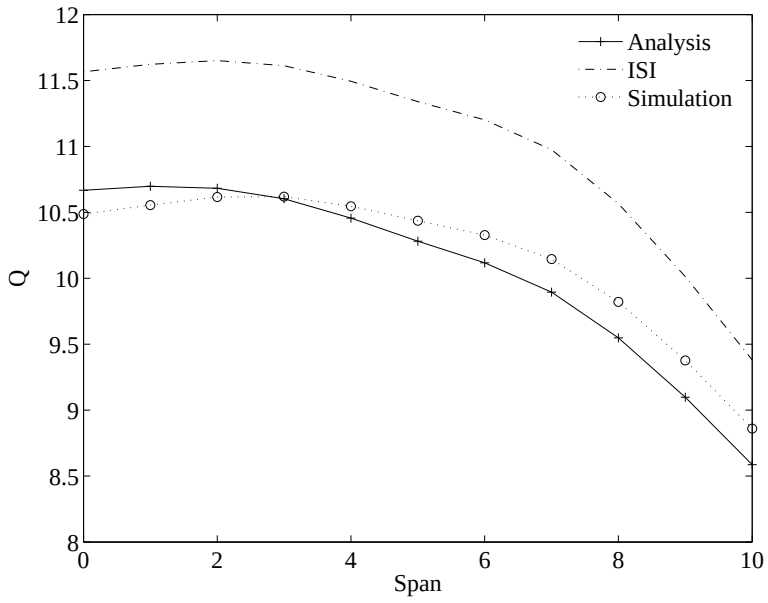

(b) Q factor

Figure 2.3: Details of the impact of ISI and crosstalk on a 2.5 Gbps system.

In the following plots, we show that our technique holds for wide ranges of system parameters. In Figs. 2.3(a) and 2.3(b), we provide data for a 2.5 Gbps network with no dispersion compensation and no noise. In this case, the crosstalk is enhanced by the propagation through nonlinear fiber.

An important attribute of our analytical method is the inclusion of the potential detuning f_s of the crosstalk signal with respect to the main signal power. Consider Figs. 2.4(a) and 2.4(b), where signal variances and Q, respectively, are plotted as a function of the detuning at several points in the network. We notice that Q is actually strongly dependent on the detuning, with higher values corresponding to higher detunings. This is expected because the electrical filter tends to attenuate detuned crosstalk. Other system parameters (square pulse shape, NZ-DSF fiber, high power) can lead to modulation instability at non-zero detuning levels [10,11,45]; our system, which uses SMF fiber and Gaussian pulse shapes, does not exhibit this nonlinear phenomenon. Our model predicts the network performance well for the whole range of detunings. We did not consider higher detunings as highly detuned crosstalk can be filtered out.

In Figs. 2.5(a), 2.5(b), 2.6(a) and 2.6(b), we show that our technique is still valid for practical ranges of main signal powers and crosstalk attenuations despite the small signal approximation. We tested the analytical technique for main signal peak powers up to 10 mW; at such powers, nonlinear effects on the main signal dominate over crosstalk effects and the Q factor decreases below 6 after just a few spans. For lower powers, crosstalk is an important impairment and our analysis predicts the correct values for Q. Similarly, we accurately predict Q for crosstalk attenuation up to -20 dB; if the crosstalk is stronger (e.g., -15 dB), our approximations become inaccurate, but as seen on Fig. 2.6(b), such situations not of practical interest as the Q factor is below 6 as early as the input of the first span (span "0", just after the first OXC).

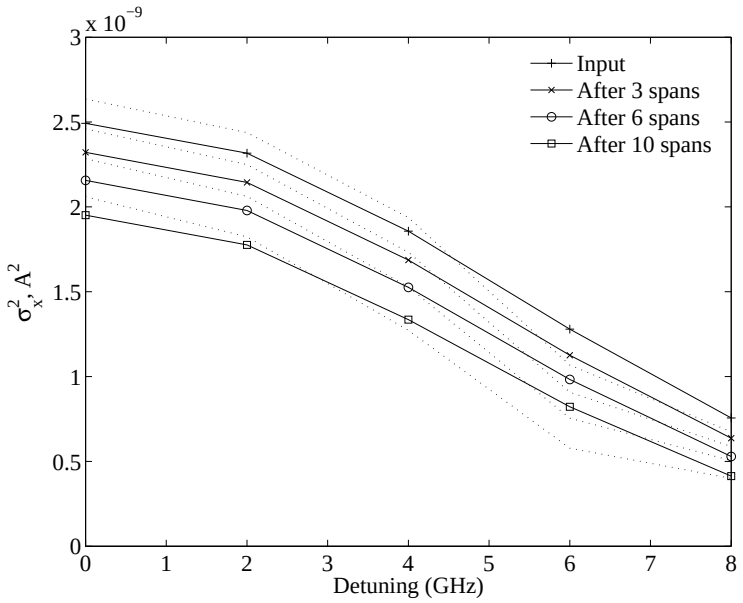

(a) Variance

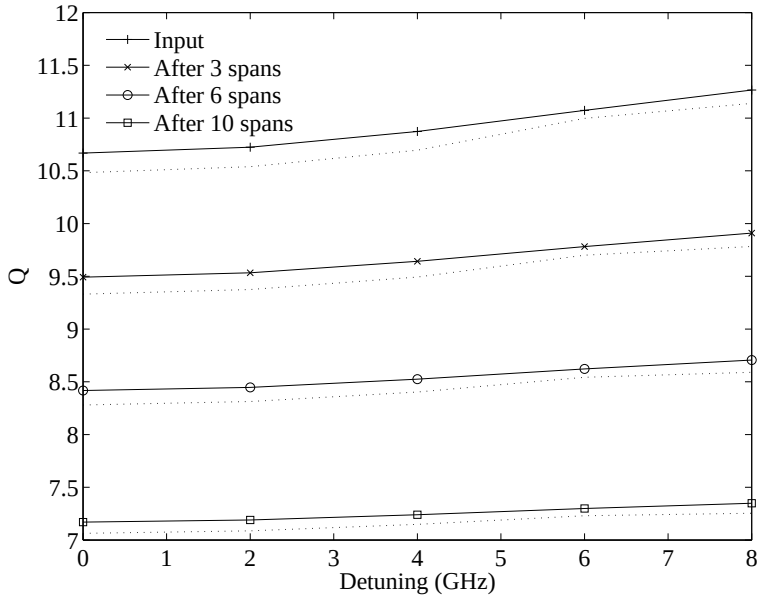

(b) Q factor

Figure 2.4: Impact of detuning.

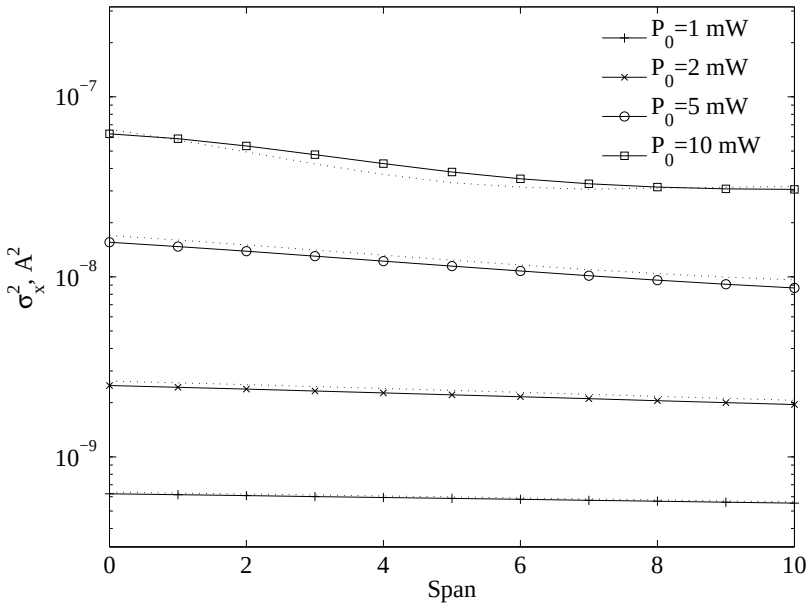

(a) Variance

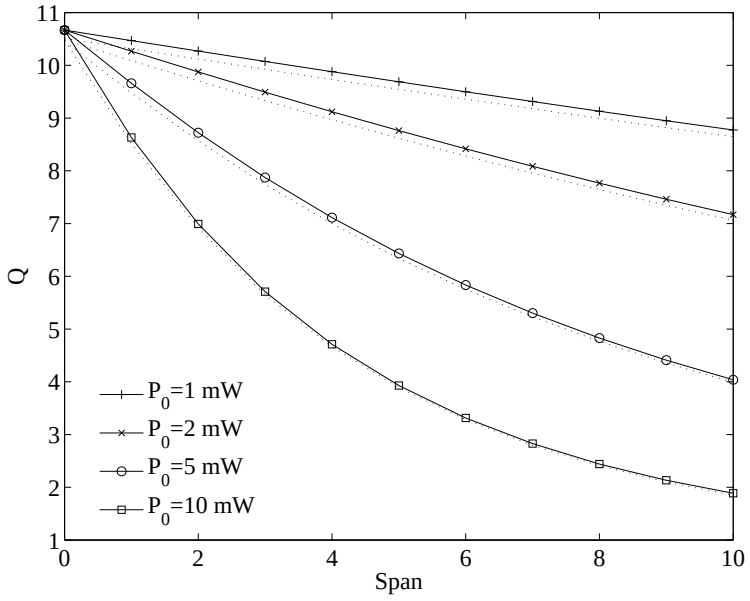

(b) Q factor

Figure 2.5: Impact of the main signal peak power.

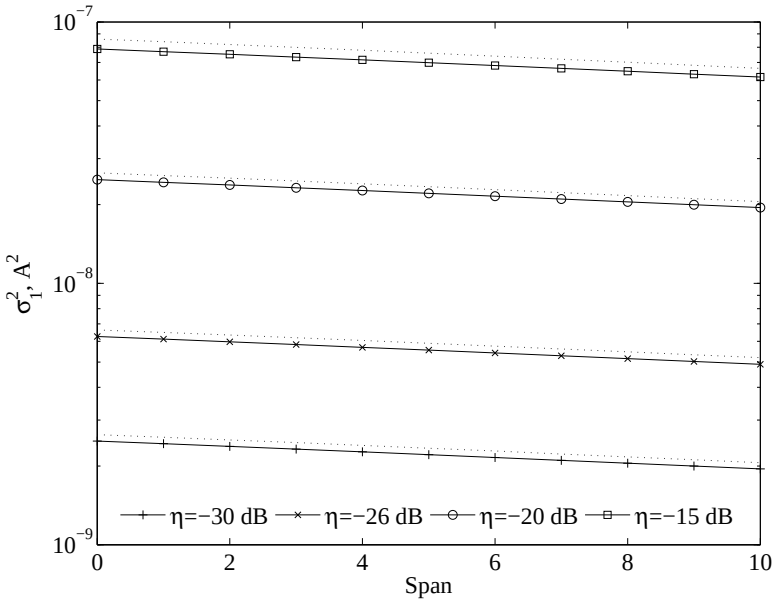

(a) Variance

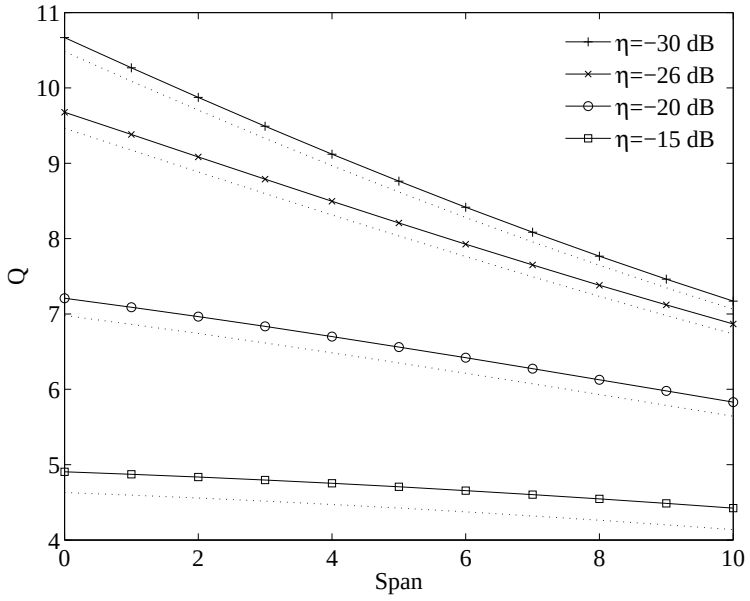

(b) Q factor

Figure 2.6: Impact of the crosstalk attenuation.

2.3.2.3 Effects of Network Topology

In this section, we consider a tandem network of several segments with total length fixed to 1200 km. Again, each OXC inserts a single crosstalk component and noise impact is ignored. We study the OXC insertion penalty on Q in the lightpath. The following topologies are considered: a single segment of 12 spans (1x12 spans), 2 segments of 6 spans each (2x6 spans), and 3 segments of 4 spans each (3x4 spans).

As shown in Figs. 2.7(a) and 2.7(b), the insertion of an OXC is clearly visible for each topology and results in a sharp drop in the Q factor. The drop in Q is more pronounced after the first OXCs than after the last OXCs, because the marginal effect of adding one crosstalk term is largest at the beginning of the fiber. Again, our analytical model predicts the performance of such networks accurately.

2.4 Semi-analytical method for RZ signals

The CW assumption models accurately networks with NRZ signaling, as was seen in the previous section. However, the CW assumption is not applicable to RZ signaling, which is is becoming popular in optical networks [54]. In this section, we extend the analytical method presented in the previous section to RZ signals, at the cost of a moderate increase in complexity.

2.4.1 Semi-analytical evaluation of crosstalk impact

We can compute the sample means μ_0, μ_1 and the variances σ_0^2 and σ_{ISI}^2 by simulating the transmission of a small number of bits forming, for instance, a de Bruijn sequence of length 32 [55], using the standard Split-Step Fourier method [56]. In any such

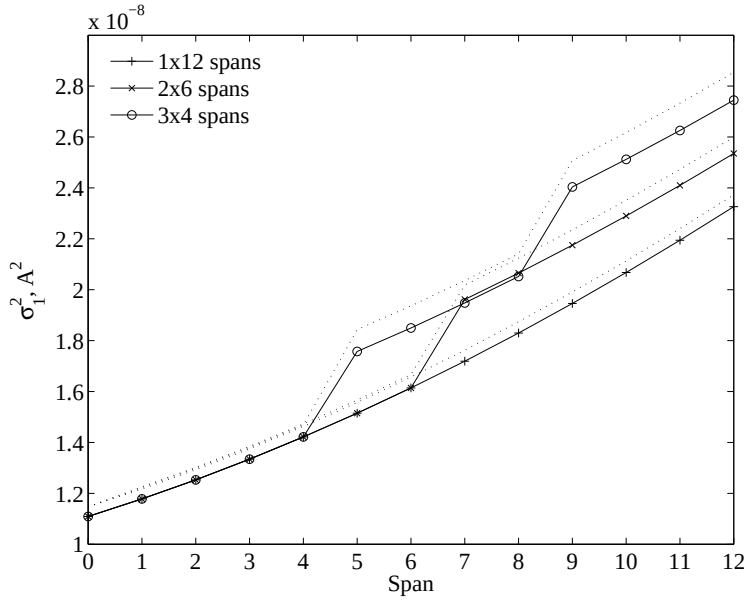

(a) Variance

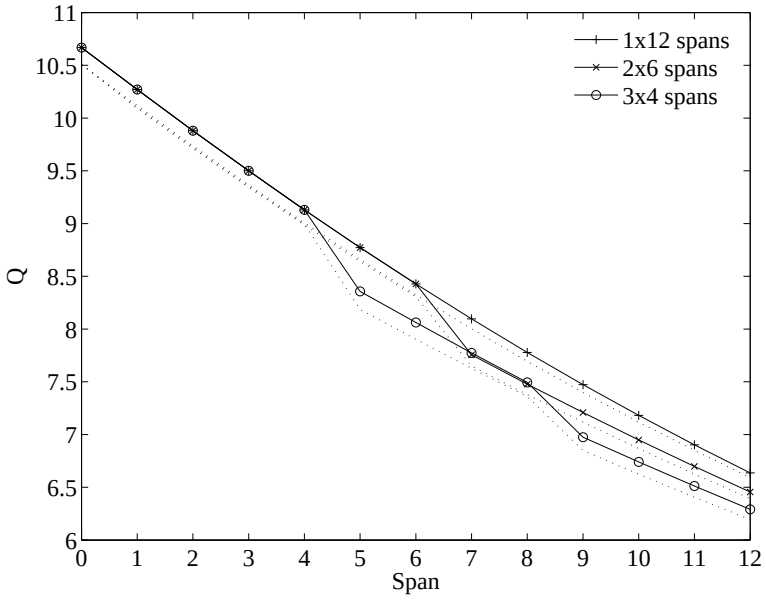

(b) Q factor

Figure 2.7: Impact of the network topology.

sequence, one of the bits is an isolated "1", which is assumed to be ISI-free. We use that bit as a reference bit (ISI and crosstalk-free) to identify the effect of crosstalk.

Computing σ_{nx}^2 using Monte Carlo simulations is time consuming because of the number of parameters involved (random delay, phase, bits); here, we seek to reduce the amount of simulations required to determine σ_{nx}^2. Using a fully analytical model assuming a CW pump for the main signal, we derived in Section 2.3.1 an expression for the output pulse shape of a crosstalk bit and then obtained σ_{nx}^2 from it. With a modulated main signal however, the output crosstalk pulse shape depends on the delay τ. Indeed, intuitively, a crosstalk pulse with delay $\tau = 0$ (i.e., when most of the crosstalk power resides at the time where the main signal power at its peak value) is more affected by fiber nonlinearity than a crosstalk pulse with delay $\tau = T_b/2$ (when most of the crosstalk power resides at the time when the main signal power is close to 0). To overcome this issue, we need to consider the transmission of more than a single bit to derive the crosstalk bit pulse shape and hence σ_{nx}^2.

Let $g_{\tau,\varphi}(t)$ be the complex envelope of the optical field at the output of the fiber (before the receiver) of a crosstalk pulse launched with delay τ and phase φ into the fiber; let $\sqrt{P(t)}\exp(j\theta(t))$ be that of a signal pulse with no crosstalk added. We also denote by $m \in \{0, 1\}$ the value of the crosstalk bit. Here, we neglect ISI between the main signal bits (ISI is accounted for by σ_{ISI}^2) and study the transmission of a single signal pulse corrupted by crosstalk such that the complex envelope $s_{out}(t)$ of the signal before the receiver is:

$$s_{out}(t) = \sqrt{P(t)}\exp(j\theta(t)) + m g_{\tau,\varphi}(t). \tag{2.38}$$

Splitting the output crosstalk pulse shape into in-phase ($g_{\tau,\varphi}^I(t)$) and quadrature

$(g^{Q}_{\tau,\varphi}(t))$ components with respect to the main signal phase $\theta(t)$, we obtain:

$$s_{out}(t) = \exp\left(j\theta(t)\right)\left(\sqrt{P(t)} + m\left(g^{I}_{\tau,\varphi}(t) + jg^{Q}_{\tau,\varphi}(t)\right)\right) \tag{2.39}$$

and then, projecting each component on $(\exp(j\varphi), \exp(-j\varphi))$, we have:

$$\begin{aligned} s_{out}(t) &= \exp\left(j\theta(t)\right)\Big(\sqrt{P(t)} + m\left(g^{I+}_{\tau}(t)\exp(j\varphi) + g^{I-}_{\tau}(t)\exp(-j\varphi)\right. \\ &\quad \left. + jg^{Q+}_{\tau}(t)\exp(j\varphi) + jg^{Q-}_{\tau}(t)\exp(-j\varphi)\right)\Big). \end{aligned} \tag{2.40}$$

We denote by $f(t)$ the electrical filter impulse response and by $*$ the convolution operation. We call ρ the responsivity of the square-law detector. The current due to crosstalk is:

$$\begin{aligned} i(t) &= \rho f(t) * \left(\left|\sqrt{P(t)}\exp\left(j\theta(t)\right) + mg_{\tau,\varphi}(t)\right|^2 - P(t)\right) \\ &\approx \rho f(t) * \left(2\sqrt{P(t)}m\left(g^{I+}_{\tau}(t)\exp(j\varphi) + g^{I-}_{\tau}(t)\exp(-j\varphi)\right)\right) \end{aligned} \tag{2.41}$$

Averaging over the signal and crosstalk bits and the phase φ, and since $E_{\varphi}[\exp(j\varphi)] = 0$, the variance of $i(t)$ becomes:

$$\sigma^2_{nx}(t) = 4\int_{-\frac{T_b}{2}}^{\frac{T_b}{2}} \frac{\rho^2}{T_b}\left|f(t) * \left(\sqrt{P(t)}g^{I+}_{\tau}(t)\right)\right|^2 \mathrm{d}\tau. \tag{2.42}$$

At the sampling time $t = T_b/2$, the crosstalk variance is $\sigma^2_{nx} = \sigma^2_{nx}(T_b/2)$. Therefore, to compute σ_{nx}, we need to know $\left(f(t) * g^{I+}_{\tau}(t)\right)\big|_{t=T_b/2}$ for all values of τ.

The proposed semi-analytic method uses a short simulation to find an estimate $\hat{g}^{I+}_{\tau}(t)$ of $g^{I+}_{\tau}(t)$ for all τ. Consider the pulse trains depicted in Fig. 2.8, showing 4-bit long (0,0,1,0) signal pulse sequences. We surround a single 'one' bit by 'zero'

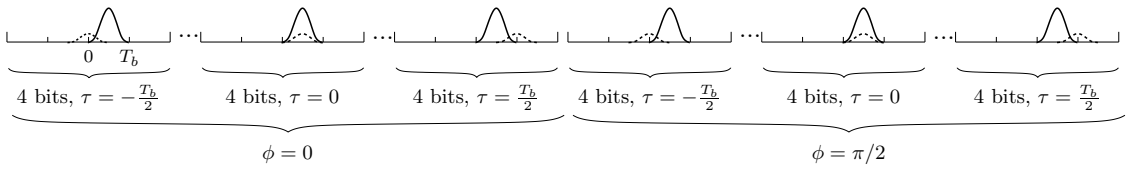

Figure 2.8: Transmitted signal in the simulation part of the semi-analytical method. Plain line: main signal; dashed line: crosstalk signal (amplitude vs. time). The transmitted signal is the sum of these two signals, and we perform a simulation for each of $\phi = 0$ and $\phi = \pi/2$.

bits to isolate the crosstalk effect from the ISI effect. We add a crosstalk pulse to this 4-bit sequence, with variable delay, and phase $\phi = 0$ with respect to the main pulse; if we use N discrete samples per bit for our simulations, then we generate N 4-bit sequences, each with a different delay of $-N/2$ to $N/2 - 1$ samples between the crosstalk pulse and the main pulse. Then, we generate another set of $4N$ bits changing the phase between main pulses and crosstalk pulses to $\phi = \pi/2$. This yields a total of $8N$ pulses to be simulated through the fiber lightpath. Before the receiver, we obtain $2N$ signals, each representing an aggregated 4 bit-long sequence,

$$s^{out}_{k,\phi}(t) \approx \sqrt{P(t)} \exp j\theta(t) + g_{\tau_k,\phi}(t) \tag{2.43}$$

with $\tau_k = kT_b/N$ ($k \in \{-N/2, \cdots, N/2 - 1\}$) and $\phi \in \{0, \pi/2\}$.

Due to the crosstalk detuning ω_s, a time *walk-off* appears between the crosstalk and the main signal. In real systems, the crosstalk bit may move by more than a bit period and interfere with other main pulses — a behavior we cannot capture by simulating short, 4-bit long time frames. To cancel this simulation artifact and account for walk-off, we shift the crosstalk pulse shape after each span by the amount of walk-off $t_{wo} = \beta_2 \omega_s L$, where β_2 is the second-order linear dispersion and L is the fiber span length [57].

Now, in order to determine $g_{\tau_k}(t)$ for all τ_k, we subtract from each $s^{out}_{k,\phi}(t)$ the pulse shape of a crosstalk-free and ISI-free bit. Denoting by $\Re\{z\}$ the real part of a complex number z, and using (2.40) with $\varphi = 0$ and $\varphi = \pi/2$, we obtain estimates of $g^{I+}_{\tau_k}(t)$ for all N values of τ_k:

$$\begin{aligned}\hat{g}^{I+}_{\tau_k}(t) &= \frac{1}{2}\Re\left\{\exp\left(-j\theta(t)\right)(s^{out}_{k,0}(t) - \sqrt{P(t)}\exp j\theta(t))\right\} \\ &\quad -\frac{j}{2}\Re\left\{\exp\left(-j\theta(t)\right)(s^{out}_{k,\frac{\pi}{2}}(t) - \sqrt{P(t)}\exp j\theta(t))\right\}. \qquad (2.44)\end{aligned}$$

We obtain an estimate of the power variance using (2.42) for $t = T_b/2$:

$$\hat{\sigma}^2_{nx} = \left(\frac{\rho^2}{N}\sum_{k=-N/2}^{N/2-1} 4\left|f(t) * \left(\sqrt{P(t)}\hat{g}^{I+}_{\tau_k}(t)\right)\right|^2\right)\Bigg|_{t=T_b/2}. \qquad (2.45)$$

This variance can now be used in the Q factor equation to estimate BERs.

2.4.2 Validation by simulation of the semi-analytical technique

In this section, we validate our new semi-analytical method through simulation. In each of the following plots, plain lines are obtained using the semi-analytical model and dotted lines come from simulations. Unless otherwise stated, the baseline system we study is made of 50 km-long spans of standard NZ-DSF; the input signal is a train of 10 Gbps Gaussian RZ pulses with a peak power of 2 mW at the input corrupted by 0-detuned, -30 dB attenuated crosstalk. The electrical filter bandwidth is 7 GHz and the detector responsivity is arbitrarily set to 1 A/W. All other parameters are the same as in Table 2.2.

First, in Fig. 2.9, we show how our method accounts for both ISI and crosstalk

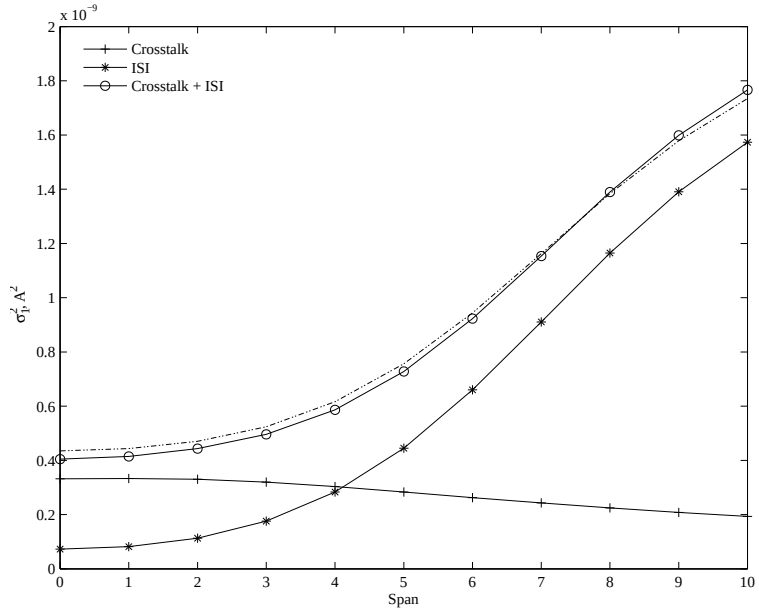

Figure 2.9: Power variance for crosstalk and ISI for different values of the propagation distance.

variations. Crosstalk impairment dominates until the fourth span and decreases slightly, while ISI increases early in the lightpath. The semi-analytical method is able to predict accurately the variance σ_1^2 for both ISI and crosstalk dominated cases.

Then, in Fig. 2.10, we vary the input peak power between 1 and 10 mW. Higher power leads to increased non-linear effects and the higher order terms that we have neglected in the analysis become larger. However, we find good agreement between the semi-analytical method and simulation for powers up to 5 mW. As in Section 2.3.2.2, we observe a discrepancy between our model and the simulation for 10 mW signals, which are impractical for proper network operation.

Last, in Fig. 2.11, we investigate the impact of crosstalk detuning on system performance; for this configuration, we observe that detuned crosstalk has a lower impact than non-detuned crosstalk on the system performance, which can be explained by the removal of part of the crosstalk frequency spectrum by the narrow

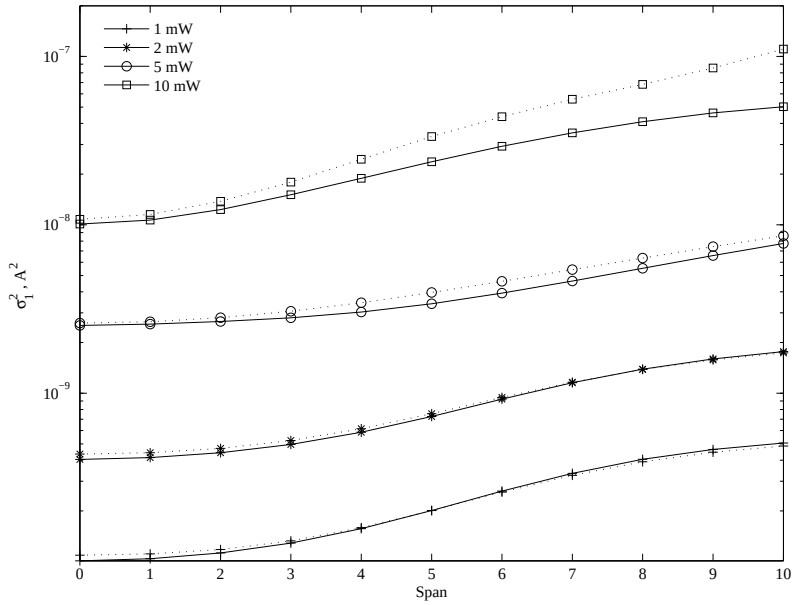

Figure 2.10: Power variance as a function of the propagation distance for different input powers.

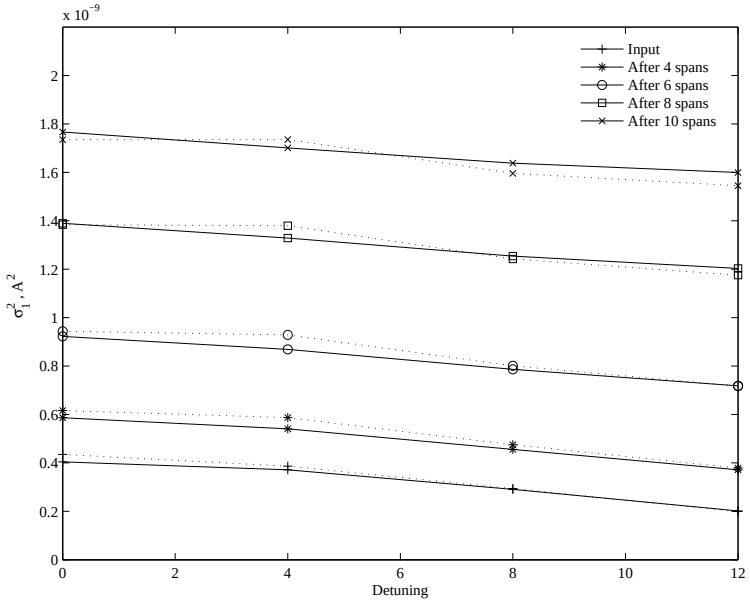

Figure 2.11: Power variance as a function of the crosstalk detuning f_s for different values of the propagation distance.

electrical filter. Nevertheless, system performance exhibits a dependence on the detuning, which should therefore be accounted for when designing all-optical networks. Again, our semi-analytical method predicts the power variance well for the detuning levels tested, but divergence appears near the end of the lightpath when the detuning, and hence the walk-off, is large. This is because our walk-off compensation method is actually a one-shot correction to model the crosstalk bit transmission in the fiber; in the real system, walk-off would occur and a crosstalk bit could be enhanced by several different main signal bits if the walk-off becomes larger than T_b. We do not account for this effect in this semi-analytical method. However, the 4-GHz detuned crosstalk case is practically out-of-band and the walk-off effect is typically mitigated by the utilization of low-dispersive fibers or dispersion compensation, which is not included in Fig. 2.11, and we are able to predict σ_1^2 for large metropolitan networks.

This semi-analytical method is faster than performing full simulations. The full simulation requires transmitting 32768 bits because 1024 sets of random values of φ and τ are needed to obtain a value of the Q factor within a tight confidence interval. With the semi-analytical method, we only need to simulate the transmission of $32+8N$ bits (the value of N is typically 16 to 64) to account for both ISI and delay randomness, hence a speedup on the order of 2 orders of magnitude, to be compared with a speedup of 3 orders of magnitude if we use the CW assumption.

2.5 Summary

In this chapter, we developed fast and accurate perturbation theory models for in-band crosstalk penalty by propagation through non-linear fiber. Our models holds for wide physical parameter ranges: power, crosstalk detuning and attenuation, presence of noise, network length and topology, presence of dispersion compensators, pulse

shape. Model failure occurred only for extreme parameter values, which would not be used in real networks. Both OXC insertion and transmission effects have a strong negative impact on the Q factor, and neither can be overlooked when designing long-haul or even metropolitan networks.

Only crosstalk effects have been accounted for, neglecting all other physical effects (insertion losses, inter-channel effects, PMD) to focus on the performance degradation due to crosstalk. However, other effects can be included in our analysis, for instance modeling those as additional variance terms as we have done for noise. A direct application of our work is the inclusion of crosstalk impairments in routing and wavelength assignment problems, which is the topic of the next two chapters of this dissertation.

Chapter 3

Cross-Layer Adaptive Routing and Wavelength Assignment in All-Optical Networks

In WDM all-optical networks where electrical regeneration is not available, physical impairments due to propagation in the fibers, amplifier noise, leaks between channels (interchannel crosstalk) and in the switches (node crosstalk, which we studied in Chapter 2) cannot be removed at the physical layer. These effects may cause calls (especially between physically distant nodes) to be rejected because they cannot meet minimum Quality of Service (QoS) requirements, as measured by signal bit-error rates. It is possible to mitigate physical layer effects at the network layer using appropriate Routing and Wavelength Assignment (RWA) algorithms. We present new RWA algorithms which account for physical impairments in their design and increase QoS and fairness among users without sacrificing low blocking probabilities in metropolitan-sized networks. We also present RWA algorithms that can sharply decrease blocking probabilities in regional-sized networks using optional channel coding. All algorithms are evaluated through simulation in realistic scenarios and shown

to successfully mitigate physical layer effects and to perform better in terms of QoS and network access fairness than traditional algorithms. Parts of this chapter were published in [58, 59, 60].

3.1 Introduction

In this chapter, we present four new RWA algorithms (SP2, HQ, MMQ, MMQ2) that belong to the class of *adaptive* RWA algorithms [34], which are known to perform well in terms of blocking probabilities. The new RWA algorithms are QoS-aware in the sense that they ensure (during admission control) that all lightpaths in the network meet a QoS (BER) constraint without disrupting previously established lightpaths, and that they explicitly account for QoS when determining which lightpath a call should use. Furthermore, SP2 and MMQ2 implement the so-called *protecting threshold* technique described in [36] where short lightpaths are not established when free wavelengths are sparse, to keep more resources for longer lightpaths and hence enhancing fairness in the network. We evaluate our new QoS-aware algorithms against the traditional SP (Shortest Path) algorithm on a realistic large metropolitan-sized network and show gains in performance in terms of average call BER and fairness, without sacrificing low blocking probability.

The algorithms discussed above are able to mitigate physical layer effects. However, in the case of larger networks where some node pairs have no viable paths satisfying QoS even with just ISI and accumulated noise, none of the algorithms discussed above is able to establish lightpaths for these pairs. This leads to high blocking probability and low fairness. In [61], a new class of RWA algorithms was proposed to address this issue. These algorithms implement optional coding: they try to establish several lightpaths for calls that would otherwise violate the QoS con-

straint; coding is used on each of these lightpaths. By using coding only on the lightpaths that require it, we minimize the amount of coding to be performed by the system. In this dissertation, we evaluate RWA with optional coding in scenarios with crosstalk impairments in addition to ISI and noise only, for BER and fairness in addition to blocking probability. We show using simulations over a regional-sized network that our algorithms with optional coding decrease average call blocking probability, reduce crosstalk impact on call blocking probability, decrease average BER and improve fairness compared with the similar RWA algorithm with no optional coding capability.

This chapter is organized as follows: in Section 3.2, we present the assumptions concerning the physical layer and network modeling. In Section 3.3, we present fair QoS-aware adaptive RWA algorithms and evaluate them through simulation on a metropolitan-sized network. In Section 3.4, we present a QoS-aware adaptive RWA algorithm with optional coding, and evaluate it through simulation on a regional-sized network.

3.2 Assumptions and system description

We now state our assumptions concerning the modeled network. We consider a network of bidirectional links with C equally spaced wavelengths in each direction. Although all-optical wavelength conversion is the subject of much current research, the technology is not yet mature for deployment in the near future and thus we assume that wavelength conversion is not available. Calls are assumed to arrive in the network according to a Poisson process with average arrival rate Λ and the call durations are assumed to follow an exponential distribution with unit mean, such that Λ is the *total offered load* of the network in Erlangs. Call sources and destinations

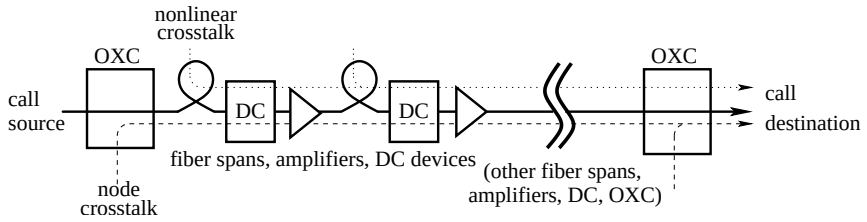

Figure 3.1: Model of a transmission lightpath (plain line) used to compute the Q factor. Each OXC can inject one or more node crosstalk components (dashed lines), and nonlinear crosstalk can originate from each span (dotted lines).

are uniformly distributed over the set of network nodes.

When a call is accepted in the network, it is assigned one (Section 3.3) or potentially several (Section 3.4) *lightpaths* by a network management system, which can be centralized or distributed[1]; a lightpath is the combination of a wavelength and a sequence of nodes and links called *route* or *path*. As in Section 2.2, the links physically consist of one or several *spans*; each span in turn consists of single mode fiber, a dispersion compensation (DC) device that compensates for the fiber chromatic dispersion, and an amplifier that compensates for the fiber linear attenuation. The receiver is modeled by a wideband optical filter (for demultiplexing purposes), followed by a photodetector per channel (a square-law device, a time sampler and a narrow electrical filter). A sample lightpath is shown in Fig. 3.1.

Because of the physical impairments sustained by signals during their transmission on a lightpath, a signal may be too degraded at reception to ensure a minimal QoS as defined by the network administrator. We measure QoS via signals BER which is related to the Q factor defined in Section 2.2.

In this chapter, we account for four of the main physical impairments which are known to affect lightpaths in all-optical networks [62]: intersymbol interference, amplifier noise, nonlinear crosstalk, and node crosstalk. Each of these effects is

[1]In the distributed case, each node needs to know at all times what calls are established in the network, in order to be able to compute Q factors when a new call arrives.

accounted for as a noise variance in the Q factor of the lightpath, that is, for a given lightpath:

$$Q = \frac{\mu_1 - \mu_0}{\sigma_0 + \sqrt{\sigma_i^2 + \sigma_n^2 + \sigma_{nlx}^2 + \sigma_{nx}^2}} \tag{3.1}$$

where σ_i^2, σ_n^2, σ_{nlx}^2 and σ_{nx}^2 are the variance contributions due to intersymbol interference, amplifier noise, nonlinear crosstalk and node crosstalk (which we studied under the name "crosstalk" in Chapter 2), respectively. As in Section 2.2, assuming a good extinction ratio, we can ignore the interference contributions (noise, nonlinear crosstalk, node crosstalk) to $(\mu_1 - \mu_0)$ and σ_0. We detail in Appendix A how to estimate each of the quantities in (3.1) using precomputed tables.

First, ISI is a single-channel effect that results from chromatic dispersion, SPM, and filtering at the receiver; ISI depends on the lightpath topology only: span lengths, amplifier and dispersion compensation devices placement, fiber and receiver physical characteristics; ISI is independent of the network state.

Second, amplifier noise is injected by each amplifier on the path and is due to the so-called Amplified Spontaneous Emission (ASE) phenomenon. Amplifier noise also depends on the lightpath topology only, and is independent of the network state.

Third, nonlinear crosstalk occurs when two (in the case of XPM) or three or four (in the case of FWM) signals propagate on different channels in the same fiber span. Signal co-propagation in optical fiber results in energy transfers between the signals resulting in impairments similar to noise. These nonlinear effects are stronger when the participating signals are on closer channels and when channel separation is tighter as is the case with DWDM systems [63]. Since nonlinear crosstalk is due to the interaction between several signals in the network, it is a network status-dependent impairment that cannot be precomputed. It is possible to compute σ_{nlx} accounting for all nonlinear crosstalk components on a lightpath by summing the

variance contributions for each nonlinear crosstalk: $\sigma^2_{nlx} = \sum_p \sigma^2_{nlx_p}$ where the sum is taken over all nonlinear interchannel interferences between any existing lightpath in the network and the considered lightpath. More details on the related computations for the variances $\sigma^2_{nlx_p}$ are provided in Appendix A.

Fourth, node crosstalk originates from signal leaks in the OXCs, either at the demultiplexing stage or inside the switching fabric. The model for the origin of node crosstalk we use here was first detailed in [8], and we restate it here for clarity. It is compatible with the model we adopted in Chapter 2, which makes no assumption regarding the origin of node crosstalk; the different types of node crosstalk we present here correspond to different values for the η attenuation parameter introduced in Chapter 2. The three types of node crosstalk we consider in this chapter are depicted in Fig. 3.2.

The first type of node crosstalk (Fig. 3.2(a)) is called co-wavelength crosstalk and comes from leaks within the switching fabric. Two lightpaths LP_1 and LP_2 enter the OXC on the same wavelength but by different input ports; because of imperfection in the switching fabric, a small part of LP_1 is leaked on LP_2 and a small part of LP_2 is leaked on LP_1. The associated crosstalk attenuation η for co-wavelength crosstalk is called "switching fabric attenuation".

The second type of node crosstalk (Fig. 3.2(b)) is called self-wavelength crosstalk. Two lightpaths enter the OXC by the same port and exit the OXC on the same port, on different wavelengths; because of imperfection at the input demultiplexer, a small part of LP_1 is leaked on LP_2 and a small part of LP_2 is leaked on LP_1.

The third type of node crosstalk (Fig. 3.2(c)) is a generalization of the second type, where LP_1 and LP_2 enter the OXC via different input ports. In this case, the crosstalk comes from the leak at the input demultiplexer of LP_2 from a third lightpath, entering the OXC on the same input port as LP_2, on the same wavelength

as LP_1. Lightpath LP_2 carries this leak and when LP_1 and LP_2 are multiplexed, LP_1 is subject to crosstalk from LP_3.

Because the frequency response of the demultiplexer is not flat over the whole transmission spectrum, we further distinguish between adjacent port and non-adjacent port crosstalk for the second and third kinds of node crosstalk. Adjacent-port crosstalk occurs when the considered lightpath (LP_1) and the lightpath that injects node crosstalk (LP_2 or LP_3) are on adjacent wavelengths, while non-adjacent port crosstalk occurs when the wavelength for those two signals are not adjacent in the transmission spectrum. This model could be further refined by making the attenuation η a function depending on the wavelength separation between considered channel and crosstalk channel; however, in this chapter, we consider that any non-adjacent port crosstalk is very small compared with adjacent port crosstalk. This assumption is valid for systems with wide grid spacing and steep passband filters at the demultiplexers. When the grid spacing becomes tighter, the non-adjacent port crosstalk terms on the wavelengths that are closest to that of LP_1 cannot be ignored anymore.

As with nonlinear crosstalk, node crosstalk is a dynamic effect that depends on the network status. It is possible to compute σ_{nx} accounting for all node crosstalk components on a lightpath by summing the variance contributions for each node crosstalk: $\sigma_{nx}^2 = \sum_q \sigma_{nx_q}^2$ where the sum is taken over all node crosstalk signals between any existing lightpath in the network and the considered lightpath. More details on the related computations for the variances $\sigma_{nx_q}^2$ are provided in Appendix A.

The aforementioned physical effects all contribute to increase the blocking probability and average BER in all-optical networks. However, as mentioned in Section 3.1, high fairness, in addition to low BER averages, is desirable. Indeed, in all-optical networks, calls between nodes that are physically distant are blocked more often than

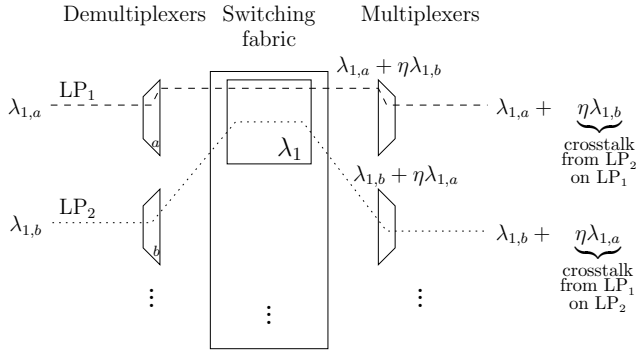

(a) Co-wavelength crosstalk

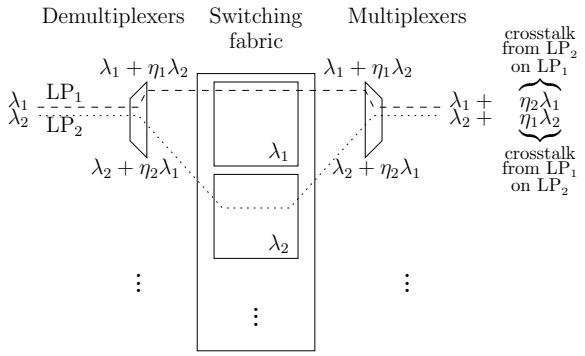

(b) Self crosstalk

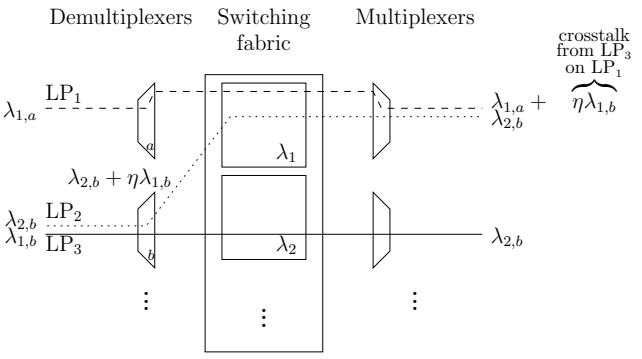

(c) Neighbor-port crosstalk

Figure 3.2: The three types of in-band crosstalk.

calls between closer nodes because both wavelength continuity and QoS constraints are harder to fulfill for longer lightpaths. Similarly, the BER for calls between physically distant calls is higher than for calls between close nodes. In this chapter, we consider two types of fairness, one applied to blocking probability, the other to BER. We design RWA algorithms which are more fair than traditional RWA algorithms in terms of blocking probability and in terms of BER. Fairness in terms of BER is important because, in the context of networks that implement Forward Error Correction (FEC) techniques — FEC requires additional bandwidth and is difficult to perform at high bitrates, — FEC could be reserved for only those paths that exhibit high BER. With RWA algorithms that are fair in terms of BER and which yield low BERs, FEC can be used on fewer paths and the BER threshold can be relaxed. In this dissertation, we use the definition of fairness introduced by Jain in [35] for circuit-switched networks but applicable to more general situations. The *fairness index* for a resource X shared between n users is a number between 0 and 1 that measures how fairly a resource is shared; a fairness index of $1/n$ indicates that a single user utilizes all of the resource while a fairness index of 1 indicates that all users utilize the resource equally. The formal definition for the fairness index f_X is:

$$f_X = \frac{\left(\sum_{k=1}^{n} x_k\right)^2}{\sum_{k=1}^{n} x_k^2} \tag{3.2}$$

where x_k is the amount of resource received by user k. In this dissertation, the users are pairs of nodes and the resource can be either blocking probability or BER. In the following section, we provide RWA algorithms that exhibit low blocking probabilities, lower BER, higher blocking probability fairness and higher BER fairness compared with traditional RWA algorithms.

3.3 Fair QoS-aware adaptive routing and wavelength assignment

3.3.1 Algorithms description

In this section we present five RWA algorithms (SP, SP2, HQ, MMQ, MMQ2) which belong to the class of adaptive RWA algorithms as defined in [34] and provide various degrees of fairness and QoS enhancements. Four of these algorithms are new (SP2, MMQ, MMQ2, HQ) and are compared with a traditional algorithm (SP).

In adaptive RWA algorithms, blocking due to the wavelength continuity constraint is reduced as follows. On a call arrival, a wavelength λ in the set of the C wavelengths in the network is selected according to a predefined order and a network topology that contains only links that are not in use by λ is determined. A route R is then tentatively selected using a shortest path algorithm on this new topology. If such a path exists then the call is accommodated on lightpath (R, λ). If such a path does not exist then the wavelength continuity condition is not fulfillable on this wavelength and the next available wavelength is chosen.

The standard *exhaustive adaptive RWA algorithm* is an adaptive RWA algorithm where, instead of considering wavelengths in a predefined order and picking the first wavelength for which a route can be found, all wavelengths are considered, thereby yielding at most C possible routes which satisfy the wavelength continuity constraint. A lightpath is established on the shortest of these routes. This standard exhaustive adaptive RWA algorithm yields low blocking probabilities but implements no QoS-awareness or fairness enhancement.

To enhance fairness in some of our algorithms, we use the technique called *protecting threshold* presented in [36]. The protecting threshold technique safeguards

Algorithm 3.1 Generic QoS-aware adaptive RWA
Input: policy, Q_{th}.
Output: lightpath LP.

```
1: for i=1 ... C do
2:    Determine altered network topology considering only links where λ_i is free
3:    Determine the shortest path SP(λ_i) in the altered network topology
4:    if Q factors for all lightpaths (including the tentative lightpath) are above
      threshold Q_th then
5:       Mark SP(λ_i) as usable
6:    end if
7: end for
8: if set of usable lightpaths is empty then
9:    return LP = ∅ (reject call)
10: else
11:   Select a lightpath ("LP") in the set of usable lightpaths according to a prede-
      fined policy (SP, SP2, HQ, MMQ, MMQ2)
12:   return LP (accept call on "LP")
13: end if
```

from the fact that longer paths are subject to more frequent blocking than shorter paths because of the wavelength continuity constraint; protecting threshold is even more relevant in the context of crosstalk-impaired networks, because longer paths are subject to higher QoS degradation due to crosstalk; here, wavelength continuity and QoS constraints are both harder to fulfill for longer paths. Protecting threshold facilitates establishing longer paths by allowing a short lightpath to be established only when the number of wavelengths that are available on the tentative paths is above a preset threshold, hereby saving resources for longer lightpaths. The drawback of protecting threshold is that calls on short paths can be blocked even if wavelengths are available and the technique can therefore be detrimental to the average blocking probability on the network. In this chapter, we implement the protecting threshold as follows: a single-hop lightpath is blocked if it would use the last wavelength available on the (unique) link that constitutes the lightpath. This corresponds to a threshold (or reservation parameter) of 2 in [36].

We provide a description of our QoS-aware adaptive RWA algorithms in Alg. 3.1. The first modification to the standard exhaustive adaptive RWA algorithm we propose concerns QoS-awareness; in this dissertation, we consider that the QoS constraint is satisfied when the Q factor of all calls in the network is above a predefined threshold Q_{th}, which corresponds to operation below a fixed minimum BER. When a lightpath is tentatively established in the network, it is therefore necessary to check that its Q factor is above the preset threshold, but this is not sufficient. Indeed, when a new lightpath is established, it injects crosstalk on all previously established lightpaths with which it shares links (nonlinear crosstalk) or nodes (node crosstalk) and therefore Q factors for those lightpaths have to be checked as well as the Q factor of the tentative lightpath. Lightpaths that share no link nor node with the tentative lightpath are not affected by the insertion of the tentative lightpath and therefore their Q factors do not need to be recomputed. Our algorithms enforce satisfaction of the QoS constraint by computing the Q factors of the tentative lightpath and of all lightpaths that share at least a link or node with the tentative lightpath (see Alg. 3.1, line 4), and by rejecting the tentative lightpath from the list of candidate lightpaths if any of these Q factors is below the preset threshold.

The second modification lies in the selection of the route among the list of (at most C) candidates and concerns both QoS awareness and fairness enhancement. We propose the following five policies to select the route on which an incoming call is to be accommodated (see Alg. 3.1, line 11):

- **SP** (shortest path) selects the wavelength that corresponds to the physically shortest path among the candidates [34]; this policy is used as a reference against which other policies are evaluated;

- **SP2** is the traditional shortest path algorithm with protecting threshold and

reservation parameter set to 2; this new policy is designed to enhance blocking probability fairness;

- **HQ** (highest Q factor) selects the candidate lightpath with the highest Q factor. This new policy is designed to decrease the average BER in the network.

- **MMQ** (max-min Q factor) is a new, QoS-aware policy. Assuming a wavelength has been chosen, inserting a lightpath increases crosstalk in the network, possibly bringing the Q factor of a previously established lightpath close to the threshold. Operation close to the Q threshold is not desirable as it makes the QoS constraint more difficult to fulfill for future incoming calls. MMQ maximizes the margin of QoS operation in the network by selecting the lightpath that maximizes (over the at most C candidates) the minimum (over the tentative lightpath itself and all lightpaths previously established in the network that the tentative lightpath crosses) Q factor. MMQ is QoS aware in the sense that its decision is based on QoS rationales. MMQ is designed to decrease the average network BER;

- **MMQ2** is MMQ augmented with the protecting threshold technique. MMQ2 is designed to not only decrease average network BER, but also increase blocking probability fairness and BER fairness.

For each policy, ties are broken by choosing the first lightpath in the list of candidates.

Our RWA algorithms require online Q factor computations, but Q factors cannot be precomputed because σ_{nlx} and σ_{nx} depend on the network status. However, it is possible to precompute all quantities in (3.1) and hence compute Q factors online using fast table lookups, as is shown in Appendix A. The QoS computation overhead incurred by our algorithms is therefore not computationally intensive. Fur-

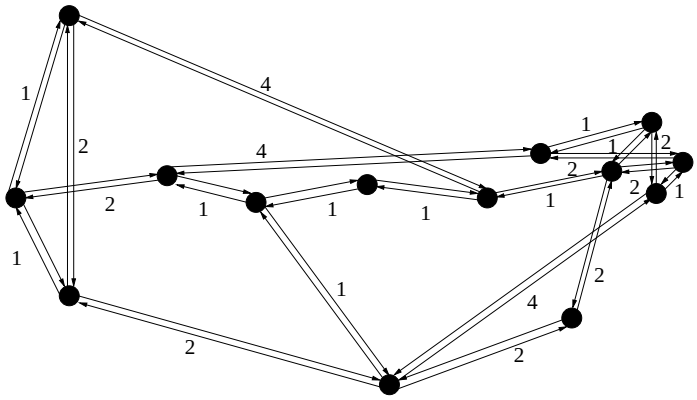

Figure 3.3: Down-scaled version of the NSF topology (scaling factor: 1/10) used to perform the simulations. On the figure, the weights represent the number of spans for the links.

thermore, since our new algorithms are based on exhaustive adaptive RWA, they have the same complexity as the reference algorithm (SP) and are much less complex than algorithms that search for an optimal solution over the complete set of possible lightpaths, which is an NP-complete problem [18].

As mentioned above, fairness-enhanced algorithms (SP2, MMQ2) may result in higher blocking probability than the reference algorithm (SP). Similarly, although HQ, MMQ and MMQ2, which are designed with QoS in mind, attempt to lower blocking probability due to the QoS constraint, the path they select is not necessarily the shortest path. Therefore these three algorithms may waste network resources and make wavelength continuity constraint harder to fulfill for future calls. In the next section, we show with simulations that the trade-offs between wavelength continuity and QoS constraints, between lower blocking probability and higher QoS, and between lower blocking probability and higher fairness, do not result in a substantial increase in overall blocking probability.

Table 3.1: Physical parameters for the simulated networks.

Description	**Value**
Span length	70 km
Signal peak power	2 mW
Bit rate	10 Gbps
Pulse shape	Super-Gaussian NRZ
Fabric crosstalk	-40 dB
Adj. port crosstalk attenuation	-30 dB
Non adj. port crosstalk attenuation	-60 dB
Crosstalk detuning	0 GHz
WDM grid spacing	25 GHz
Fiber loss	0.22 dB/km
Nonlinear coefficient	2.2 $(\text{W km})^{-1}$
Chromatic dispersion	17 ps/nm/km
Dispersion compensation length	70 km
Spontaneous-emission factor	2
Photodetector responsitivity	1 A/W
Receiver electrical bandwidth	7 GHz
Number of wavelengths (C)	8
Minimum Q factor: Q_{th}, Q_{th_1} (no coding) Q_{th_2} (Golay coding)	 6 3.6

Table 3.2: Impact of adjacent port crosstalk accumulation on the maximum transmission distance.

Crosstalk components	0, 1	2, 3	4	5, 6	7, 8	9	10
Spans	12	11	10	9	8	7	6

Table 3.3: Lengths of the shortest paths in the NSF topology.

Length (spans)	1	2	3	4	5	6	7	8
Number of paths	20	30	34	36	26	18	14	4

Table 3.4: Impact of XPM crosstalk accumulation on the maximum transmission distance.

Crosstalks components	0	1	2-8
Spans	12	9	7

3.3.2 Evaluation through simulation

We evaluate our algorithms on the NSF network topology depicted in Fig. 3.3, with the physical parameters from Table 3.1. The NSF topology we are using for our simulations is scaled down by a factor of 10 with respect to the real NSF topology to model a large metropolitan network. We have computed the maximum distance achievable in this network for a path subject to a varying number of adjacent port crosstalk signals and report the results in Table 3.2. The maximum distance achievable in the downscaled network while maintaining good QoS ($BER \leq 10^{-9}$) and assuming physical impairments due to ISI and noise only is 12 spans. (Distances much longer than 12 spans are achievable using optimized long-haul link design and components, which are not the focus of this dissertation.) Moreover, if as few as 10 adjacent port crosstalk signals are injected on a lightpath, then the maximum transmission distance on the considered lightpath is only 6 spans. We provide the distribution of the lengths of the shortest paths in the downscaled NSF topology in Table 3.3. Since the longest shortest path between any two nodes is 8 spans long with this topology, even node crosstalk can have disruptive effects in the network in terms of blocking probability due to the QoS constraint. For reference, we also show in Table 3.4 the impact of XPM on the maximum transmission distance in this network. XPM has a steeper impact than node crosstalk; if only two signals co-propagate in the network on the same route (one XPM crosstalk component case), the maximum distance each of these signals can cover is 9 spans. This maximum distance then decreases to 7 spans if as few as 3 signals (two XPM crosstalk components or more) use the same route.

In Fig. 3.4, we show the blocking probability when all physical impairments are accounted for, for all five RWA algorithms discussed above and different total offered

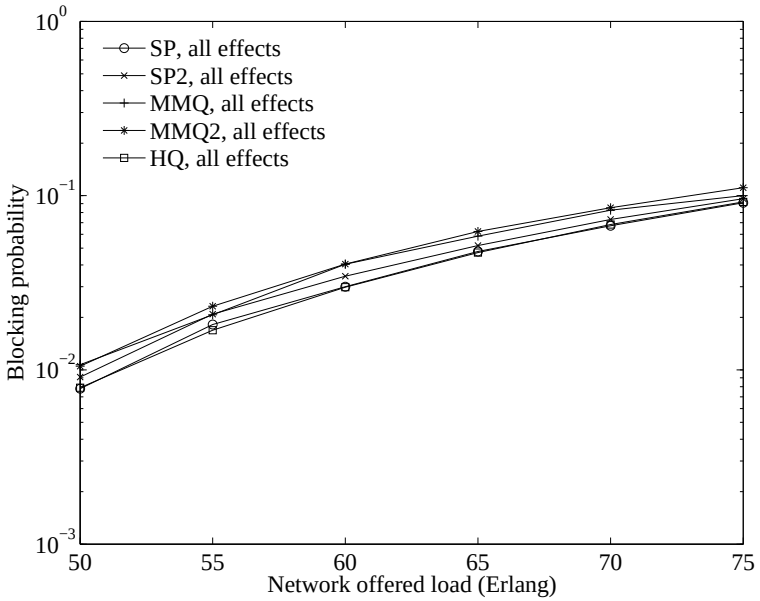

Figure 3.4: Blocking probability for the various QoS-aware RWA algorithms.

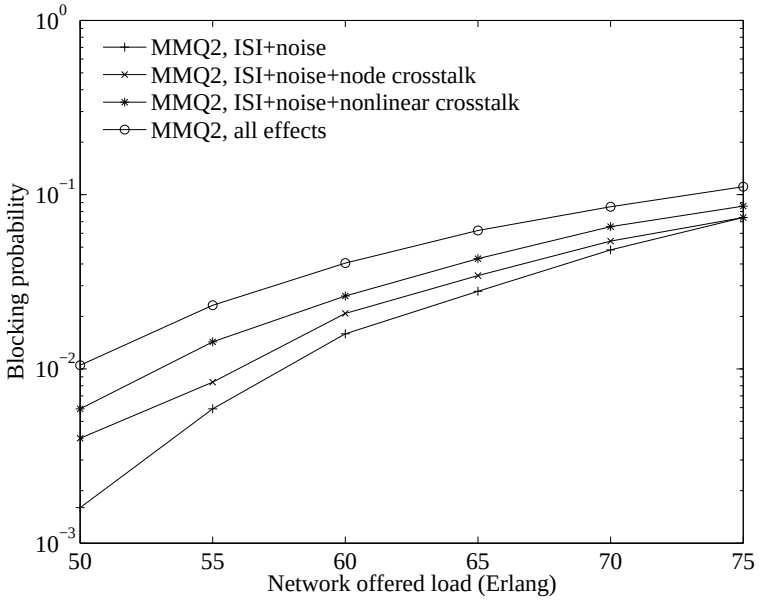

Figure 3.5: Blocking probability for separate physical impairments, for the MMQ2 algorithm.

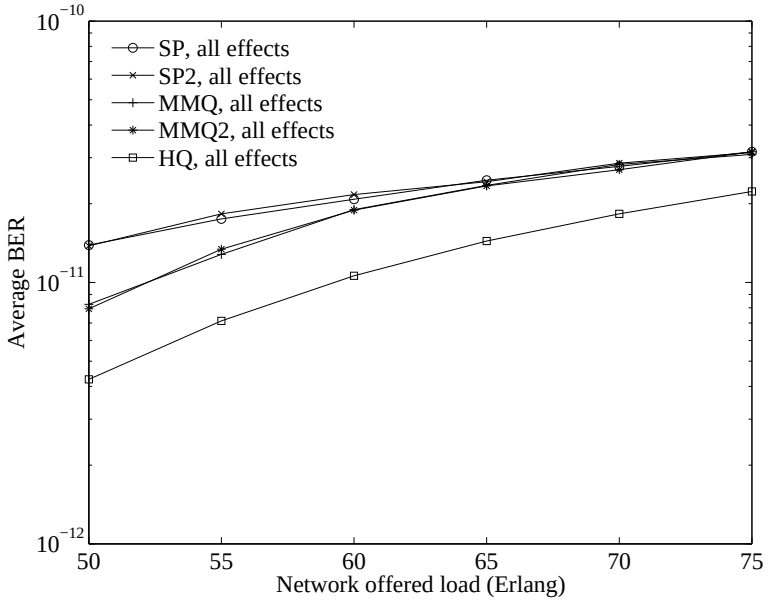

Figure 3.6: BER for the various QoS-aware RWA algorithms.

network loads. The HQ algorithm tends to perform best and the MMQ2 worst; however, the differences in average blocking probabilities for all algorithms are small and overall all algorithms perform very similarly. In Fig. 3.5, we investigate further the origin of blocking probabilities for one of the algorithms, MMQ2. The difference between the topology-related impairments only (ISI and noise) case and the all-effects (ISI, noise, nonlinear and node crosstalk) case is close to one order of magnitude in average blocking probability. Furthermore, we observe that blocking probabilities for cases including only one of the crosstalk effects are similar: impact of nonlinear crosstalk is only slightly higher than that of node crosstalk. Therefore, inclusion of both kinds of crosstalk is important when evaluating RWA algorithms for blocking probability.

The average BER in the network is shown in Fig. 3.6 for the various algorithms. As expected, all three algorithms designed with QoS in mind (MMQ, MMQ2, HQ) perform better than SP and SP2, especially for lower loads. Furthermore, MMQ and

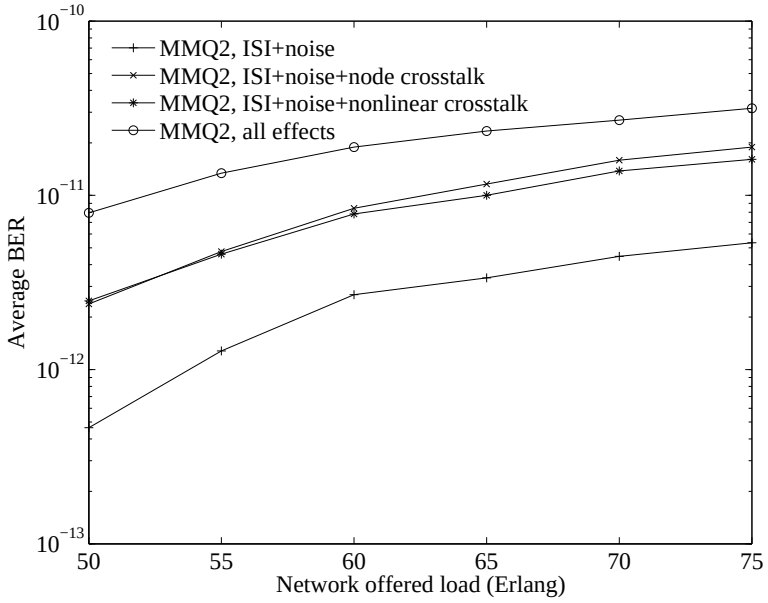

Figure 3.7: BER for separate physical impairments, for the MMQ2 algorithm.

MMQ2 perform very close to one another, showing that additionally tuning MMQ for fairness does not harm its performance in terms of BER. The HQ algorithm performs best, yielding BERs at least twice lower than those of other algorithms. The BER performance of the network is further investigated in Fig. 3.7 for the MMQ2 algorithm: physical effects are responsible for an increase of one order of magnitude for the average BER in the network, with both node and nonlinear crosstalk effects decreasing BER similarly.

We show how our algorithms perform in terms of fairness in Figs. 3.8 and 3.9; fairness indices lies between 0 and 1 with higher values being desirable. First, we study blocking probability fairness in Fig. 3.8. The MMQ2 algorithm exhibits the highest fairness even compared to SP2 which was designed to improve fairness. The HQ algorithm performs significantly lower than other algorithms as it is only designed to improve QoS. In Fig. 3.9 we study BER fairness; here, the two algorithms designed to provide high margin in terms of BER (MMQ, MMQ2) outperform all other

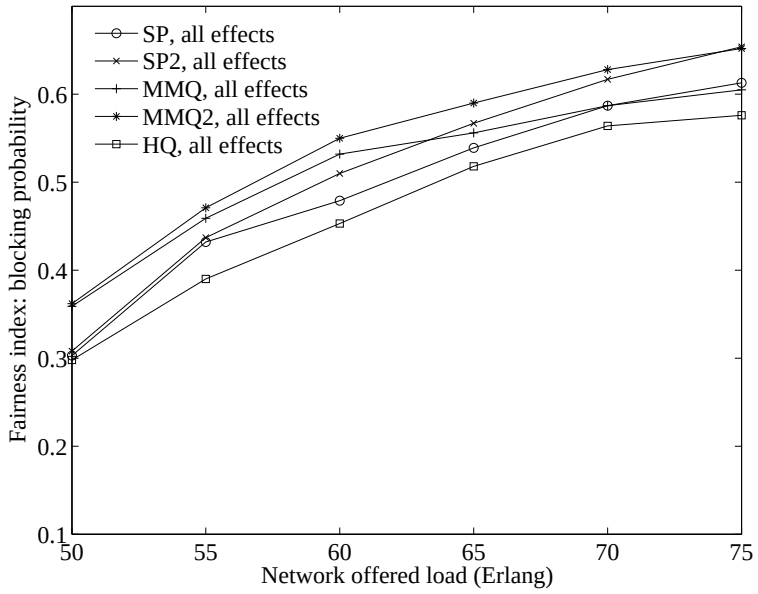

Figure 3.8: Blocking probability fairness for the various QoS-aware RWA algorithms.

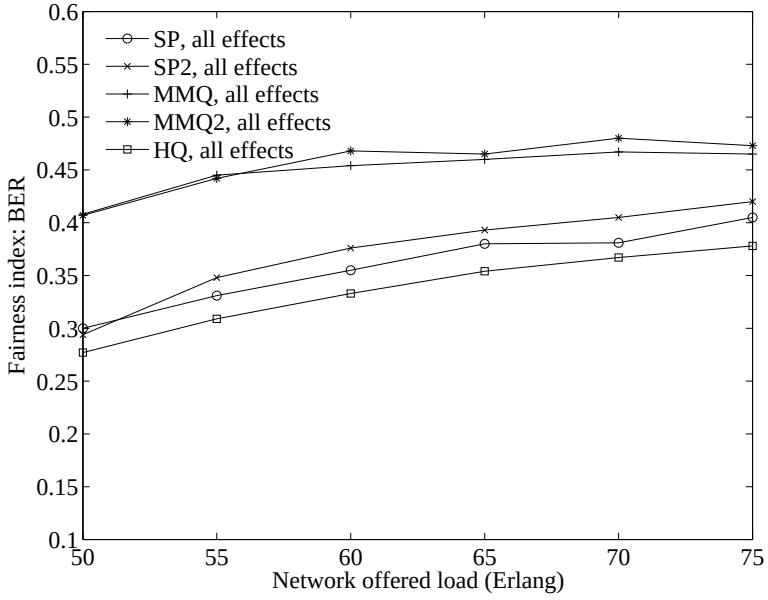

Figure 3.9: BER fairness for the various QoS-aware RWA algorithms.

algorithms. Although MMQ2 implements an additional mechanism, the protecting threshold, to improve blocking probability fairness, this mechanism has no impact on the BER fairness property of the algorithm. We also evaluated a sixth algorithm, HQ2, which implements the HQ policy augmented with the protecting threshold technique. However, for each of the metrics presented here, HQ2 was outperformed by at least one of the other five algorithms..

In this section, we have shown how different RWA algorithms could improve network performance. With the HQ algorithm, BER is greatly diminished compared with other algorithms, while MMQ/MMQ2 still perform better than the reference algorithms. Fairness, both in terms of blocking probability and BER, is improved with MMQ2 (and BER fairness is equivalently improved with MMQ) compared with all other algorithms. These results are obtained without sacrificing average blocking probability as all algorithms perform similarly for this metric.

3.4 QoS-aware adaptive routing and wavelength assignment with optional coding

3.4.1 Algorithms description

In this section, we address a problem that arises when some paths in a network are too long to meet the QoS constraint even in the absence of crosstalk. Indeed, such long paths are always blocked, independently of the network load and some customers are never given an opportunity to communicate with one another. Adding load (and crosstalk) in the network further degrades the performance in terms of blocking probability. In the previous section, with the NSF topology depicted in Fig. 3.3, all shortest paths between two nodes are 8 spans or less, and the Q factor drops

Algorithm 3.2 QoS-aware adaptive RWA with optional coding.
Input: Q_{th1},Q_{th2}.
Output: set LP of up to two lightpaths.

1: Compute LP using Alg. 3.1 with wavelength random pick (cf. Section 3.4.2) for the SP policy and $Q_{th} = Q_{th1}$
2: **if** $LP \neq \emptyset$ **then**
3: **return** LP (accept call on LP with no coding)
4: **else**
5: Compute LP_1 using Alg. 3.1 with wavelength random pick (cf. Section 3.4.2) for the SP policy and $Q_{th} = Q_{th2}$
6: **if** $LP_1 \neq \emptyset$ **then**
7: Compute LP_2 using Alg. 3.1 with wavelength random pick (cf. Section 3.4.2) for the SP policy and $Q_{th} = Q_{th2}$
8: **if** $LP_2 \neq \emptyset$ **then**
9: **return** $LP = LP_1, LP_2$ (accept call on LP_1 and LP_2 with FEC coding)
10: **end if**
11: **else**
12: **return** $LP = \emptyset$ (reject call)
13: **end if**
14: **end if**

below the threshold $Q_{th} = 6$ for paths that are 13 spans or more, using the physical parameters given in Table 3.1. Therefore, any node is reachable from any other node. Now consider the NSF topology from Fig. 3.3 where the number of spans between any two adjacent nodes is *doubled*, to model a regional-sized network. With this new, enlarged topology, some shortest paths between network nodes are now longer than the maximal achievable distance of 12 spans[2]. It can be seen in Table 3.3 that 18 shortest paths are more than 12 spans long in the enlarged topology, and hence no algorithm described in the previous section can draw the average network blocking probability below $18/(14 \times 13) \approx 0.1$. The QoS-aware adaptive RWA algorithm presented in this section overcomes this limitation by using optional FEC coding on calls that do not meet the QoS constraint.

[2]A network using new technology could be designed to achieve these distances; the network used simply provides an example of a regional-scaled network using the parameters given.

FEC coding allows to trade bandwidth utilization against higher QoS. The principle of our QoS-aware RWA algorithm with optional coding (see Alg. 3.2) is to use several lightpaths per call for calls that do not meet the QoS constraint. Data on each of these lightpaths is encoded with a FEC code such that the minimal Q factor required for the coded signal to achieve a maximal target BER after decoding is lower compared with the case where no coding is used and where a single lightpath is used for each call. Lightpaths for the same call can use the same route and different wavelengths, or different routes. In this section, we propose to use a simple code, Golay(23,12), for calls that fail to meet the QoS constraint ($Q > Q_{th_1}$ where $Q_{th_1} = 6$ for a target BER of $BER = 10^{-9}$). Since the rate of this code is approximately 1/2, the coded datastream has to use two lightpaths instead of one. The coding gain of Golay(23,12) is 4.4 dB for $BER = 10^{-9}$ [61]. After coding, the minimum required Q factor can be shown to be reduced to $Q_{th_2} = 3.6$ instead of 6 for the same BER target of $BER = 10^{-9}$, assuming that a 1 dB OSNR degradation corresponds to a 1 dB decrease of the Q factor [64]. Our RWA algorithm with optional coding employs coding only for those paths that need it in order to keep the bandwidth (number of lightpaths per call) expansion low. It uses a variation of the QoS-aware adaptive RWA algorithm (Alg. 3.1) that we described in Section 3.3 to find up to two lightpaths per call.

The QoS-aware adaptive RWA algorithm with optional coding trades bandwidth utilization in the form of the number of lightpaths used per call against looser Q factor requirements. Increasing bandwidth utilization results in higher blocking probabilities due to the wavelength continuity constraint and higher crosstalk imposed upon other lightpaths. Looser requirements on the Q factors decrease blocking probability due to the QoS constraint. In the following section, we show that the trade-off actually results in lower blocking probabilities overall on a regional-sized example.

3.4.2 Evaluation through simulation

To evaluate the QoS-aware adaptive RWA algorithm with optional coding, we use the NSF topology depicted in Fig. 3.3 where the number of spans between any two nodes has been doubled. The physical parameters for the network can be found in Table 3.1. As discussed in the previous section, about 10% ($18/(13 \times 14)$) of the shortest paths in this enlarged topology are too long to be accomodated with sufficient QoS ($BER \leq 10^{-9}$) if no coding is used. Furthermore, the (potentially two) lightpaths used by each call are computed with a slightly modified version of Alg. 3.1 and the SP policy: instead of exhaustively searching for the shortest path among all wavelengths, wavelengths are picked randomly and Alg. 3.1 stops as soon as a lightpath is found. This simplification is made to keep simulation times low and does not change the core concept of the QoS-aware adaptive RWA algorithm with optional coding, which is to trade bandwidth against QoS. We evaluate the QoS-aware adaptive RWA with optional coding algorithm against its counterpart where no coding is available and where a call that does not meet the QoS condition is rejected without being given a chance to be assigned two lightpaths instead of one. In all plots (Figs. 3.10, 3.11, 3.12), plain lines refer to algorithms where no coding is available while dashed lines refer to the algorithms where optional coding is available.

First consider Fig. 3.10; when no coding is available, blocking probabilities remain above 0.1 even for the lower load values and when the only impairments are ISI and noise. Node and nonlinear crosstalk have similar impacts on the call blocking probability, with nonlinear crosstalk having a slightly higher impact as already noticed in Section 3.3.2 for the RWA algorithms with no coding capability. When optional coding is used, and when all physical impairments are included, blocking probabilities are lowered by 0.07 to 0.1: crosstalk effects are almost, but not completely, removed

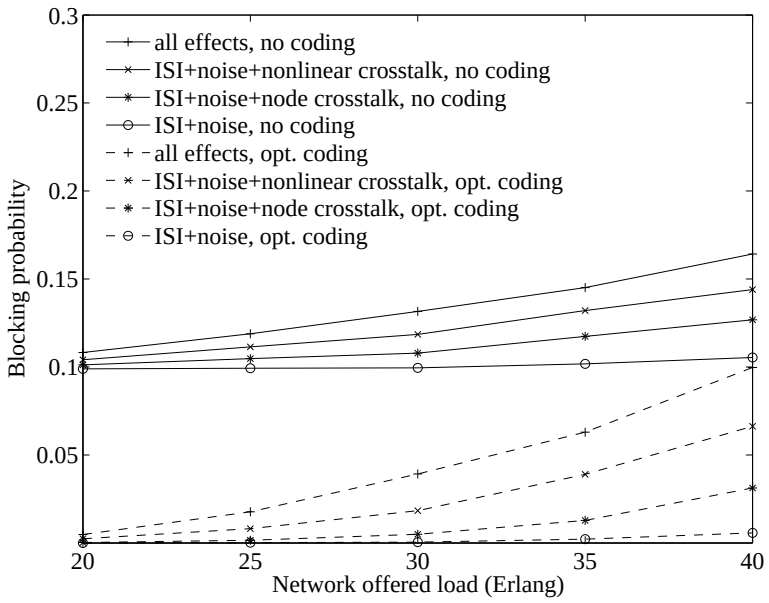

Figure 3.10: Blocking probability for separate physical impairments, for RWA algorithms with and without optional coding.

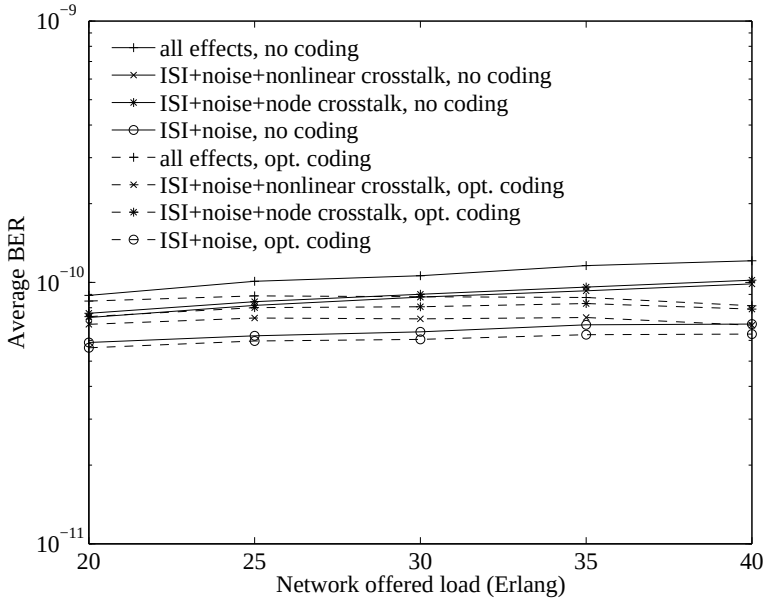

Figure 3.11: BER (after decoding) for separate physical impairments, for for RWA algorithms with and without optional coding.

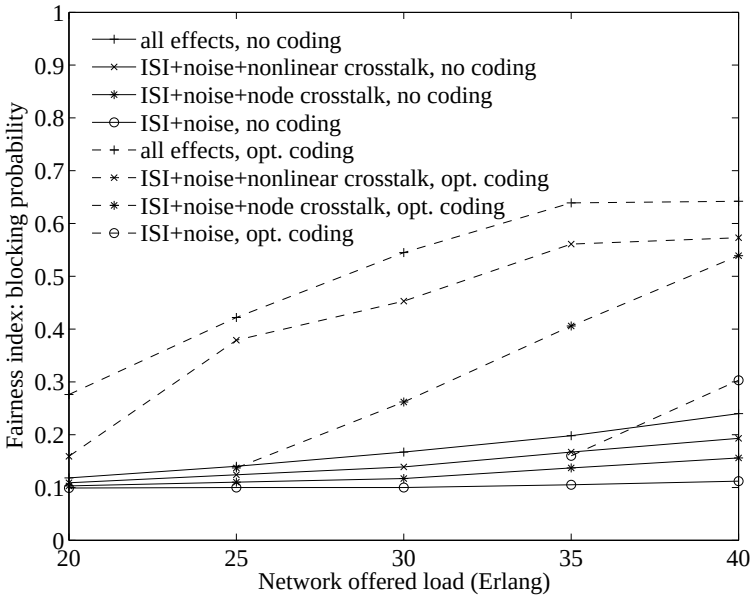

Figure 3.12: Blocking probability fairness for separate physical impairments, for RWA algorithms with and without optional coding.

by the utilization of optional coding. The trade-off mentioned in the former section overall therefore results in a blocking probability decrease. In Fig. 3.11, we show that using coding also contributes in decreasing the average BER (after coding) in the network. Coding also improves blocking probability fairness as is shown in Fig. 3.12; for instance, when no coding is available, blocking probability fairness remains between 0.1 and 0.2 while it can reach 0.6 with optional coding when all effects are included.

We have shown, using simulation on a large, regional-sized network, how optional coding could reduce blocking probability, improve QoS and improve fairness in networks where some paths are too long to be used without coding. For networks where all paths are short enough to be used without coding, our results (not shown here) show that optional coding does not decrease blocking probability. Then, the shortage of wavelengths satisfying the continuity constraint is not offset by the gains in QoS, and the bandwidth expansion vs. QoS trade-off results in high blocking probabilities.

3.5 Summary

We have presented two classes of adaptive QoS-aware Routing and Wavelength Assignment algorithms for networks with physical impairments. When networks are large and heavily loaded, some calls are blocked because chosen lightpaths would experience a poor QoS, as measured by BER. In these cases, our fair QoS-aware adaptive RWA algorithms decrease BER (HQ algorithm) and improve fairness in blocking probability and BER (MMQ, MMQ2 algorithms) without sacrificing low average call blocking probability in the network. These new RWA algorithms account for crosstalk at call admission and path selection steps, and SP2 and MMQ2 additionally implement the so-called protecting threshold technique. In still larger networks, say regional or continental-sized, where some calls would always be blocked even in the absence of crosstalk, the QoS-aware adaptive RWA algorithm with optional coding can establish calls between physically distant nodes using several lightpaths per call and coding over these lightpaths, hereby decreasing call blocking probabilities and achieving lower BER and higher fairness compared to the case where coding is not available. All algorithms are shown to mitigate physical layer effects on network operation using simulations for realistic network scenarios.

Chapter 4

Analysis of Blocking Probability in Crosstalk-Impaired Networks

In this chapter, we present an analytical technique to compute blocking probability in all-optical networks subject to physical impairments. Evaluating RWA algorithms via simulation, as we did in the previous chapter of this dissertation, is a lengthy process. Here, we present much faster analytical tools for RWA algorithms evaluation. The algorithms we evaluate in this chapter are simpler than those in Chapter 3, which are adaptive; yet, we are able to give an analytical framework for a class of QoS-aware RWA algorithms. The physical impairments we consider in this chapter are ISI, noise, and a particular type of node crosstalk, namely self-crosstalk.

4.1 Introduction

Evaluating RWA algorithms through simulations is a lengthy process, so fast, preferably analytical, tools, are needed. In this chapter, we tackle the problem of computing analytically blocking probabilities in networks subject to both wavelength blocking and QoS blocking. We consider a single instance of routing and wavelength assign-

ment, namely, fixed routing where routing tables are precomputed and contain a single path between any two nodes, and random wavelength assignment. Indeed, as is seen in Chapter 3 in the context of adaptive routing, the impact of wavelength assignment on network performance as measured by blocking probability is less than an order of magnitude.

The goal of the present chapter is to present a fast algorithm that can be used to dimension the performance of a network, rather than to compute exact blocking probabilities for specific RWA algorithms. We consider only fixed routing because adaptive routing has not been studied analytically even for networks with no QoS constraints (no-QoS case). We chose to limit the scope of this work to the fixed routing case because the no-QoS case is well understood for such routing.

The problem of analytically computing blocking probability in all-optical networks has been studied in the past, using various models and assumptions. In [65], a reduced load approximation scheme is developed and is applicable only to small networks due to its exponential computational complexity with the number of nodes in the network. Also, in [65] wavelength utilizations on different links are assumed to be independent. This independence assumption is oversimplifying especially for sparse networks where nodal degree is low. The independence assumption is relaxed in [19, 40, 41, 66, 67]. However, other oversimplifying assumptions are made in [66]. In [40], the problem of partial wavelength conversion is touched upon. The iterative algorithm presented in [19], and reused in [41], is less complex than the model used in [67] and yields accurate results, while making only a two-link correlation assumption, that is, wavelength utilization on a link of a given route depends only on that of the one previous or next link of the route. Our work reuses certain results from [19], which is applicable to large networks and arbitrary topologies; however, our technique is largely independent of the algorithm that is used to compute blocking probability due

to wavelength blocking, and can be combined with other algorithms that compute the wavelength blocking for each route.

This chapter is organized as follows. In Section 4.2, we present our model and state the assumptions used throughout this chapter. In Section 4.3, we give an overview of the algorithm presented in [19], which computes blocking probability due to wavelength continuity. We extend this technique in Section 4.4 to include blocking due to ISI, noise, and node crosstalk. Our technique is validated by simulations on various network topologies for realistic physical layer parameters in Section 4.5.

4.2 Network and crosstalk model

We present here our assumptions concerning the network, traffic, and crosstalk models used throughout this chapter. As in Chapter 3, we assume that:

- links represent optical fibers and hence are unidirectional;
- the number of wavelengths per link is fixed to a constant number C across the network;
- wavelength conversion is not available;
- call durations are exponentially distributed with mean rate $M_{R(n_1,n_2)} = 1$ for route $R(n_1, n_2)$ from node n_1 to n_2;
- call arrivals follow a Poisson process with mean rate $\Lambda_{R(n_1,n_2)}$ for route $R(n_1, n_2)$ from node n_1 to n_2. Since $M_R = 1$, the offered load in Erlangs on a route R is Λ_R. Denoting by V the set of nodes in a network, the total offered load in Erlangs in that network is $\sum_{\substack{n_1,n_2 \in V \\ n_1 \neq n_2}} \Lambda_{R(n_1,n_2)}$.

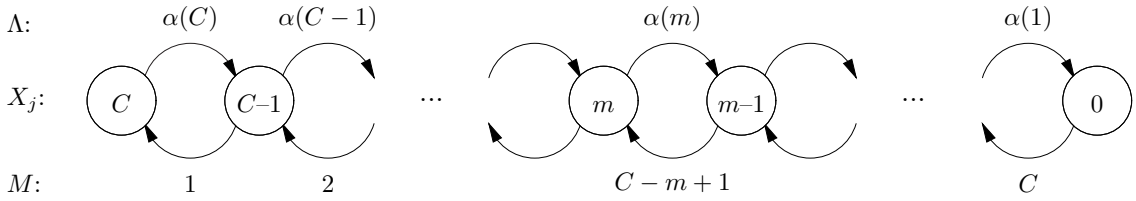

Figure 4.1: Birth-death process. The states represent the number of free wavelengths on a given link and the "Λ"s and "M"s are the transition rates.

Following [19], we also make the following assumptions concerning the traffic model. These assumptions make analysis tractable and fast, yet approximate well the behavior of all-optical networks:

- routing is fixed with no alternate paths and wavelength assignment is random pick;
- given m wavelengths are free on link j, the time until a call that uses j arrives is assumed to be exponentially distributed with parameter $\alpha_j(m)$ [68], such that the number of free wavelengths on link j is modeled as a birth-death process as illustrated in Fig. 4.1;
- wavelength occupancies on disjoint routes are independent of each other;
- numbering the links of a given route sequentially from source to destination: the state of wavelength i on link j of a route R is independent of the state of some other wavelength $k \neq i$ on the previous link $j-1$ on the same route, given the state of wavelength i on link $j-1$ or given the state of wavelength k on link j;
- the state of wavelength k on link j of route R is independent of the state of wavelength k on other links of R given the state of wavelength k on the previous link $j-1$ on R (locality assumption).

This work, as do [19] and [41], uses the ergodicity of the system. The blocking probability for a route in a network is actually a time average (average of blockings per unit of time), but the analytical method computes ensemble averages (average of blockings over the set of possible network states). Therefore, the blocking probabilities we compute are equivalent to blocking rates. Moreover, event orders are not important to compute these rates. More specifically, in a real network, if call C_1 arrives and is blocked because establishing C_1 would cause the Q factor of some other call C_2 already established to cross the threshold Q_{th} then C_1 is rejected; in our analysis, since it is the Q factor of C_2 that crosses the threshold, C_2 is rejected. Averaging over all network states in the analysis yields the blocking rate in the real network.

We model the physical layer as follows. ISI and noise are modeled as in Chapter 3, and interchannel crosstalk is ignored; rather, we focus on a single type of node crosstalk: self-crosstalk, as defined in Section 3.2. Self-crosstalk occurs when two signals enter an OXC through the same port and exit the OXC also on the same port, but on different wavelengths as shown in Fig. 3.2(b). This kind of crosstalk is due to imperfect demultiplexer filters. Other types of crosstalk are ignored here because fabric crosstalk is generally weaker than port crosstalk. Also, we do not distinguish between adjacent and non-adjacent channel crosstalk. This assumption is accurate when the demultiplexer frequency response is flat in the cut-off region.

Our analytical work is based on crosstalk component counting (Section 4.4.1); crosstalk component counts are then linked to QoS blocking (Section 4.4.2). Our method can be generalized easily to more than just self-crosstalk. For instance, a small modification of how crosstalk components are counted permits one to replace self-crosstalk effects by co-wavelength crosstalk effects in our analysis. Such a modification is useful in cases where the primary source of crosstalk is the switching

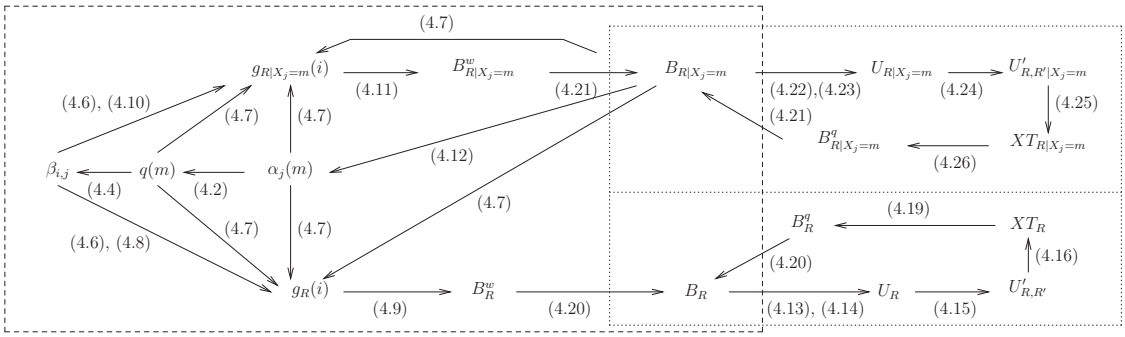

Figure 4.2: Iterative algorithm to compute blocking probability of an all-optical network. The portion in the dashed box computes the blocking probability due to the wavelength continuity constraint and was first published in [19]. Our extensions to compute the blocking probability due to QoS are in the dotted boxes.

fabric, in the case of non-MEMS switches for instance [3]. Similarly, another simple modification in the crosstalk counting part of our analysis permits accounting for neighbor-port crosstalk as defined in Section 3.2. Furthermore, our analytical method can compute blocking probabilities if several of these crosstalks are present in the case where the crosstalk attenuations are the same. Our method cannot be simply adapted to compute blocking probabilities in cases when crosstalks with different attenuations are present, for instance, if both adjacent and non-adjacent crosstalks are attenuated differently, or if switching fabric and port crosstalk have different attenuations. Indeed, when different attenuations are present in the network, the wavelength equivalence assumption is no longer valid.

4.3 Wavelength blocking

In this section, we give a brief overview on how the blocking probability due to the wavelength continuity constraint can be determined. The technique presented here was published in [19] and was based on [36]. We repeat it for the sake of

completeness and to make explicit how our technique to compute QoS blocking and the technique to compute wavelength blocking interact; however our QoS blocking computation technique could be adapted to other wavelength blocking computation techniques. We provide a pictorial version of the algorithm in the dashed box of Fig. 4.2. The edges are labeled by the corresponding equation numbers and we use the same notations as in [19], except for minor differences to make our derivations easier to follow. The algorithm is iterative and revolves around the computation of the state-dependent arrival rates $\alpha_j(m)$. Those rates are first assumed to be known and are used to compute a number of quantities, leading ultimately to the blocking probability for each route (Section 4.3.1). In Section 4.3.2, we make explicit the state-dependent arrival rate calculations.

4.3.1 Blocking due to wavelength continuity

We seek to compute here the blocking probability due to the wavelength continuity constraint B_R^w for each route R. Since, in this section, we ignore QoS blocking, the blocking probability B_R for route R is equal to the blocking probability due to wavelength continuity constraint B_R^w.

We denote by X_j the number of free wavelengths on link j and define $q_j(m)$ for link j and number of wavelengths m as:

$$q_j(m) = Pr(X_j = m). \tag{4.1}$$

Since the number of free wavelengths on a link is assumed to follow a birth-death

process, the probabilities $q_j(m)$ are given by [19]:

$$q_j(m) = \frac{\frac{C(C-1)...(C-m+1)}{\alpha_j(1)\alpha_j(2)...\alpha_j(m)}}{1 + \sum_{k=1}^{C} \frac{C(C-1)...(C-k+1)}{\alpha_j(1)\alpha_j(2)...\alpha_j(k)}}. \tag{4.2}$$

Note that $q_j(m)$ depends on the state-dependent arrival rates $\alpha_j(m)$, which are computed in Section 4.3.2. Define $Y_{i,j}$ as the state of wavelength i on link j, that is, $Y_{i,j} = 0$ if wavelength i is free on j and $Y_{i,j} = 1$ if wavelength i is used on j. Define $\beta_{i,j}$ as the probability that a given set of i wavelengths is free on link j. Assuming random wavelength assignment, this is equivalent to:

$$\beta_{i,j} = Pr\left(Y_{1,j} = 0, \ldots, Y_{i,j} = 0\right). \tag{4.3}$$

It is shown in [19] that:

$$\beta_{i,j} = \sum_{m=i}^{C} q_j(m) \frac{\binom{m}{i}}{\binom{C}{i}}. \tag{4.4}$$

We now seek to compute the probability $g_R(i)$ that a given set of i wavelengths is free on route R. First define $\eta_{i,j}$ as the conditional probability that wavelength i is free on link j given that any $i-1$ other wavelengths are free:

$$\eta_{i,j} = Pr\left(Y_{i,j} = 0 | Y_{1,j} = 0, \ldots, Y_{i-1,j} = 0\right). \tag{4.5}$$

It follows from the definition and the wavelength equivalence assumption that:

$$\begin{aligned} \eta_{i,j} &= \beta_{i,j} \quad \text{if } i = 1, \\ &= \tfrac{\beta_{i,j}}{\beta_{i-1,j}} \quad \text{otherwise.} \end{aligned} \tag{4.6}$$

Define $Pl_R^{(j)}$ as the probability that a call using some wavelength on link j of route R is not using the following link $j+1$ of R. The quantity $Pl_R^{(j)}$ is approximated as the ratio between the arrival rate of traffic on link j that does not continue on the following link of route R to the total arrival rate of the accepted traffic on link j:

$$Pl_R^{(j)} = \frac{\sum\limits_{\substack{R':j\in R' \\ j+1\notin R'}} \sum\limits_{m=1}^{C} \Lambda_R B^w_{R'|X_j=m} q_j(m)}{\sum\limits_{m=1}^{C} \alpha_j(m) q_j(m)}, \tag{4.7}$$

where $B^w_{R|X_j=m}$ is the wavelength blocking probability on route R given m wavelengths are free on link j, and is derived in the next section.

Given a route R and numbering sequentially the links of R from 1 (first link) to H (last link), it can then be shown as in [19] that:

$$g_R(i) = \beta_{i,H} \prod_{j=1}^{H-1} \prod_{k=1}^{i} \frac{\eta_{k,j}}{\eta_{k,j} + Pl_R^{(j)}(1-\eta_{k,j})}. \tag{4.8}$$

Using the inclusion-exclusion principle and assuming no blocking due to QoS, the blocking probability B_R on route R is [19]:

$$B_R = B_R^w = 1 - \sum_{i=1}^{C} (-1)^{i-1} \binom{C}{i} g_R(i). \tag{4.9}$$

4.3.2 State-dependent arrival rates

We now determine the state-dependent arrival rates $\alpha_j(m)$. First, let $g_{R|X_j=m}(i)$ be the probability that a given set of i wavelengths are free on route R given m wavelengths are free on link j. If $i > m$ then $g_{R|X_j=m}(i) = 0$, otherwise we can adapt

(4.8) to account for the additional condition "$X_j = m$":

$$\begin{aligned} g_{R|X_j=m}(i) &= \beta_{i,H} \frac{\binom{m}{i}}{\binom{C}{i}} \prod_{\substack{n=1 \\ n\neq j}}^{H-1} \prod_{k=1}^{i} \frac{\eta_{k,n}}{\eta_{k,n}+Pl_R^{(n)}(1-\eta_{k,n})} && \text{if } j \neq H \\ &= \frac{\binom{m}{i}}{\binom{C}{i}} \prod_{n=1}^{H-1} \prod_{k=1}^{i} \frac{\eta_{k,n}}{\eta_{k,n}+Pl_R^{(n)}(1-\eta_{k,n})} && \text{if } j = H \end{aligned} \tag{4.10}$$

if link j is on route R, and $g_{R|X_j=m}(i) = g_R(i)$ otherwise.

Similarly, the blocking probability $B_{R|X_j=m}$ on route R given m wavelengths are free on link j, assuming no blocking due to QoS, is:

$$B_{R|X_j=m} = B^w_{R|X_j=m} = 1 - \sum_{i=1}^{m} (-1)^{i-1} \binom{C}{i} g_{R|X_j=m}(i) \tag{4.11}$$

if link j is on route R, and $B_{R|X_j=m} = B_R$ otherwise.

The state-dependent arrival rates $\alpha_j(m)$ are given by:

$$\alpha_j(m) = \sum_{R:j\in R} \Lambda_R \left(1 - B^w_{R|X_j=m}\right). \tag{4.12}$$

The iterative algorithm which computes the blocking probability due to wavelength constraint uses the previous quantities as follows, and is further illustrated in Fig. 4.2. The values for $\alpha_j(m)$ are initialized to $\alpha_j(0) = 0$ and $\alpha_j(m) = \sum_{R:j\in R} \Lambda_R$ for each link j and for $m = 1, \ldots, C$, and the blocking probabilities B_R, B^w_R, $B_{R|X_j=m}$ and $B^w_{R|X_j=m}$ are initialized to 0 for each route R, link j and number of wavelengths $m = 1, \ldots, C$. The quantities $q(m)$, $\beta_{i,j}$, $g_R(i)$, B_R, $g_{R|X_j=m}(i)$, $B_{R|X_j=m}$ and $\alpha_j(m)$ are then computed iteratively using (4.1)-(4.12) until the difference between the values of B_R for each route R between two successive iterations is small enough to indicate convergence at a required precision.

4.4 QoS blocking

In this section, we present an extension to the algorithm detailed in the previous section. The aim of the extension is to compute the QoS blocking probability in all-optical networks with physical impairments. More specifically, the extension computes the blocking probability B_R^q due to ISI, noise, and node crosstalk blocking for all routes R. As in Chapter 3, a new call is blocked due to insufficient QoS when its BER or the BER of a call that has already been established is below a predefined threshold Q_{th}, should the new call be established.

In this section, we assume that the blocking probabilities B_R^w and $B_{R|X_j=m}^w$ are known for all routes R, all links j and all wavelength counts m. These quantities were computed in the previous section, with $B_R^w = B_R$ and $B_{R|X_j=m}^w = B_{R|X_j=m}$, respectively. We give a pictorial version of our technique in the dotted boxes in Fig 4.2. Notice that our method is independent of the algorithm used to compute the blocking probabilities B_R^w: the intersection between the dashed and dotted boxes is reduced to the blocking probabilities B_R^w (lower dotted box) and $B_{R|X_j=m}^w$ (upper dotted box). Our method can be combined with any other algorithm that computes the blocking probability for each route. The algorithm we used to compute B_R^w requires the computation of state-dependent arrival rates, and hence we provide here a modification to the state-dependent arrival rates computations accounting for QoS blocking. However, if our method were used with an algorithm that computes B_R^w, yet does not require state-dependent arrival rates computations, then our method would still hold by simply ignoring state-dependent arrival rates computations.

To compute the blocking probability due to QoS, we first assume that the blocking probabilities B_R^w are known and we determine the distribution of the number of crosstalk components XT_R that impair each route R in Section 4.4.1. Then, we relate

the blocking probability due to QoS to the crosstalk distributions in Section 4.4.2, and we show how the state-dependent arrival rates computations should be modified from Section 4.3.2 in Section 4.4.3. We derive the time complexity of the algorithm in Section 4.4.4.

4.4.1 Distribution of the number of crosstalk terms

Denote by $U_R(k)$ the probability that $k = 0, \ldots, C$ calls are established on route R; $U_R(k)$ accounts only for calls that use exactly route R, not for calls that use only part of route R or that use a route that includes R. To determine the distribution U_R for each route R, we make the approximation that U_R is binomial. Indeed, the utilization of a wavelength on some route R can be viewed as a Bernoulli trial with probability of success p_R, the probability that the corresponding call is established[1]. The probability that a call is established on route R is the per-wavelength arrival rate for calls on route R, multiplied by the probability that a call is actually accepted on R, that is:

$$p_R = \frac{\Lambda_R}{M_R}\frac{1 - B_R}{C} = \Lambda_R \frac{1 - B_R}{C} \tag{4.13}$$

since, with no loss of generality, the service rates M_R are assumed to be unity.

The probability that exactly k calls are established on route R is therefore:

$$U_R(k) \approx \binom{C}{k} p_R^k (1 - p_R)^{C-k}, k = 0, 1, \ldots, C. \tag{4.14}$$

Let $I_R^{xt} = \{R_1, \ldots, R_p\}$ be the set of the routes that are potential sources of crosstalk for lightpaths established on route R. The set I_R^{xt} is determined for each route R as follows.

[1]The wavelengths statuses are statistically identical but not independent, hence the binomial distribution we use is an approximation

Consider route R consisting of the sequence of s nodes $(r_1, \ldots, r_s)$. Consider a route R' consisting of the sequence of nodes $(r'_1, \ldots, r'_l)$. Route R' can inject self-crosstalk at node r_n $(n = 1, \ldots, s)$ of R if the input (respectively, output) ports for R and R' at node r_n are the same. That is, $R' \in I_R^{xt}$ when:

- $n = 1$ (if r_n is the first node of R): R and R' start with the same link, i.e., $(r_1, r_2) = (r'_1, r'_2)$. In this case, crosstalk occurs at the multiplexer used to add wavelengths to the network.

- $n = s$ (if i is the last node of R): R and R' end with the same link, i.e., $(r_{s-1}, r_s) = (r'_{l-1}, r'_l)$.

- $1 < n < s$ (the other cases): R and R' share two consecutive links separated by node r_n, i.e., there exists $v \in \{2, \ldots, \min(s-1, l-1)\}$ such that $(r_{n-1}, r_n, r_{n+1}) = (r'_{v-1}, r'_v, r'_{v+1})$.

When a route R' shares more than one node where crosstalk can occur with route R, it cannot inject just one crosstalk component on R. Rather, the number of crosstalk components that route R' can inject on R can only be a multiple of the number of nodes in common between R and R'. Call $n_{xt}(R, R')$ the number of common nodes between routes R and R' where crosstalk can occur, and $U'_{R,R'}(k)$ the probability that some route R' injects k crosstalk components on route R. From the definitions of U' and n_{xt}, we have:

$$U'_{R,R'}(k) = \begin{cases} U_{R'}(k/n_{xt}(R, R')) & \text{if } k \text{ is a multiple of } n_{xt}(R, R'), \\ 0 & \text{otherwise.} \end{cases} \tag{4.15}$$

Let $XT_R(k)$ be the probability that route R is subject to exactly k crosstalk components. The total number of crosstalk components k seen by route R is the sum of

all crosstalk components injected at each node of R by all routes that intersect R. Here, we make the further approximation that the probabilities for establishing different routes are independent and that $U'_{R,R'}$ describe independent random variables. This approximation is compatible with the wavelength occupancy independence and the locality assumptions from Section 4.2. Therefore, $*$ denoting the convolution operator, and with $I_R^{xt} = \{R_1, \ldots, R_p\}$, the distribution of XT_R can be computed as follows:

$$XT_R = U'_{R,R_1} * \ldots * U'_{R,R_p}. \tag{4.16}$$

4.4.2 Blocking probability due to QoS

In this section, we exhibit the relation between the physical layer (impact of crosstalk on QoS) and the network layer (distribution of the number of crosstalk components). Assuming that physical layer impairments are due to ISI, noise and self-crosstalk only, the Q factor Q_R for a route R is:

$$Q_R = \frac{\mu_{1,R} - \mu_{0,R}}{\sigma_{0,R} + \sqrt{\sigma_{i,R}^2 + \sigma_{n,R}^2 + n\sigma_{x,R}^2}} \tag{4.17}$$

where $\mu_{0,R}$ and $\mu_{1,R}$ are the means of the received "0" and "1" samples, $\sigma_{0,R}$ is the standard deviation of the received "0" samples, $\sigma_{i,R}$, $\sigma_{n,R}$, $\sigma_{x,R}$ are the standard deviations of the "1" samples due to ISI, noise and single crosstalk interference, respectively, and n is the number of crosstalk signals that interfere with the considered lightpath (assuming these are all equal). Using the techniques described in Chapters 2 and 3, we can precompute $\mu_{1,R}$, $\mu_{0,R}$, $\sigma_{0,R}$, $\sigma_{i,R}$ and $\sigma_{x,R}$ for all routes in the network. Since the quantities $\mu_{1,R}$, $\mu_{0,R}$, $\sigma_{0,R}$, $\sigma_{i,R}$ and $\sigma_{x,R}$ are known for each route in the network, we can compute the maximum number of crosstalk components $N_R^{\max}$ a

route R can accommodate to maintain a Q factor above a predetermined threshold Q_{th}:

$$N_R^{\max} = \left\lfloor \frac{\left(\frac{\mu_1-\mu_0}{Q_{th}} - \sigma_{0,R}\right)^2 - \sigma_{i,R}^2 - \sigma_{n,R}^2}{\sigma_{x,R}^2} \right\rfloor . \tag{4.18}$$

Therefore, the probability that a lightpath is blocked because it does not meet the QoS constraint is the probability that this lightpath is subject to $N_R^{\max}$ crosstalk components or more, that is:

$$B_R^q = \sum_{k>N_R^{\max}} XT_R(k). \tag{4.19}$$

The blocking probabilities due to wavelength continuity and due to QoS are related by:

$$B_R = B_R^w + (1 - B_R^w)B_R^q \tag{4.20}$$

Indeed, a call can be blocked due to QoS only if a wavelength is available on the route the call is assigned, that is, when the call is not blocked due to the wavelength continuity constraint.

4.4.3 State-dependent arrival rates

As shown in Section 4.3, the state-dependent arrival rates $\alpha_j(m)$ depend on $B_{R|X_j=m}$, the blocking probabilities conditioned on the number of free wavelengths on link j. Similarly to (4.20), these blocking probabilities depend in turn on the conditional blocking probabilities due to QoS:

$$B_{R|X_j=m} = B_{R|X_j=m}^w + \left(1 - B_{R|X_j=m}^w\right) B_{R|X_j=m}^q. \tag{4.21}$$

We now determine the conditional probabilities $B^q_{R|X_j=m}$, which are needed to compute the state-dependent arrival rates $\alpha_j(m)$. First, we compute the probability $p_{R|X_j=m}$ that a given lightpath is established on route R given m wavelengths are free on link j, and the probability $U_{R|X_j=m}(k)$ that R is used by exactly k lightpaths given m wavelengths are free on link j.

If j is not a link of R, then $p_{R|X_j=m} = p_R$ and $U_{R|X_j=m} = U_R$. If j is a link of R then at most m wavelengths are free on R. Consider the case where j is a link of route R. The probability that a given lightpath is established on route R given m wavelengths are free on link j is now:

$$p_{R|X_j=m} = \frac{\Lambda_R}{M_R}\frac{1 - B_{R|X_j=m}}{C} = \Lambda_R\frac{1 - B_{R|X_j=m}}{C}. \tag{4.22}$$

since $M_R = 1$ for each route R.

We adapt (4.14) accounting for the fact that m, not C, wavelengths at most can be used by a lightpath on R:

$$U_{R|X_j=m}(k) = \begin{cases} \binom{m}{k}\left(p_{R|X_j=m}\right)^k\left(1 - p_{R|X_j=m}\right)^{m-k} & k = 0, \ldots, m, \\ 0 & k = m+1, \ldots, C. \end{cases} \tag{4.23}$$

The probability that route R' injects k crosstalk components of route R, given m wavelengths are free on R, follows from (4.15):

$$U'_{R,R'|X_j=m}(k) = \begin{cases} U_{R|X_j=m}(k/n_{xt}(R,R')) & \text{if } k \text{ is a multiple of } n_{xt}(R,R'), \\ 0 & \text{otherwise.} \end{cases} \tag{4.24}$$

The distribution of XT_R given m wavelengths are free on link j is:

$$XT_{R|X_j=m} = U'_{R,R_1|X_j=m} * \ldots * U'_{R,R_p|X_j=m}, \tag{4.25}$$

and the blocking probability due to QoS conditioned on the state of link j is:

$$B^q_{R|X_j=m} = \sum_{k>N_R^{\max}} XT_{R|X_j=m}(k). \tag{4.26}$$

The state dependent arrival rates $\alpha_j(m)$ are then computed using (4.12) and (4.20), with $B^w_{R|X_j=m}$ replaced by $B_{R|X_j=m}$.

4.4.4 Computational complexity

We determine here the computational complexity of our technique for one iteration of the algorithm. In practice, the algorithm runs through just a few iterations before the blocking probabilities converge and the algorithm terminates. Denote by N the number of nodes in the network, L the number of links, A the maximum number of nodes on a route, D the maximum number of routes intersecting any given route ($D = \max_R |I^{xt}_R|$), C the number of wavelengths. The number of routes is $N(N-1) = O(N^2)$.

The computation of B^w_R is dominated by the computations of $Pl^{(j)}_R$ and $g_{R|X_j=m}(i)$ ((4.7) and (4.10)). The time complexity for computing all values of $Pl^{(j)}_R$ and $g_{R|X_j=m}(i)$ are, respectively, $O(N^4AC)$ and $O(N^2C^3AL)$. Overall the time complexity needed to compute all B^w_R is $O(N^2CA(N^2 + C^2L))$.

Now consider our extensions to compute B^q_R. The statistics required to compute the Q factors are precomputed. The complexity of the computations that lead to B^q_R is dominated by the computations of (4.25). Each $U'_{R,R'|X_j=m}$ can be

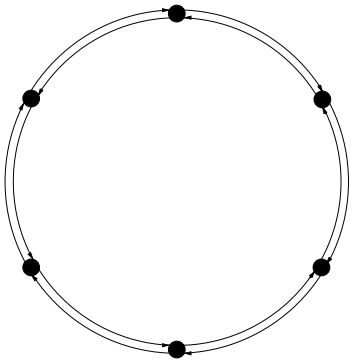

Figure 4.3: Ring of 6 nodes. Each link is a span of 70-km of SMF.

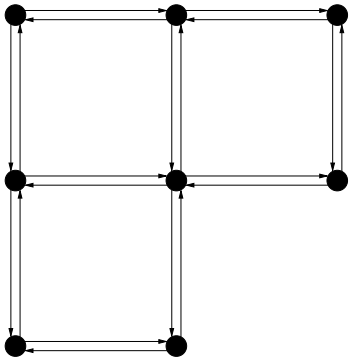

Figure 4.4: Mesh of 8 nodes. Each link is a span of 70-km of SMF.

represented as a vector of at most AC elements. To compute each $XT_{R|X_j=m}$, we need to convolve at most D of these vectors, which can be done in time $O((AC)^D D \log(AC))$ with FFTs. The time complexity of (4.25) and thus of our extensions is $O(N^2 LC(AC)^D D \log(AC))$. The time complexity of the full algorithm is hence $O(N^2 C(A(N^2 + C^2 L) + L(AC)^D D \log(AC)))$. On comparable hardware, computing blocking probabilities through simulations typically took several hours, while analysis took only a few minutes at most — a gain of one to three orders of magnitude in running time.

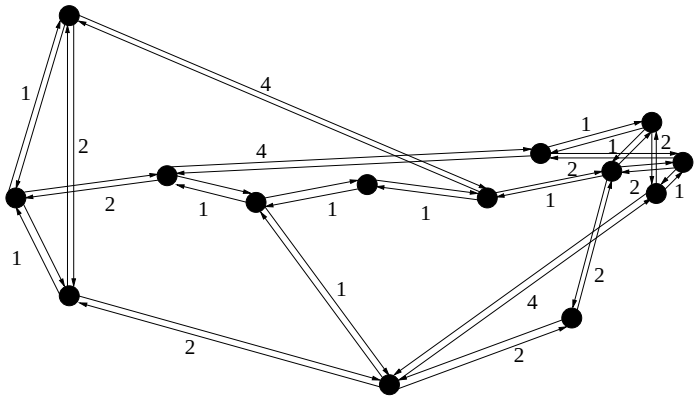

Figure 4.5: Down-scaled version of the NSF topology (scaling factor: 1/10). On the figure, the weights represent the number of 70-km long spans for the links.

4.5 Validation by simulation results

In this section, we evaluate our analytical model for blocking probability in all-optical networks impaired by crosstalk. Evaluation is performed on three different topologies of increasing complexity: a ring of 6 nodes (Fig. 4.3), a mesh of 8 nodes (Fig. 4.4), and the NSF topology (Fig. 4.5). The physical parameters are chosen to emulate regional-sized networks; unless otherwise stated, we used the parameters given in Table 4.1. Let B, B^w, and B^q be the mean (taken over the set of the node pairs) blocking probability, blocking probability due to the wavelength constraint, and blocking probability due to QoS, respectively. The analytical results are obtained by stopping the iterative algorithm when the difference for the blocking probabilities between two successive iterations differ by less than 1% for each route. The simulation results are obtained by simulating the routing and wavelength assignment of 10^5 calls. We use separate counters to determine blockings due to wavelength and due to QoS to compute B_w, B_q, and B using (4.20). Each data point is obtained by repeating this process 10 times in order to compute 95% confidence intervals, which are shown on the plots.

Table 4.1: Physical parameters for the simulated networks.

Description	**Value**
Span length	70 km
Signal peak power	2 mW
Bit rate	10 Gbps
Pulse shape	Super-Gaussian NRZ
Port crosstalk	-30 dB
Crosstalk detuning	0 GHz
WDM grid spacing	25 GHz
Fiber loss	0.22 dB/km
Nonlinear coefficient	2.2 $(\text{W km})^{-1}$
Chromatic dispersion	17 ps/nm/km
Dispersion compensation length	70 km
Spontaneous-emission factor	2
Photodetector responsitivity	1 A/W
Receiver electrical bandwidth	7 GHz
Minimum Q factor	6

Similar to the analysis, simulations use precomputed tables to compute Q factors; however, in the simulation, we consider that crosstalk is propagated from the node where the leak occurs to the end of the considered lightpath, while in the analysis we assume that crosstalk is propagated on the whole considered lightpath, irrespective of where the leak occurs, as can be seen in (4.17). With the physical parameters given in Table 4.1, it was shown in Chapter 2 that the crosstalk variance decreases slowly with the propagation distance; therefore, our analytical method tends to underestimate crosstalk variances by assuming longer propagation distances, and hence to underestimate QoS blocking.

We first present results for the ring of 6 nodes topology with 32 wavelengths per link ($C = 32$) in Fig. 4.6. For this set of parameters, blocking probability due to wavelength continuity is several orders of magnitude lower than that due to QoS, and therefore $B^q \approx B$. Our technique estimates accurately blocking probability in a wide operation range (blocking probabilities varying over 4 orders of magnitude).

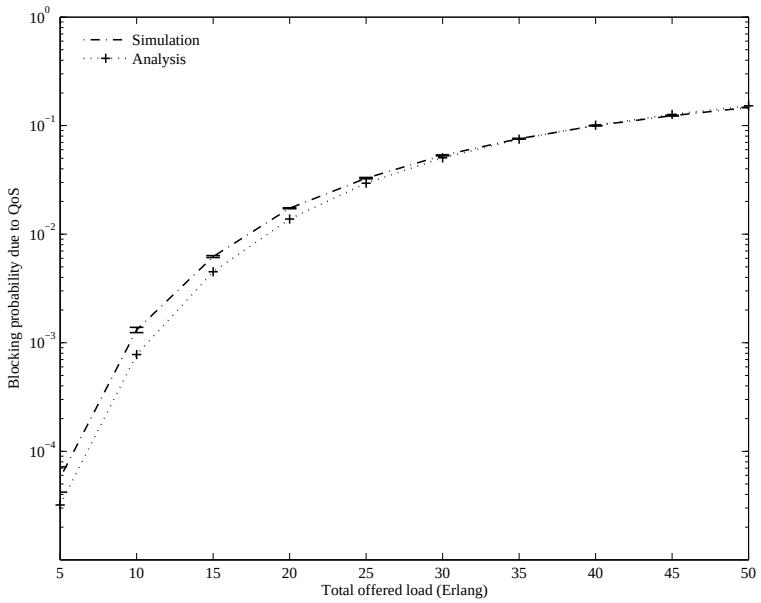

Figure 4.6: Blocking probability for the ring of 6 nodes, 32 wavelengths, -30 dB crosstalk.

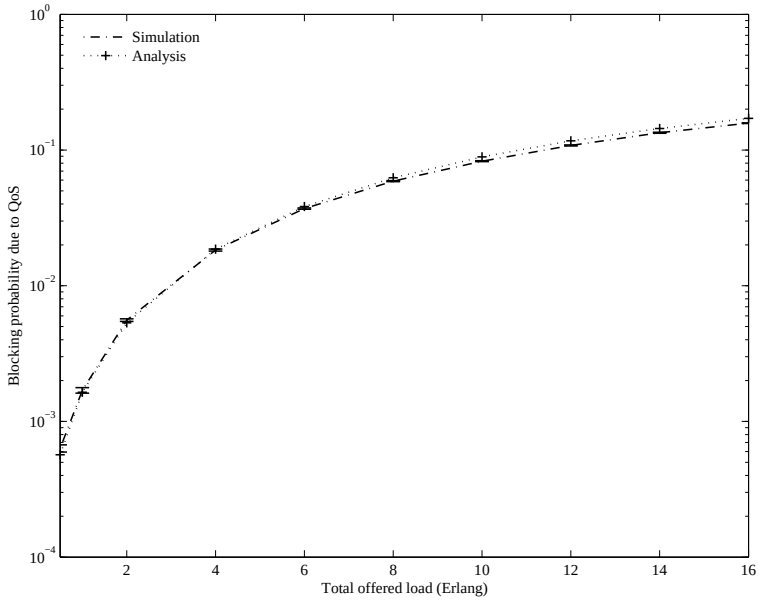

Figure 4.7: Blocking probability for the mesh of 8 nodes, 16 wavelengths, -25 dB crosstalk.

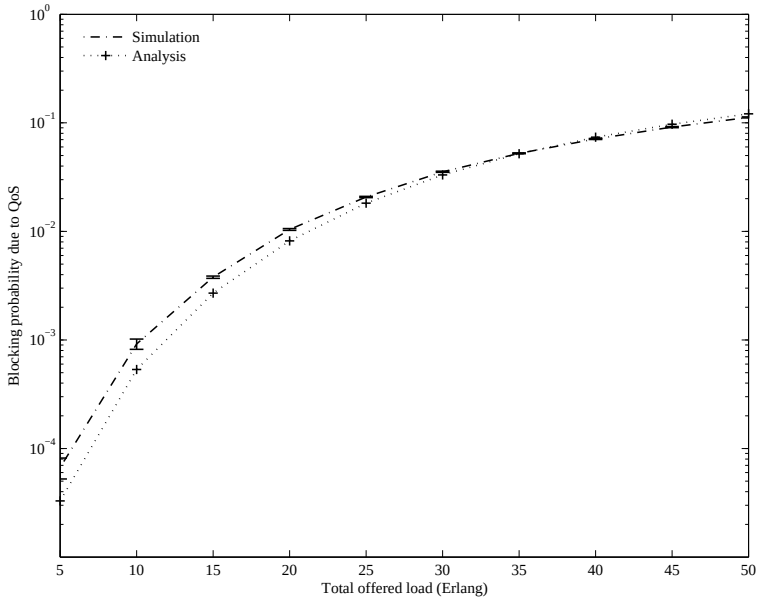

Figure 4.8: Blocking probability for the mesh of 8 nodes, 16 wavelengths, -30 dB crosstalk.

In Figs. 4.7 and 4.8, we show the blocking probability due to QoS for the mesh of 8 nodes with 16 wavelengths ($C = 16$) for 2 levels of crosstalk: -25 dB and -30 dB. Again, in this case, blocking probability due to wavelength continuity is very small compared to that due to QoS and hence we do not report it. The mesh network of 8 nodes is more dense than the ring of 6 nodes, and the analytical results are very close to the simulations.

We define the gain in load of a network as follows: given a target blocking probability B_t, a reference crosstalk level η_r, and a crosstalk level η, the gain in load for crosstalk level η is the ratio between the load in Erlang such that the call blocking probability in the network for crosstalk level η is B_t, and the load in Erlang such that the call blocking probability in the network for crosstalk level η_r is B_t. It can be seen in Fig. 4.9, where B_t was fixed to 0.001 and η_r to -25 dB, that crosstalk level has a dramatic influence on the admissible load in the network; for instance, if crosstalk

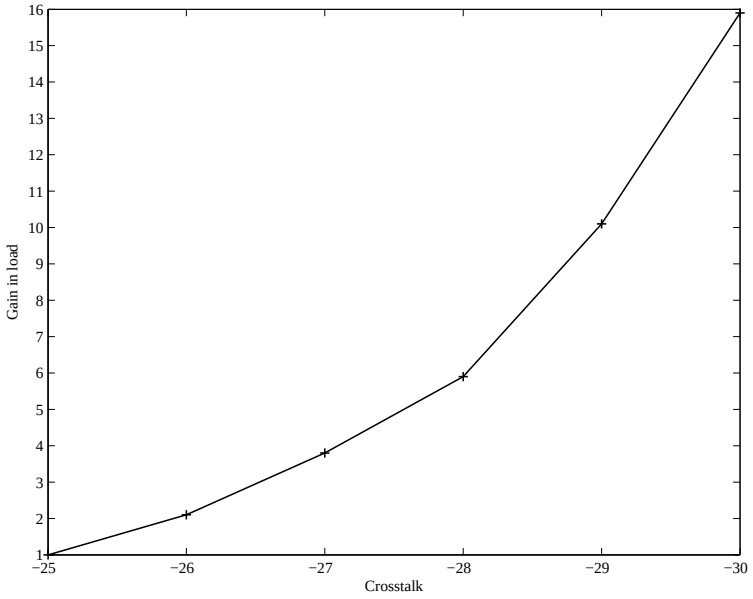

Figure 4.9: Gain in load for the mesh of 8 nodes for a target blocking probability of $B_t = 0.001$; by construction, a gain of 1 corresponds to -25 dB crosstalk.

level drops by only 5 dB from -25 dB to -30 dB, then the network can be loaded 16 times more while still achieving a 0.001 average call blocking probability.

In Fig. 4.10, we report blocking probability for the scaled NSF topology with 16 wavelengths ($C = 16$). Again B^w is negligible compared to B^q and we report B^q only. Our model is very accurate over more than 3 orders of magnitude in terms of blocking probability. Fig. 4.11 depicts the scenario where the number of wavelengths is 8 ($C = 8$) instead of 16. In this case, blocking due to wavelength continuity is not negligible. We report total blocking probability, as well as blocking probability due to wavelength continuity and due to QoS. For loads lower than 30 Erlangs, QoS blocking dominates wavelength blocking, and the converse is true for loads above 30 Erlangs. Our analytical results predict this behavior accurately.

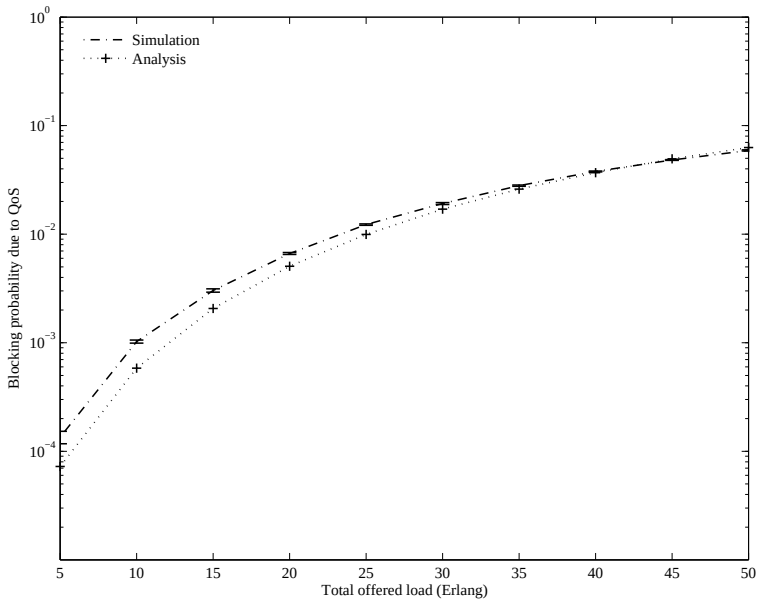

Figure 4.10: Blocking probability for the NSF network, 16 wavelengths, -30 dB crosstalk.

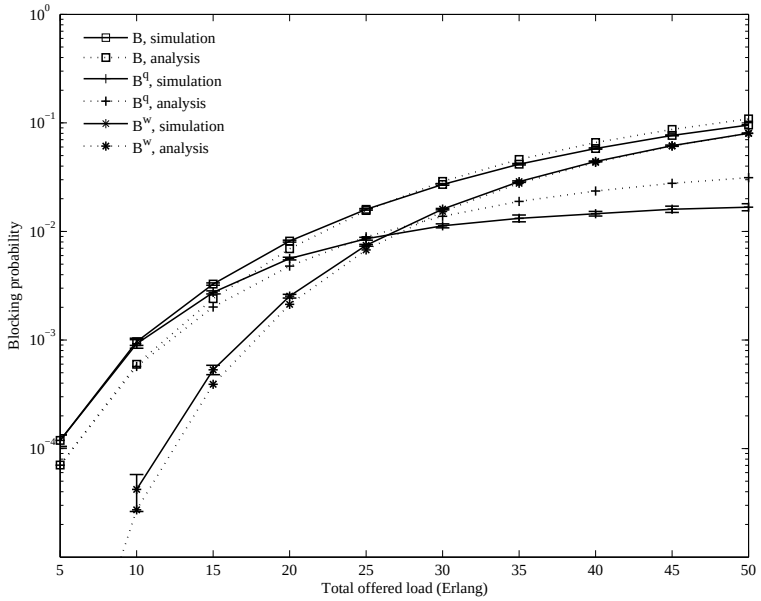

Figure 4.11: Blocking probability for the NSF network, 8 wavelengths, -30 dB crosstalk.

4.6 Summary

In this chapter, we presented an iterative technique to compute the blocking probability in all-optical networks impaired by ISI, noise, and node self-crosstalk. Starting from a published method that computes blocking probability due to wavelength continuity, we were able to compute blocking probability due to QoS. Our technique, which is independent of the algorithm used to compute wavelength blocking, was evaluated on various topologies for realistic physical layer parameters and shown to match closely simulation results.

Chapter 5

Conclusions and future work

The goal of this dissertation was to study a physical effect particular to all-optical networks, namely, node crosstalk, and techniques to mitigate physical impairments through a crosslayer technique: Routing and Wavelength Assignment.

We have shown that node crosstalk should be accounted for when designing all-optical networks. In Chapter 2, we developed fast analytical and semi-analytical techniques to compute the impact of crosstalk on signal transmission, as measured by its Q factor, which is related to signal BER. Using the technique we developed, we can account for many physical parameters including the detuning between crosstalk and impaired signal. The technique was evaluated for wide ranges of system parameters and the impact of crosstalk was compared with impact of other impairments such as ISI and noise. Depending on the physical characteristics of the network and the transmission lengths involved, the impact of node crosstalk dominates, is equivalent to, or is dominated by other effects. However the impact of node crosstalk on light-path BER cannot be neglected. Node crosstalk is difficult to remove with hardware because it is in-band with legitimate signals, and hence other techniques are needed to mitigate its effects.

This impact in terms of BER has direct implications in terms of network operations. To maintain high Quality of Service in networks, some calls are blocked because their BER is below a predetermined threshold, even if network resources were sufficient to accommodate the call otherwise. We estimated in Chapter 3 the separate impacts on call blocking probability of ISI and noise, node crosstalk, and crosstalk due to interchannel interactions (nonlinear crosstalk). It was shown that each physical impairment had different but non-negligible consequences on the call blocking probability in all-optical networks. Routing and wavelength assignment algorithms we developed account for crosstalk at call admission time. We evaluated our algorithms on realistic large-scale networks; we showed that we were able to partially remove the impact of the physical layer on blocking probability using simply software, network-layer techniques, which are far less costly than hardware-based physical-layer. Moreover, our RWA algorithms exhibit desireable properties such as higher fairness among the network users compared with standard algorithms. In Chapter 4, we evaluated analytically a reduced class of RWA algorithms, accounting for QoS blocking due to ISI, noise, and a specific kind of node crosstalk: adjacent-port node crosstalk. Very good agreement was found between our analytical method and simulations.

The context of this dissertation was the evaluation and design of realistic, next generation all-optical network, and we purposefully ignored the impact of signal regeneration on network performance. Signal regeneration can be done electrically, in which case the network is no longer all-optical, but a translucent network (for instance, a network of small all-optical "clouds" isolated by electronic switches). Since the topic of this dissertation was all-optical networks and was motivated by the prospect of the complete removal of electrical bottlenecks in optical networks, we did not study those hybrid networks. A second type of regeneration is all-optical

regeneration, which is still at the experimental design stage and was hence ignored. However, all-optical regeneration will be soon available and should therefore be added to future enhancements of our network model. All-optical regeneration will improve the SNR of crosstalk-impaired signals, however detection errors may be added by the regenerators. A model for all-optical regeneration is needed, and its impact on end-to-end BER as well as on RWA operation and design, should be studied.

We studied networks with datarates of typically 10 Gbps. Future networks will use datarates of 40 Gbps or more. At such speeds, polarization mode dispersion (PMD), which does not affect recent 10 Gbps systems and hence was safely ignored, must be included in the network model. PMD is not easy to include in our proposed model because, unlike the effects we studied, PMD is a time-varying effect (it is, for instance, a temperature-dependant effect). A lightpath with good BER at establishment time could start exhibiting a poor BER while it is in use, due to the PMD effect. It is possible to account for PMD with our model using a worst-case assumption, hereby leading to over-designing the system. Statistical models for PMD and appropriate mitigation techniques, such as using multipath diversity by transmitting data between source and destination over multiple, disjoint paths, could be studied.

In Chapter 3, some of the algorithms we presented implement the protecting threshold technique; we used a threshold of 2 wavelengths to determine whether a short (single-hop) or a long (multi-hop) path could be established. Although it is possible to use other values for the threshold and for the distinction between short and long paths, our goal was to give a proof of concept for the protecting threshold technique applied to QoS-aware adaptive RWA algorithms – such fine tuning is left for future work. Also, we assumed the existence of a centralized network management system; application of our algorithms to non-centralized, distributed networks is also left for future work.

Finally, our analytical model for RWA algorithms is the first to include QoS blocking, however it fails to account for crosstalks with different levels, that is, differentiating adjacent and non-adjacent port crosstalk. This is due to the reliance of the technique on the wavelength equivalence assumption. Relaxing this assumption would pave the way for inclusion of more complex crosstalk models, such as adjacent and non-adjacent port (node) crosstalk but also nonlinear crosstalk.

Appendix A

Q-factor computation

In this appendix, we present a fast technique to compute the Q factor of a signal in a homogeneous network where all spans have the same physical characteristics. Since the technique is based on the utilization of precomputed tables, little computation is needed at call admission time, and the technique can be used in real time while operating a network. We consider a signal over a lightpath LP, depicted in Fig. 3.1, subject to physical impairments. The physical impairments we account for here are ISI, ASE noise, node crosstalk, and nonlinear crosstalk.

Recall from Section 3.2 that the Q factor for a signal can be computed as, at the end of its associated lightpath:

$$Q = \frac{\mu_1 - \mu_0}{\sigma_0 + \sigma_1} = \frac{\mu_1 - \mu_0}{\sigma_0 + \sqrt{\sigma_i^2 + \sigma_n^2 + \sum_p \sigma_{nxp}{}^2 + \sum_q \sigma_{nlxq}{}^2}} \tag{A.1}$$

where μ_0 and σ_0^2 are the mean and variance of the "0" samples after photodetection, μ_1 and σ_1^2 are the mean and variance of the "1" samples after photodetection; the variance σ_1^2 is split into terms due to ISI: σ_i^2, noise: σ_n^2, node crosstalk: $\sum_p \sigma_{nxp}{}^2$, and nonlinear crosstalk: $\sum_p \sigma_{nlxp}{}^2$. The sums in (A.1) are taken over the sets of

Table A.1: Table containing the ISI terms used to compute Q.

Spans	0	1	2	...	N
μ_0	$\mu_0(0)$	$\mu_0(1)$	$\mu_0(2)$	...	$\mu_0(N)$
μ_1	$\mu_1(0)$	$\mu_1(1)$	$\mu_1(2)$	...	$\mu_1(N)$
σ_0^2	$\sigma_0^2(0)$	$\sigma_0^2(1)$	$\sigma_0^2(2)$	...	$\sigma_0^2(N)$
σ_i^2	$\sigma_i^2(0)$	$\sigma_i^2(1)$	$\sigma_i^2(2)$	...	$\sigma_i^2(N)$

interfering lightpaths. For node crosstalk, the set of interfering lightpath was defined in Section 3.2. For nonlinear crosstalk, the interfering lightpaths are those that have at least one span in common with the lightpath which Q factor we seek to compute.

In this Appendix, we show how to compute each of the terms in (A.1) using precomputed tables.

A.1 Load independent terms

Assuming physically identical fiber spans over LP, the ISI terms μ_0, μ_1, σ_0, σ_i only depend on the number of spans k of lightpath LP. We can precompute $\mu_0(k)$, $\mu_1(k)$, $\sigma_0(k)$, $\sigma_i(k)$ after each span k where k is an integer smaller than the maximal number of spans N on a lightpath in the network (see Table A.1). If the maximum number of spans on a lightpath N is not known a priori, it can be replaced by an upper bound: the total number of spans in the network. For each of the aforementioned statistics, there is no simple analytical relation between the statistics at span k and the same statistics at span $k+1$. Indeed, these quantities depend on fiber dispersion, nonlinearity, pulse shape, filter parameter, etc. Therefore, simulation are required; although we present here one technique to compute the values in Table A.1, the technique to compute Q factors presented here makes no assumption regarding how the values in Table A.1 are computed.

When computing the Q factor of a lightpath of k spans, the values of μ_0, μ_1, σ_0,

Table A.2: Table containing the ASE noise variances used to compute Q.

Spans	0	1	2	...	N
σ_n^2	$\sigma_n^2(0)$	$\sigma_n^2(1)$	$\sigma_n^2(2)$	...	$\sigma_n^2(N)$

σ_i in (A.1) are replaced by the the quantities $\mu_0(k)$, $\mu_1(k)$, $\sigma_0(k)$, $\sigma_i(k)$, respectively, precomputed as follows. We simulate using a well-known, fast technique such as the Split-Step Fourier method (SSF, [56]) the transmission of a short train of bits with the desired input pulse shape in N spans of fiber. An appropriate pseudo-random sequence for the train of pulses is the de Bruijn sequence [55], which includes all possible bit patterns of length m in a 2^m-bit long sequence. The total number of pulses 2^m whose transmission is simulated is therefore related to the number of ISI patterns to be accounted for. For instance, considering a pulse, if the ISI of the system we study is known to come only from the pulses that are immediate neighbors to the considered pulse, then we can simulate the transmission of $2^3 = 8$ bits to account for ISI at the physical layer. After transmission through k spans, the signal is passed through the modelled receiver and the sample means (μ_0, μ_1) and variances (σ_0^2, σ_i^2) of the sent "0" and "1" bits are computed.

A.2 ASE noise

Like the ISI terms, the ASE noise variances σ_n^2 are precomputed for a varying number of spans (see Table A.2); designating by $\sigma_n^2(k)$ the variance due to ASE noise after k spans, the Q factor of a lightpath of k spans is computed by replacing σ_n^2 by $\sigma_n^2(k)$ in (A.1).

The data in Table A.2 can be obtained, for instance, by (slow) simulations, or using the fast analytical method described in [53], which assumes an amplifier with flat gain and constant gain regardless of the input power.

Table A.3: Table containing the node crosstalk variances used to compute Q.

Spans	0	1	2	...	N
σ_x^2	$\sigma_x^2(0)$	$\sigma_x^2(1)$	$\sigma_x^2(2)$	...	$\sigma_x^2(N)$

A.3 Node crosstalk term

In Chapter 2, we presented a semi-analytical method to compute the variance $\sigma_x^2(k)$ from node crosstalk propagated through k fiber spans. The results for these computations, for a given attenuation η_0, are recorded in a table (see Table A.3). Again, the technique presented to compute Q factors makes no assumption regarding the algorithm used to fill Table A.3.

Consider that a signal $s(t)$ is subject to a single node crosstalk component $s_p(t)$ indexed by p as in (A.1) injected by another lightpath LP_p. As stated above, the case where several crosstalk components are present is dealt with by summing up the variances $\sigma_{nx_p}^2$ over the set of crosstalk components that are injected by lightpaths crossing LP. A model was given in Section 3.2 to determine the set of lightpaths injecting crosstalk on LP. The computations presented here do not assume any particular model for the origin of crosstalk.

The variance $\sigma_{nx_p}^2$ is determined using $\sigma_x^2(k)$ from Table A.3 as follows. The node crosstalk signal $s_p(t)$ is characterized by its attenuation with respect to the power of the signal $s(t)$, and the location where $s_p(t)$ starts co-propagating with signal $s(t)$; $s(t)$ and $s_p(t)$ co-propagate from the intersection of the LP and LP_p to the end of LP. Calling η the power attenuation of the crosstalk signal, and k the number of spans of LP from the intersection of LP with LP_p to the last node of LP, the variance $\sigma_{nx_p}^2$ is given by:

$$\sigma_{nx_p}^2 = \frac{\eta}{\eta_0}\sigma_x^2(k). \tag{A.2}$$

A.4 Nonlinear crosstalk term

The nonlinear crosstalk term, $\sigma_{nlx} = \sum_q \sigma_{nlx_q}^2$, is a sum of nonlinear crosstalk terms coming from XPM between signal $s(t)$ on lightpath LP and a single signal $s_q(t)$ on lightpath LP_q, or FWM between $s(t)$ and up to three signals $s_{q_1}(t)$, $s_{q_2}(t)$, $s_{q_3}(t)$ on lightpaths LP_{q_1}, LP_{q_2}, and LP_{q_3}, respectively. The sum is taken over the set of signals that co-propagate with $s(t)$ on one or more segments of LP. As in Section 2.2, we split the lightpath LP into segments; each segment corresponds to the part of the lightpath between two consecutive nodes. Consider a nonlinear interaction (XPM or FWM) indexed by q in the sum above. We consider that signals before and after an OXC are statistically independent and therefore each variance $\sigma_{nlx_q}^2$ due to a nonlinear interaction q is a sum of variances over the segments LP_{q_1}, ..., LP_{q_n}, where signals $s(t)$ and $s_q(t)$ or $s_{q_1}(t)$, $s_{q_2}(t)$, $s_{q_3}(t)$ co-propagate:

$$\sigma_{nlx_q}^2 = \sum_{r=1}^{n} \sigma_{nlx_{q,r}}^2 \tag{A.3}$$

Consider the nonlinear interaction q between signals $s(t)$ and $s_q(t)$ (XPM) or $s_{q_1}(t)$, $s_{q_2}(t)$, $s_{q_3}(t)$ (FWM) over a k-span long segment LP_r. We show how to compute the variance associated to this nonlinear interaction $\sigma_{nlx_{q,r}}^2$ using a table of precomputed data. Let C be the number of WDM channels in the system. Suppose that the nonlinear interaction q we study is XPM, and let ℓ be the channel number of the signal $s_q(t)$ relative to the channel of $s(t)$. That is, if $s(t)$ is on channel $1 \leq a \leq C$ and $s_q(t)$ is on channel $1 \leq b \leq C$ then $\ell = b - a \in \{-C+1, \ldots, C+1\} \setminus \{0\}$. We can compute the standard deviation $\sigma_{XPM}(\ell)$ after one span due to XPM between signals separated by ℓ channels, using for instance the technique described in [48]. Then, the variance $\sigma_{nlx_{q,r}}^2$ after k spans is, for XPM:

$$\sigma_{nlx_{q,r}}^2 = k^2 \sigma_{XPM}^2(\ell). \tag{A.4}$$

Table A.4: Table containing the nonlinear crosstalk variances due to XPM used to compute Q.

Channel separation (ℓ)	0	1	2	...	N
σ^2_{XPM}	$\sigma^2_{XPM}(0)$	$\sigma^2_{XPM}(1)$	$\sigma^2_{XPM}(2)$	...	$\sigma^2_{XPM}(N)$

Table A.5: Table containing the nonlinear crosstalk variances due to FWM used to compute Q.

ℓ	**m**	**n**	$\sigma^2_{FWM}(\ell, m, n)$
$-C+2$	$-C+1$	-1	$\sigma^2_{FWM}(-C+2, -C+1, -1)$
$-C+3$	$-C+1$	-2	$\sigma^2_{FWM}(-C+3, -C+1, -2)$
$\vdots$	$\vdots$	$\vdots$	$\vdots$
$C-1$	$C-2$	-1	$\sigma^2_{FWM}(-C+1, C-2, -1)$

Noting that the effects of XPM depend only on the absolute channel count between two signals, we have $\sigma_{XPM}(-\ell) = \sigma_{XPM}(\ell)$ for all ℓ. Therefore, we can compute variances due to XPM interaction in a network using only the precomputed values of $\sigma_{XPM}(\ell)$ for each channel count $\ell \in \{1, \ldots, C-1\}$ (see Table A.4).

Now suppose that the nonlinear (FWM) interaction q is between the four signals $s(t)$, $s_{q_1}(t)$, $s_{q_2}(t)$, $s_{q_3}(t)$; similar to XPM, we denote by ℓ, m, n the channel numbers of signals $s_{q_1}(t)$, $s_{q_2}(t)$, $s_{q_3}(t)$ relative to the channel of signal $s(t)$. FWM occurs when $m = \ell + n$, $m \neq l$, $\ell \neq 0$, and $n \neq 0$ (the cases where $m = l$ or $\ell = 0$ or $m = 0$ actually corresponds to XPM). Also, the cases where $\ell < 0$ and $n > 0$ simultaneously are symmetric to other cases already accounted for, and can be ignored. Again, using for instance [48], we can compute the variance $\sigma^2_{FWM}(\ell, m, n)$ due to the FWM between the four signals $s(t)$, $s_{q_1}(t)$, $s_{q_2}(t)$, $s_{q_3}(t)$ for all $\ell, m, n \in \{-C+1, \ldots, C+1\}$ with $m = \ell + n$, $m \neq l$, and either $\ell \geq 0$ or $n \leq 0$, after one span (see Table A.5). The variance $\sigma^2_{nlx_{q,r}}$ after k spans is, for FWM:

$$\sigma^2_{nlx_{q,r}} = k^2 \sigma^2_{FWM}(\ell, m, n). \tag{A.5}$$

Bibliography

[1] Lambda optical systems networks, http://www.lambdaopticalsystems.com/.

[2] Movaz networks, http://www.movaz.com/.

[3] A.E. Willner, M.C. Cardakli, O.H. Adamczyk, Y.-W. Song, and D. Gurkan. Key building blocks for all-optical networks. *IEICE Transactions on Communications*, pages 2166–2177, October 2000.

[4] M. Wu and W.I. Way. Fiber nonlinearity limitations in ultra-dense WDM systems. *IEEE/OSA Journal of Lightwave Technology*, 22(6):1483–1498, June 2004.

[5] J. Zhou, R. Cadeddu, E. Casaccia, C. Cavazzoni, and M.J. O'Mahony. Crosstalk in multiwavelength optical cross-connect networks. *IEEE/OSA Journal of Lightwave Technology*, 14(6):1423–1435, June 1996.

[6] E. Iannone, R. Sabella, M. Avattaneo, and G. De Paolis. Modeling of in-band crosstalk in WDM optical networks. *IEEE/OSA Journal of Lightwave Technology*, 17(7):1135–1141, July 1999.

[7] Y. Shen, K. Lu, and W. Gu. Coherent and incoherent crosstalk in WDM optical networks. *IEEE/OSA Journal of Lightwave Technology*, 17(5):759–764, May 1999.

[8] T. Deng, S. Subramaniam, and J. Xu. Crosstalk-aware wavelength assignment in dynamic wavelength-routed optical networks. In *Proceedings of the IEEE International Conference on Broadband Networks (Broadnets)*, pages 140–149, San Jose, CA, USA, October 2004.

[9] N. Antoniades, A. Boskovic, I. Tomkos, N. Madamopoulos, M. Lee, I. Roudas, D. Pastel, M. Sharma, and M.J. Yadlowsky. Performance engineering and topological design of metro WDM optical networks using computer simulation. *IEEE Journal on Selected Areas in Communications*, 20(1):149–165, January 2002.

[10] E. Ciaramella and F. Curti. Impairments due to the interplay between node crosstalk and nonlinear propagation in all optical transport networks. *IEEE Photonics Technology Letters*, 11(5):563–565, May 1999.

[11] E. Ciaramella and F. Curti. Experimental assessment of node crosstalk limitations enhanced by nonlinear effects in all optical transport networks. *IEEE Photonics Technology Letters*, 11(6):7511–753, June 1999.

[12] L. Gillner, C.P. Larsen, and M. Gustavsson. Scalability of optical multiwavelength switching networks: crosstalk analysis. *IEEE/OSA Journal of Lightwave Technology*, 17(1):58–67, January 1999.

[13] T. Gyselings, G. Morthier, and R. Baets. Crosstalk analysis of multiwavelength optical cross connects. *IEEE/OSA Journal of Lightwave Technology*, 17(8):1273–1283, August 1999.

[14] I. Roudas, N. Antoniades, T. Otani, T.E. Stern, R.E. Wagner, and D.Q. Chowdhury. Accurate modeling of optical multiplexer/demultiplexer concatenation in transparent multiwavelength optical networks. *IEEE/OSA Journal of Lightwave Technology*, 20(6):921–936, June 2002.

[15] J. Sun. Influence of crosstalk on the scalability of WDM cross-connect networks. *Optoelectronics, IEE Proceedings*, 149(2):59–64, April 2002.

[16] F.B. Shepherd and A. Vetta. Lighting fibers in a dark network. *IEEE Journal on Selected Areas in Communications*, 22(9):1583–1588, November 2004.

[17] I. Chlamtac, A. Ganz, and G. Karmi. Lightpath communications: a novel approach to high bandwidth optical WANs. *IEEE Transactions on Communications*, 40(7):1171–1182, July 1992.

[18] H. Zang, J.P. Jue, and B. Mukherjee. A review of routing and wavelength assignment approaches for wavelength-routed optical WDM networks. *Optical Networks Magazine*, 1(1):47–60, January 2000.

[19] A. Sridharan and K.N. Sivarajan. Blocking in all-optical networks. *IEEE/ACM Transactions on Networking*, 12(2):384–397, April 2004.

[20] G. Karmous-Edwards. Global e-science collaboration. *IEEE Computing in Science and Engineering*, 7(2):67–74, March-April 2005.

[21] E. Mannie. Generalized Multi-Protocol Label Switching (GMPLS) Architecture. RFC 3945 (Proposed Standard), October 2004.

[22] C. Qiao and M. Yoo. Optical burst switching (OBS) - a new paradigm for an optical Internet. *Journal of High Speed Networks*, 8(1):69–84, March 1999.

[23] M. Ali and L. Tancevski. Impact of polarization-mode dispersion on the design of wavelength-routed networks. *IEEE Photonics Technology Letters*, 14(5):720–722, May 2002.

[24] I.E. Fonseca, R.C. Almeida, M.R.N. Ribeiro, and H. Waldman. Algorithms for FWM-aware routing and wavelength assignment. In *Proceedings of the IEEE International Microwave and Optoelectronics Conference (IMOC)*, volume 2, pages 707–712, Iguazu Falls, Parana, Brazil, September 2003.

[25] I.E. Fonseca, M.R.N. Ribeiro, R.C. Almeida, and H. Waldman. Preserving global optical QoS in FWM impaired dynamic networks. *IEEE Electronics Letters*, 40(3):191–192, February 2004.

[26] A. Jukan and G. Franzl. Path selection methods with multiple constraints in service-guaranteed WDM networks. *IEEE/ACM Transactions on Networking*, 12(1):59–72, February 2004.

[27] M.A.C. Lima, A. César, and A.F.R. Arújo. Optical network optimization with transmission impairments based on genetic algorithm. In *Proceedings of the SBMO/IEEE International Microwave and Optoelectronics Conference (IMOC)*, volume 1, pages 361–365, Iguazu Falls, Parana, Brazil, September 2003.

[28] J.F. Martins-Filho, C.J.A. Bastos-Filho, E.A.J. Arantes, S.C. Oliveira, L.D. Coelho, J.P.G. de Oliveira, R.G. Dante, E. Fontana, and F.D. Nunes. Novel routing algorithm for transparent optical networks based on noise figure and amplifier saturation. In *Proceedings of the IEEE International Microwave and Optoelectronics Conference (IMOC)*, volume 2, pages 919–923, 2003.

[29] D. Penninckx and C. Perret. New physical analysis of 10-gb/s transparent optical networks. *IEEE Photonics Technology Letters*, 15(5):778–780, May 2003.

[30] Y. Huang, J.P. Heritage, and B. Mukherjee. Connection provisioning with transmission impairment consideration in optical WDM networks with high-speed

channels. *IEEE/OSA Journal of Lightwave Technology*, 23(3):982–993, March 2005.

[31] B. Ramamurthy, D. Datta, H. Feng, J.P. Heritage, and B. Mukherjee. Impact of transmission impairments on the teletraffic performance of wavelength-routed optical networks. *IEEE/OSA Journal of Lightwave Technology*, 17(10):1713–1723, October 1999.

[32] X. Yang and B. Ramamurthy. Dynamic routing in translucent WDM optical networks: the intradomain case. *IEEE/OSA Journal of Lightwave Technology*, 23(3):955–971, March 2005.

[33] T. Deng and S. Subramaniam. Adaptive QoS routing in dynamic wavelength-routed optical networks. In *Proceedings of the IEEE International Conference on Broadband Networks (Broadnets)*, pages 184–193, Boston, MA, USA, October 2005.

[34] A. Mokhtar and M. Azizoğlu. Adaptive wavelength routing in all-optical networks. *IEEE/ACM Transactions on Networking*, 6(2):197–206, April 1998.

[35] R. Jain, D. Chiu, and W. Hawe. A quantitative measure of fairness and discrimination for resource allocation in shared computer systems, September 1984. DEC Research Report TR-301.

[36] A. Birman and A. Kershenbaum. Routing and wavelength assignment methods in single-hop all-optical networks with blocking. In *Proceedings of the IEEE Conference on Computer Communications (INFOCOM)*, volume 2, pages 431–438, Boston, MA, USA, April 1995.

[37] H. Harai, M. Murata, and H. Miyahara. Performance of alternate routing methods in all-optical switching networks. In *Proceedings of the IEEE Conference on Computer Communications (INFOCOM)*, volume 2, pages 516–524, Kobe, Japan, April 1997.

[38] S. Thiagarajan and A. Somani. Capacity fairness of WDM networks with grooming capabilities. *SPIE Opt. Networks Mag.*, 2(3):24–31, May-June 2001.

[39] M. Köhn. Improving fairness in multi service multi layer networks. In *Proceedings of the 7th International Conference on Transparent Optical Networks (ICTON)*, pages 53–56, Barcelona, Spain, July 2005.

[40] S. Subramaniam, M. Azizoğlu, and A.K. Somani. All-optical networks with sparse wavelength conversion. *IEEE/ACM Transactions on Networking*, 4(4):544–557, August 1996.

[41] K. Lu, G. Xiao, and I. Chlamtac. Analysis of blocking probability for distributed lightpath establishment in WDM optical networks. *IEEE/ACM Transactions on Networking*, 13(1):187–197, February 2005.

[42] Y. Pointurier and M. Brandt-Pearce. Analytical study of crosstalk propagation in all-optical networks using perturbation theory. *IEEE/OSA Journal of Lightwave Technology*, 23(12):4074–4083, December 2005.

[43] Y. Pointurier and M. Brandt-Pearce. Study of crosstalk propagation in all-optical networks using perturbation theory. In *Proceedings of the IEEE International Conference on Electronics, Circuits and Systems (ICECS)*, pages 147–150, Gammarth, Tunisia, December 2005.

[44] E.L. Goldstein and L. Eskildsen. Scaling limitations in transparent optical networks due to low-level crosstalk. *IEEE Photonics Technology Letters*, 7(1):93–94, January 1995.

[45] H. Kim and T.S. El-Bawab. Enhancement of node-induced crosstalk by nonlinear effects in nonzero dispersion shifted-fiber rings with optical add-drop multiplexers. *Fiber and Integrated Optics, Taylor & Francis*, 20(6):625–635, 2001.

[46] G.P. Agrawal. *Nonlinear Fiber Optics*. Academic Press, 2001.

[47] H. Takahashi, K. Oda, and H. Toba. Impact of crosstalk in an arrayed-waveguide multiplexer on NxN optical interconnection. *IEEE/OSA Journal of Lightwave Technology*, 14(6):1097–1105, June 1996.

[48] B. Xu and M. Brandt-Pearce. Comparison of FWM- and XPM-induced crosstalk using the Volterra Series Transfer Function method. *IEEE/OSA Journal of Lightwave Technology*, 21(1):40–53, January 2003.

[49] E.L. Goldstein, L. Eskildsen, C. Lin, and Y. Silberberg. Polarization statistics of crosstalk-induced noise in transparent lightwave networks. *IEEE Photonics Technology Letters*, 7(11):1345–1347, November 1995.

[50] S.D. Dods, J.P.R. Lacey, and R.S. Tucker. Performance of WDM ring and bus networks in the presence of homodyne crosstalk. *IEEE/OSA Journal of Lightwave Technology*, 17(3):388–396, March 1999.

[51] G. Bosco, A. Carena, V. Curri, R. Gaudino, P. Poggiolini, and S. Benedetto. A novel analytical approach to the evaluation of the impact of fiber parametric gain on the bit error rate. *IEEE Transactions on Communications*, 49(12):2154–2163, December 2001.

[52] A. Carena, V. Curri, R. Gaudino, P. Poggiolini, and S. Benedetto. New analytical results on fiber parametric gain and its effects on ASE noise. *IEEE Photonics Technology Letters*, 9(4):535–537, December 2001.

[53] B. Xu and M. Brandt-Pearce. Analysis of noise amplification by a CW pump signal due to fiber nonlinearity. *IEEE Photonics Technology Letters*, 16(4):1062–1064, April 2004.

[54] C. Yu, L.-S. Yan, T. Luo, Y. Wang, Z. Pan, and A.E. Willner. Width-tunable optical RZ pulse train generation based on four-wave mixing in highly nonlinear fiber. *IEEE Photonics Technology Letters*, 17(3):636–638, March 2005.

[55] N.G. de Bruijn. A combinatorial problem. *Nederl. Akad. Wetensch., Proc.*, 49:758–764, 1946.

[56] G.P. Agrawal. *Fiber-Optic Communications Systems*. John Wiley & Sons, Inc., 2002.

[57] R. Hui, K.R. Demarest, and C.T. Allen. Cross-phase modulation in multi-span WDM optical fiber systems. *IEEE/OSA Journal of Lightwave Technology*, 17(6):1018–1026, June 1999.

[58] Y. Pointurier and M. Brandt-Pearce. Fair Routing and Wavelength Assignment in all-optical networks. In *Proceedings of the IEEE/OSA Optical Fiber Conference (OFC)*, page OFG3, Anaheim, CA, USA, March 2006.

[59] Y. Pointurier, M. Brandt-Pearce, T. Deng, and S. Subramaniam. Fair QoS-aware adaptive Routing and Wavelength Assignment in all-optical networks. In *Proceedings of the IEEE International Conference on Communications (ICC)*, Istanbul, Turkey, June 2006.

[60] Y. Pointurier, M. Brandt-Pearce, and B. Xu. Reduction of crosstalk in WDM networks with optional FEC coding. In *Proceedings of the IASTED International Conference on Optical Communication Systems and Networks (OCSN)*, Banff, Alberta, Canada, July 2006.

[61] B. Xu. Concatenated codes-based bit-rate adaptation for blocking probability reduction in WDM networks. *IEEE Photonics Technology Letters*, 17(9):1983–1985, September 2005.

[62] B. Mukherjee. WDM optical communication networks: Progress and challenges. *IEEE Journal on Selected Areas in Communications*, 18(10):1810–1824, October 2000.

[63] E. Ciaramella. Impairments in extremely dense WDM systems. *IEEE Photonics Technology Letters*, 14(6):804–806, June 2002.

[64] X. Liu, X. Wei, S. Chandrasekhar, and A.H. Gnauck. Increased OSNR gains of Forward-Error Correction in nonlinear optical transmissions. *IEEE Photonics Technology Letters*, 15(7):999–1001, July 2003.

[65] A. Birman. Computing approximate blocking probabilities for a class of all-optical networks. In *Proceedings of the IEEE Conference on Computer Communications (INFOCOM)*, volume 2, pages 651–658, Boston, MA, USA, April 1995.

[66] R.A. Barry and P.A. Humblet. Models of blocking probability in all-optical networks with and without wavelength changers. *IEEE Journal on Selected Areas in Communications*, 14(5):858–867, June 1996.

[67] Y. Zhu, G.N. Rouskas, and H.G. Perros. A path decomposition approach for computing blocking probabilities in wavelength-routing networks. *IEEE/ACM Transactions on Networking*, 8(6):747–762, December 2000.

[68] S.-P. Chung, A. Kasper, and K.W. Ross. Computing approximate blocking probabilities for large loss networks with state-dependent routing. *IEEE/ACM Transactions on Networking*, 1(1):105–115, February 1993.